Information measures of quantum systems

* * *

Collective Rydberg excitations of an atomic gas confined in a ring lattice

Tesis Doctoral presentada por

Beatriz M. Olmos Sánchez

Tesis Doctoral dirigida por:

Jesús Sánchez-Dehesa Moreno-Cid
Rosario González Férez
Igor Lesanovsky

Departamento de Física Atómica, Molecular y Nuclear

Universidad de Granada

- Dña. Rosario González Férez, Doctora en Ciencias Físicas y Profesora Titular del Departamento de Física Atómica, Molecular y Nuclear de la Facultad de Ciencias de la Universidad de Granada,

- D. Igor Lesanovsky, Doctor in Physics and Lecturer in the School of Physics and Astronomy of the University of Nottingham y

- D. Jesús Sánchez-Dehesa Moreno-Cid, Doctor en Física, Doctor en Matemáticas y Catedrático del Departamento de Física Atómica, Molecular y Nuclear de la Facultad de Ciencias de la Universidad de Granada,

MANIFIESTAN:

Que la presente memoria titulada: "Information measures of quantum systems and collective Rydberg excitations of an atomic gas confined in a ring lattice", presentada por Beatriz Montserrat Olmos Sánchez para optar al Grado de Doctora en Física, ha sido realizada bajo nuestra dirección en el Departamento de Física Atómica, Molecular y Nuclear y el Instituto Carlos I de Física Teórica y Computacional de la Universidad de Granada,

2 de Febrero de 2010

Fdo.: Rosario González Férez

Fdo.: Igor Lesanovsky

Fdo.: Jesús Sánchez-Dehesa Moreno-Cid

Fdo.: Beatriz Montserrat Olmos Sánchez

Título de Doctor con Mención Europea

Con el fin de obtener la Mención Europea en el Título de Doctor (aprobada en Junta de Gobierno de la Universidad de Granada el 5 de Febrero de 2001), se han cumplido, en lo que atañe a esta Tesis Doctoral y a su Defensa, los siguientes requisitos:

1. La memoria está escrita parcialmente en inglés y en español.

2. Uno o más de los miembros del tribunal provienen de una Universidad europea no española.

3. Una parte de la defensa se ha realizado en inglés.

4. Una parte de esta Tesis Doctoral se ha realizado en Inglaterra, en la School of Physics and Astronomy de la Universidad de Nottingham.

Agradecimientos/Acknowledgements

Escribir los agradecimientos es comprometido y difícil, porque sé que mucha gente sólo se leerá esta página de la tesis. Quiero dedicársela a todos los que han significado algo o mucho para mí durante estos cuatro años, ya que la suma de todo es lo que me trae al punto en el que me encuentro. Allá vamos:

- A mis directores de tesis. A Jesús, por haber depositado tu confianza en mí. Desde el principio, cuando decidiste darme una oportunidad de empezar en el mundo de la investigación, hasta el final, donde has sabido darme la libertad suficiente, aunque siempre pendiente de mi avance. A Rosario, por haber sido no sólo un gran punto de apoyo para continuar trabajando durante los últimos años, sino también una amiga con la que poder charlar siempre que me ha hecho falta. To Igor, for being both a patient and a hard supervisor. For having taught me so much and having asked always for a bit more when you knew I could give it.

- To the people I met in Innsbruck. Peter Zoller, for giving me the great opportunity of being there and learn so much. Maggie and Michael, sharing the office with you both was really great, talking about fashion and/or video games. Markus and Sebastian, contando chistes and dancing salsa. Gemma, bailando rock and roll mientras hablábamos catalán (vale, hablabas, jejeje). Claudiu, for all the chats on the terrace. You all made me feel sad when I had to leave, and make me remember those five months with a smile, see you soon!

- To the people in Nottingham. Peter, Thomas, Olga, Lucia, Anton, Sonali, Ivette, Céline, Marta and the rest, because you all make Nottingham feel a bit more like home.

- A Sandra, Su y Carmen, a mis antonias. Por lo que nos hemos reído y llorado juntas estos años, que cumplamos muchos más.

- A Dani, Jorge, Pablo, Antonio, Alex, (no me mareéis con los órdenes alfabéticos o no, eh?) por las noches frikis con cerveza y Big Bang Theory, El Núcleo y Torque, por Naruto y Narute, porque ahora digo con orgullo: !yo también soy friki! Jesús, por lo anterior y más, por no dejar que me rindiera.

- A Paqui y Lidia, por aullarle a la luna conmigo. Por haber hecho de nuestra última temporada en Granada (al menos de momento), algo memorable. Estoy a la espera de las coordenadas de la próxima.

- A Pili y Rake, por seguir ahí. Por ser alguien con quien poder contar, pase lo que pase; por lo cómoda que me siento con vosotras aunque no nos veamos tan a menudo como debiéramos. Ha sido y seguirá siendo un placer crecer y veros crecer al mismo tiempo. Y Pili, a ver si nos dan el Nobel, no?

- A Sheila, que ha andado el camino conmigo desde que éramos compañeras de prácticas hasta que nos ha tocado corregirlas, y ha aguantado conmigo que la gente todavía no sepa quién es Sheila y quién Bea (deberíamos ponernos identificación como en los congresos...). Por avisarme de los plazos, sin ti habría perdido la beca por no echar un papel, fijo. Por ser mi amiga, por ser única.

- A mi hermano, por haber hecho de mi niñez un juego y haberse convertido como quien no quiere la cosa en una persona maravillosamente diferente a mí de la que me siento orgullosa siempre.

- A mis padres. ¿Por qué? Bueno, porque soy todo lo que vosotros me habéis dado. Por haber permitido, pacientes, que cometiera errores y aprendiera de ellos, por animarme y ayudarme. Porque siempre me habéis hecho ver los malos momentos con mejor cara, ya sea con un buen consejo o un buen abrazo. Por decir que soy una llorona porque soy muy inteligente. En fin, por estar ahí, y darme la certeza de que tengo un punto apoyo constante e incondicional, que no es poco. Os quiero muchísimo.

- Y a Igor, por todo lo que has sido, eres y serás.

Contents

Foreword

This thesis encompasses two parts. In the first one, which is called 'Information measures of quantum systems', we present a contribution to the information theory of quantum mechanical systems and theory of special functions. In the second part, entitled 'Collective Rydberg excitations of an atomic gas confined in a ring lattice', we move to a different topic situated in the realm of ultracold atoms, Rydberg gases and complex many-body systems. In the following we briefly outline the contents of the thesis. A more detailed introduction and motivation can be found at the beginning of the respective parts.

In Part I, the Fisher information, which is a local information-theoretic measure, is both mathematically and physically studied. We do this by focussing on two applications which explicitly show those two aspects of the previous measure. Firstly, we determine the (translationally invariant) Fisher information of the multidimensional hydrogenic systems in both position and momentum spaces. To do so, we exploit the algebraic properties of the special functions which control the wavefunctions of the quantum states of these systems; namely, the Laguerre and Gegenbauer polynomials and the hyperspherical harmonics. The results are explicitly given in terms of the dimensional parameter and the hyperquantum numbers of the state. Secondly, the role of the Fisher information in estimation theory is highlighted. In particular, the parameter-based Fisher information the orthogonal polynomials Jacobi, Laguerre, Gegenbauer and Grosjean are analytically derived in terms of the polynomial degree and the parameter(s) which characterize them.

In Part II, we study a gas of ultracold Rydberg atoms trapped in a ring lattice and analyze thoroughly its excitation properties. First, the system is studied in the perfect blockade regime, that is, the double excitation of neighboring sites of the ring is neglected. In this framework, we first consider the time evolution of local properties, like the density of Rydberg states, the correlations and the entanglement, by means of the numerical solution of the Schrödinger equation. We find that the expectation values of certain observables, for example the number of Rydberg atoms, equilibrate after a short period of time, that is, they acquire a constant value with small fluctuations. The origin of this thermalization of a closed quantum system and its relation to the microcanonical ensemble is then further investigated. Moreover, we focus on a regime where the laser field is much stronger than the interaction between Rydberg atoms. Here, we find that the system is analytically solvable and allows us to access entangled many-particle states. We characterize these states by means of, for example, their correlations and outline a possible experimental route towards their excitation.

Prólogo

Esta memoria de tesis doctoral consta de dos partes. En la primera, titulada 'Medidas de información de sistemas cuánticos', se presenta una contribución a la teoría de información de sistemas mecano-cuánticos y a la teoría de funciones especiales. La segunda parte del trabajo, bajo el título de 'Excitaciones Rydberg colectivas de un gas atómico confinado en una red circular', está enmarcada en el campo de la física de átomos ultrafríos, estados Rydberg y sistemas multiparticulares complejos. A continuación se describen brevemente los contenidos de esta memoria de tesis. Al principio de cada una de las partes, se presentará una introducción y motivación más detalladas de las mismas.

En la Parte I, se estudia la información de Fisher, que es una medida teórica de información de carácter local. Este objetivo se aborda desde un punto de vista tanto matemático como físico. En primer lugar, se determina la información de Fisher (traslacionalmente invariante) de los sistemas hidrogenoides multidimensionales tanto en el espacio de posiciones como en el de momentos. Para ello, se hace un uso exhaustivo de las propiedades algebraicas de las funciones especiales que controlan las funciones de onda de los estados cuánticos de estos sistemas, es decir, los polinomios de Laguerre y Gegenbauer junto con los armónicos hiperesféricos. El resultado obtenido depende explícitamente de la dimensión y de los números cuánticos del correspondiente estado. A continuación, se pone de manifiesto el papel que juega la información de Fisher en la teoría de estimación de parámetros. En particular, se deriva analíticamente la información de Fisher con respecto al parámetro que caracteriza los polinomios ortogonales de Jacobi, Laguerre, Gegenbauer y Grosjean.

En la Parte II, se analizan las propiedades espectrales y dinámicas de un gas de átomos Rydberg confinado en una red óptica circular monodimensional excitados mediante un campo láser. Este estudio se comienza abordando el régimen de bloqueo perfecto, donde se considera prohibida la excitación simultánea de dos átomos situados en pozos contiguos de la red. En este caso, se investiga la evolución temporal de varias magnitudes físicas, tales como la densidad de estados Rydberg, la correlación y el entrelazamiento, mediante la resolución numérica de la ecuación Schrödinger. Este régimen se caracteriza por el estado de equilibrio que alcanzan algunos de los valores esperados de los observables alrededor del cual muestran pequeñas fluctuaciones. Se ha hecho especial hincapié en el análisis del origen de la termalización de este sistema cuántico aislado, investigando su relación con el conjunto microcanónico. A continuación, se considera el régimen dominado por la interacción con el campo láser. Se muestra que en este caso el sistema es analíticamente resoluble, y permite la creación de estados multiparticulares entrelazados. Se han estudiado las propiedades de dichos estados, y propuesto un esquema experimental para excitarlos.

Part I.

Information measures of quantum systems

1. Introduction

In the last few years, the application of information-theoretic ideas and techniques to the study of multielectronic systems has proved to be an interesting new channel of cross-fertilization between atomic and molecular physics, D-dimensional physics and theory of information [1, 2, 3, 4, 5, 6, 7, 8, 9, 10, 11, 12, 13, 14, 15]. This line of research has been addressed to the most relevant measures of information (Renyi and Shannon entropies, Fisher information...) for several quantum-mechanical potentials of a specific form [16, 17, 18] such as hydrogenic systems with standard and non-standard dimensionalities [19, 20], circular membranes [21], confined systems [22, 23] and, in general, many-electron systems [14, 24, 25, 26, 27]. However, the analytic determination of these information-theoretic measures has not yet been possible even for the single-particle systems with an analytically solvable Schrödinger equation, whose corresponding wavefunctions describing their physical states are controlled by special functions of mathematical physics (classical orthogonal polynomials, spherical harmonics, Bessel functions...). This is due to the lack of knowledge of the information-theoretic properties of special functions despite of the many results provided by the theory of the orthogonal polynomials and potential theory [19, 28, 29, 30, 31, 32].

The Fisher information is a gradient functional of the involved probability density, that is, it has the property of locality in the sense that it is very sensitive to irregularities of the distribution. This is not the case for the Renyi and Shannon entropies, which are power and logarithmic functionals of the probability density. This part of the thesis is mainly focused on the analytical determination of the Fisher information of the D-dimensional single-particle systems subject to Coulomb potentials.

The Fisher information was originally introduced in 1925 by R.A. Fisher in the theory of statistical estimation [33]. In a system, let us consider the problem of estimating a parameter with definite but unknown value θ by means of N measurements $\mathbf{y} \equiv \{y_1, \ldots y_N\}$. The data obtained fluctuate around the real value θ with a noise obeying a random noise distribution, so that the set of measurements can be given as

$$\mathbf{y} = \theta + \mathbf{x},$$

where $\mathbf{x} \equiv \{x_1, \ldots x_N\}$ are the values of the noise. These data are used to form an estimate $\hat{\theta}(\mathbf{y})$ of the parameter θ, and the whole measurement process is called to be 'smart' when the estimate obtained by this procedure is closer to the real value of the parameter than any of the data contained in $\mathbf{y}$. In this framework, the Fisher information arises as a measure of the expected error estimating a parameter in a smart measurement, i.e., from an imperfect observation in the presence of some random noise.

The system is specified by a likelihood or conditional probability law given by the family of probability densities $\rho_\theta(\mathbf{y}) \equiv \rho(\mathbf{y} \mid \theta)$. The Fisher information of the measurement process governed by $\rho_\theta(\mathbf{y})$ is defined as [33]

$$I(\theta) := \int \left[\frac{\partial \ln \rho_\theta(\mathbf{y})}{\partial \theta} \right]^2 \rho_\theta(\mathbf{y}) d\mathbf{y} = \int \frac{\left[\frac{\partial \rho_\theta(\mathbf{y})}{\partial \theta} \right]^2}{\rho_\theta(\mathbf{y})} d\mathbf{y}, \tag{1.1}$$

where the integrals are over all the corresponding space. It can be formally shown from this definition and the mean-square error of the estimate $\hat{\theta}(\mathbf{y})$

$$\sigma^2(\theta) \equiv \int \left[\hat{\theta}(\mathbf{y}) - \theta \right]^2 \rho_\theta(\mathbf{y}) d\mathbf{y},$$

that they accomplish the so-called Cramer-Rao inequality [34]

$$\sigma^2(\theta)I(\theta) \geq 1. \tag{1.2}$$

Hence, the Fisher information is formally seen to be a measure of the ability to estimate the parameter θ, i.e., it gives the minimum error in estimating θ given the probability density $\rho_\theta(\mathbf{y})$.

Note that the Fisher information (1.1) explicitly depends, in general, upon the parameter θ. There is an important exception to this rule. For the sake of simplicity, let us assume that there is only one measurement, i.e., $N = 1$. In the particular case where the noise fluctuations x are independent of the size of θ, i.e., shift invariance, the probability density accomplishes

$$\rho_\theta(y) = \rho(y - \theta) = \rho(x),$$

and the equation (1.1) reduces to

$$I = \int \frac{\left[\frac{\partial \rho(x)}{\partial x}\right]^2}{\rho(x)} dx. \tag{1.3}$$

Here, the Fisher information is a functional that gives a measure of the amount of gradient and that is sensitive to local changes of the probability distribution. This definition of the so-called **translationally-invariant Fisher information** is important since in fact a vast number of physical systems obey this shift invariance. In particular, this property holds for any isolated quantum mechanical system subject to a central potential centered in θ.

Nowadays, the Fisher Information is being used in numerous scientific areas ranging from statistics [33, 35, 36], information theory [34] and signal analysis [37], to quantum physics [6, 11]. This measure is also the main theoretic tool of the Extreme Physical Information principle (EPI), a general variational principle which allows to derive numerous fundamental equations of physics [4, 5, 6, 11, 15], such as Maxwell, Dirac, Klein-Gordon and Schrödinger equations, as well as thermodynamics' first law among others. It has been also shown that using the EPI leads to obtain as well the non-equilibrium thermodynamics [9].

This information-theoretic quantity has, among other characteristics, a number of important properties beyond the mere non-negativity, which deserve to be resembled here:

1. Additivity for independent events. If $\rho_\theta(y, z) = \rho_\theta^{(1)}(y) \cdot \rho_\theta^{(2)}(z)$, then

$$I\left[\rho_\theta(y, z)\right] = I\left[\rho_\theta^{(1)}(y)\right] \cdot I\left[\rho_\theta^{(2)}(z)\right]$$

2. Scaling invariance. The Fisher information is invariant under sufficient transformations $y = t(z)$, so that

$$I\left[\rho_\theta(y)\right] = I\left[\rho_\theta(z)\right].$$

   This property is not only closely related to Fisher's maximum likelihood method [38] but also it is very important for the theory of statistical inference.

3. The previously cited Cramer-Rao inequality [34]. It states that the reciprocal of the Fisher information $I(\theta)$ bounds from below the mean square error of an unbiased estimator $f \equiv \hat{\theta}(y)$ of the parameter θ; i.e.,

$$\sigma^2(f) \geq \frac{1}{I(\theta)},$$

   where $\sigma^2(f)$ denotes the variance of f. This inequality, which lies at the heart of statistical estimation theory, shows how much information the distribution provides about a parameter.

4. Relation to other information-theoretic properties. The Fisher information is related to the so-called Shannon entropy [39] of the probability distribution $\rho_\theta(y)$ defined as

$$S(\rho_\theta) := -\int \rho_\theta(y) \ln \rho_\theta(y) dy, \qquad (1.4)$$

via the elegant de Bruijn's identity [34, 40, 41]. More precisely, let ρ_θ be the convolution probability density of any probability density ρ with the normal density with zero mean and variance $\theta > 0$. Then, the following relation stands,

$$\frac{\partial}{\partial \theta} S(\rho_\theta) = \frac{1}{2} I(\rho_\theta).$$

Moreover, the Fisher information $I(\rho_\theta)$ satisfies, under proper regularity conditions, the limiting property [6, 11, 42]

$$I(\rho_\theta) = \lim_{\epsilon \to 0} \frac{2}{\epsilon^2} D\left(\rho_{\theta+\epsilon} \| \rho_\theta\right), \qquad (1.5)$$

where

$$D(p\|q) := \int p(y) \ln \frac{p(y)}{q(y)} dy \qquad (1.6)$$

denotes the relative or cross entropy (Kullback-Leibler divergence) of the probability density $p(y)$ and a reference distribution $q(y)$. There exist further connections of the Fisher information with other information-theoretic properties, as well as with expectation values of logarithmic and power functions of the probability distribution; see, e.g., [2, 43, 44].

5. Applications in quantum physics. The Fisher information $I(\rho_\theta)$ plays a fundamental role in the quantum-mechanical description of physical systems. It has been shown

   a) to be a measure of both disorder and uncertainty of a probability distribution, as thoroughly discussed in the Refs. [4, 6, 11];

   b) to be a measure of nonclassicality for quantum systems [7, 8];

   c) to describe, some factor apart, various macroscopic quantities such as the kinetic [1, 41] and the Weiszäcker energies [2, 3];

   d) to derive numerous fundamental equations in physics, such as the Schrödinger and Klein-Gordon equations of motion [5, 11] as well as the Euler equation of the density functional theory [10], from the principle of minimum Fisher information, in a similar way as the Shannon entropy is the starting point of the maximum entropy methods;

   e) to predict some non-linear spectral phenomena, such as the avoided crossings of energy levels encountered in atomic and molecular systems under strong external electric and magnetic fields [13], and correlations in many-electron systems [12];

   f) to be involved in numerous uncertainty inequalities [40, 41, 45, 46];

   g) to detect the transition state and the stationary points of a chemical reaction, as well as the bond breaking/forming regions of elementary ones [27].

In this part of the thesis, we present our contributions to the present knowledge on this information quantity in two chapters. In Chapter 2, we calculate the so-called translationally-invariant Fisher information of an important quantum system: the D-dimensional hydrogenic atom. We perform this task by a direct application of the definition given in (1.3) to the probability distribution obtained squaring the wavefunction that describes the dynamics of the system. We obtain the corresponding results in a closed analytical form (for both position and momentum spaces) and find that they can be expressed in terms of the hyperquantum numbers, which describe the

corresponding energy eigenstate. In a second stage (Chapter 3), we perform the fundamental task of calculating the Fisher information of the classical families of polynomials with respect to the parameters that characterize them. In particular, we treat the Laguerre, Jacobi, Gegenbauer and Grosjean polynomials and express the results in terms of their degree and corresponding parameter. At the end of each of these two chapters, we analyze and discuss the results obtained. The research carried out in this part has given as a result the following publications:

- J.S. Dehesa, S. López-Rosa, B. Olmos and R.J. Yáñez, "Information measures of hydrogenic systems, Laguerre polynomials and spherical harmonics", *J. Comput. Appl. Math.*, vol. 179, p. 185, 2005.

- J.S. Dehesa, S. López-Rosa, B. Olmos and R.J. Yáñez, "The Fisher information of D-dimensional hydrogenic systems in position and momentum spaces", *J. Math. Phys.*, vol. 47, p. 052104, 2006.

- J.S. Dehesa, B. Olmos and R.J. Yáñez, "Parameter-based Fisher information of orthogonal polynomials", *J. Comput. Appl. Math.*, vol. 214, p. 136, 2008.

2. Fisher information of D-dimensional hydrogenic systems

The quantum state of a many-particle system is in general described by the physical solution $\Psi(\mathbf{r})$ of the time-independent Schrödinger equation

$$H\Psi(\mathbf{r}) = E\Psi(\mathbf{r}),$$

where H is the Hamiltonian (independent of time) that drives the dynamics and E is the energy of the corresponding state. The spatial distribution of the system is then given by the probability density $P(\mathbf{r}) = |\Psi(\mathbf{r})|^2$, so that most of the physical information of the state is contained in this probability distribution.

One can characterize the information-theoretic content of a general probability distribution $P(\mathbf{r})$ by means of two different and complementary quantities among others: the Shannon entropy and the Fisher information. The Shannon entropy [39, 47] is a logarithmic functional of the probability density (1.4). It has been shown that it is a global measure of the smoothness (or disorder) of $P(\mathbf{r})$. On the other hand, the so-called translationally-invariant Fisher information (we will refer to it in this chapter simply as Fisher information) is defined as the gradient functional of the density

$$I = \int \frac{[\nabla P(\mathbf{r})]^2}{P(\mathbf{r})} d\mathbf{r}, \tag{2.1}$$

so it has the property of locality because it is sensitive to local rearrangements of the position variable $\mathbf{r}$. I is actually a measure of the degree of disorder of the system described by the corresponding probability distribution $P(\mathbf{r})$. The higher this quantity is, the more concentrated is the single-particle density (more gradient content), the smaller the uncertainty and the higher the accuracy is when predicting the localization of the particle (see Fig. 2.1).

However, the analytical determination of the Fisher information from first principles is not a simple task, not even for single-particle systems. In this chapter we shall perform the analytical calculation of the position and momentum Fisher information of a known and very important quantum system: the D-dimensional hydrogenic atom. So, the momentum hydrogenic orbitals (i.e., the solution to the non-relativistic, time-independent Schrödinger equation in momentum space) will also be studied. This is not only because the momentum eigenstates have usually been avoided
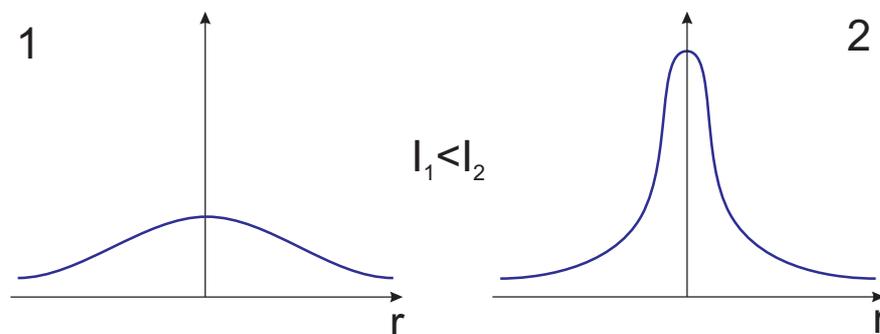
Figure 2.1.: The translationally-invariant Fisher information gives a measure of the gradient content of a probability distribution, i.e., the more concentrated the distribution, the bigger the Fisher information.

in favor of the position ones up until recently, but also because of (i) their conceptual importance, (ii) the distribution of momenta for real (D=3) atomic systems and specifically for hydrogen atom [48] is nowadays experimentally accessible in atomic, molecular and nuclear experiments, specially since the advance of the modern spectroscopy, (iii) the scattering phenomena are more conveniently viewed in numerical simulations by means of momentum space (see, e.g., [49]) and (iv) they play a very relevant role in numerous other physical processes with atoms and molecules which are governed by simple functions of the momentum transfer [50].

The chapter is structured as follows. First, the known position and momentum wavefunctions of the hydrogenic system in D dimensions are described in detail, and the corresponding probability densities are explicitly shown. Then, we find closed expressions for the Fisher information of the hydrogenic eigenstates in terms of the D quantum numbers which characterize them in position and momentum spaces, respectively. Finally, some concluding remarks are given.

2.1. The hydrogenic problem in D dimensions

In this section we fix our notation and we describe in hyperspherical coordinates the wavefunctions of the D-dimensional hydrogenic eigenstates, i.e., the solutions to the non-relativistic, time-independent Schrödinger equation in D dimensions. The configuration (or position) and momentum spaces are considered, and the associated probability distributions are obtained.

The position and momentum hydrogenic eigenstates in D-dimensions are known to be conformed in polar coordinates by an angular and a radial part. The angular part, which is common to both cases, is given in terms of the hyperspherical harmonics because of the radially symmetric character of the Coulomb potential. The radial part is controlled by the Laguerre and Gegenbauer polynomials in the position and momentum representations, respectively.

2.1.1. D-dimensional central potential

The D-dimensional time-independent Schrödinger equation for a particle moving in a central potential $V_D(r)$ reads (in atomic units)

$$\left(-\frac{1}{2\mu}\nabla_D^2 + V_D(r)\right)\Psi\left(\mathbf{r}\right) = E\Psi\left(\mathbf{r}\right), \tag{2.2}$$

where μ is the reduced mass of the system and ∇_D^2 stands for the Laplacian operator in D dimensions. Due to the symmetry of the problem, we work in hyperspherical coordinates $\mathbf{r} \equiv (r, \theta_1, \ldots, \theta_{D-1}) \equiv (r, \Omega_{D-1})$ related to the Cartesian set $(x_1, \ldots, x_D)$ as

$$x_1 = r \sin\theta_1 \sin\theta_2 \ldots \sin\theta_{D-2} \cos\theta_{D-1}$$
$$x_2 = r \sin\theta_1 \sin\theta_2 \ldots \sin\theta_{D-2} \sin\theta_{D-1}$$
$$x_3 = r \sin\theta_1 \sin\theta_2 \ldots \cos\theta_{D-2}$$
$$\vdots$$
$$x_{D-1} = r \sin\theta_1 \cos\theta_2$$
$$x_D = r \cos\theta_1,$$

with $0 \leq \theta_i \leq \pi$, $i = 1, ..., D-2$, $0 \leq \theta_{D-1} \leq 2\pi$ for $D \geq 2$ and such that $\sum_{i=1}^{D} x_i^2 = r^2$. In this framework, the gradient operator ∇_D reads

$$\nabla_D = \frac{\partial}{\partial r}\hat{r} + \frac{1}{r}\sum_{i=1}^{D-1}\frac{1}{\prod_{k=1}^{i-1}\sin\theta_k}\frac{\partial}{\partial\theta_i}\hat{\theta}_i, \tag{2.3}$$

so the Laplacian operator yields

$$\nabla_D^2 = \frac{1}{r^{D-1}} \frac{\partial}{\partial r} r^{D-1} \frac{\partial}{\partial r} - \frac{\Lambda^2}{r^2}, \tag{2.4}$$

with Λ being the generalized angular momentum in D dimensions, that depends on the $D-1$ hyperangular coordinates Ω_{D-1} [51, 52]. Λ^2 then reads

$$\Lambda^2 = -\sum_{i=1}^{D-1} \frac{(\sin\theta_i)^{i-D+1}}{\prod_{k=1}^{i-1} \sin\theta_k^2} \frac{\partial}{\partial\theta_i} \left[(\sin\theta_i)^{D-1-i} \frac{\partial}{\partial\theta_i} \right],$$

and satisfies the eigenvalue equation

$$\Lambda^2 \mathcal{Y}_{\{\nu\}}(\Omega_{D-1}) = l(l+D-2)\mathcal{Y}_{\{\nu\}}(\Omega_{D-1}). \tag{2.5}$$

Here, $\mathcal{Y}_{\{\nu\}}(\Omega_{D-1})$ stand for the hyperspherical harmonics [51], that depend on the $D-1$ quantum numbers $\{\nu\} \equiv (l \equiv \nu_1, \nu_2, \ldots, \nu_{D-1})$ corresponding to the respective hyperangular coordinates. These numbers can take integer values accomplishing the constraints $l = 0, 1, \ldots$ and $l \equiv \nu_1 \geq \nu_2 \geq \cdots \geq \nu_{D-2} \geq |\nu_{D-1}| \geq 0$. Using the so-called partial harmonics $Y_{\nu_i, \nu_{i+1}}^{(i)}(\theta_i)$, that are solutions to

$$-\frac{1}{(\sin\theta_i)^{D-1-i}} \frac{\partial}{\partial\theta_i} \left[(\sin\theta_i)^{D-1-i} \frac{\partial}{\partial\theta_i} Y_{\nu_i, \nu_{i+1}}^{(i)}(\theta_i) \right] \tag{2.6}$$

$$= \left[\nu_i \left(\nu_i + D - i - 1 \right) - \frac{\nu_{i+1} \left(\nu_{i+1} + D - i - 2 \right)}{\sin^2\theta_i} \right] Y_{\nu_i, \nu_{i+1}}^{(i)}(\theta_i),$$

for $i = 1, \ldots, D-2$, the hyperspherical harmonics can be written as

$$\mathcal{Y}_{\{\nu\}}(\Omega_{D-1}) = \frac{e^{im\theta_{D-1}}}{\sqrt{2\pi}} \prod_{k=1}^{D-2} Y_{\nu_k, \nu_{k+1}}^{(k)}(\theta_k). \tag{2.7}$$

One can easily see, taking into account the normalization of these partial harmonics

$$\int_0^\pi \left[Y_{\nu_i, \nu_{i+1}}^{(i)}(\theta_i) \right]^2 (\sin\theta_i)^{D-i-1} d\theta_i = 1, \tag{2.8}$$

that the corresponding orthonormality relation for the hyperspherical harmonics reads

$$\int_{\Omega_{D-1}} d\Omega_{D-1} \mathcal{Y}_{\{\nu\}}(\Omega_{D-1}) \mathcal{Y}_{\{\nu'\}}(\Omega_{D-1}) = \delta_{\{\nu\}\{\nu'\}}, \tag{2.9}$$

where the integral is over the generalized solid angle Ω_{D-1} with volume element

$$d\Omega_{D-1} = \left(\prod_{i=1}^{D-2} (\sin\theta_i)^{D-1-i} d\theta_i \right) d\theta_{D-1}. \tag{2.10}$$

Coming back to our initial problem of solving the Schrödinger equation (2.2) and substituting the multidimensional Laplacian operator (2.4) into it, one has

$$\left[-\frac{1}{2\mu} \left(\frac{\partial^2}{\partial r^2} + \frac{D-1}{r} \frac{\partial}{\partial r} - \frac{\Lambda^2}{r^2} \right) + V_D(r) \right] \Psi(\mathbf{r}) = E\Psi(\mathbf{r}).$$

This equation can be simplified by means of the Ansatz

$$\Psi_{E,\{\nu\}}(\mathbf{r}) = R_{E,l}(r)\mathcal{Y}_{\{\nu\}}(\Omega_{D-1}).$$

Thus, taking into account the eigenvalue equation (2.5), the radial part $R_{E,l}(r)$ satisfies the radial Schrödinger equation

$$\left[-\frac{1}{2\mu} \left(\frac{\partial^2}{\partial r^2} + \frac{D-1}{r} \frac{\partial}{\partial r} - \frac{l(l+D-2)}{r^2} \right) + V_D(r) \right] R_{E,l}(r) = ER_{E,l}(r). \tag{2.11}$$

So far, the only assumption we have made is that the potential is central, i.e., it only depends on the radial coordinate. Let us now focus on the Coulomb potential.

2.1.2. Electron distribution in position space

Substituting the Coulomb central potential in equation (2.11), i.e., $V_D(r) = -\frac{Z}{r}$ with Z being the atomic number of the atom, it yields

$$\left[-\frac{1}{2\mu} \left(\frac{\partial^2}{\partial r^2} + \frac{D-1}{r} \frac{\partial}{\partial r} - \frac{l(l+D-2)}{r^2} \right) - \frac{Z}{r} \right] R_{E,l}(r) = E R_{E,l}(r). \tag{2.12}$$

Given the structure of the equation, it is convenient to introduce the reduced radial functions $u_{E,l}(r) = r^{\frac{D-1}{2}} R_{E,l}(r)$ in order to eliminate the first derivative, obtaining

$$\left[\frac{\partial^2}{\partial r^2} - \frac{L(L+1)}{r^2} + \frac{2\mu Z}{r} \right] u_{E,L}(r) = -2\mu E u_{E,L}(r), \tag{2.13}$$

where we have used the notation for the grand orbital quantum number

$$L = l + \frac{D-3}{2}.$$

With the introduction of this generalized quantum number L, the resulting equation reads exactly like the 3D hydrogenic atom with L taking the place of the orbital quantum number (note that, in fact, $L(D = 3) = l$). Thus, we proceed in a similar way to the one used to solve the standard hydrogen atom, starting by making the following changes of variable and notation

$$E = -\frac{Z^2 \mu}{2\eta^2} \qquad \rho = \frac{2\mu Z}{\eta} r,$$

so that the equation (2.13) reads

$$\left[\frac{\partial^2}{\partial \rho^2} - \frac{L(L+1)}{\rho^2} + \frac{\eta}{\rho} - \frac{1}{4} \right] u_{\eta,L}(\rho) = 0. \tag{2.14}$$

We consider now the asymptotic behavior of the equation. The solution when $\rho \to 0$ yields $u_{\eta,L}(\rho) \sim \rho^{L+1}$ and when $\rho \to \infty$, $u_{\eta,L}(\rho) \sim e^{-\rho/2}$. With this, one finds that the solutions $\{E, R(r)\}$ to the eigenvalue problem (2.12) are

$$E_\eta = -\frac{Z^2 \mu}{2\eta^2} \qquad R_{\eta,L} = \mathcal{N}_{\eta,L} \sqrt{\frac{\omega_{2L+1}}{\rho^{D-2}}} L_{\eta-L-1}^{(2L+1)}(\rho), \tag{2.15}$$

where $\omega_\alpha(\rho) = \rho^\alpha e^{-\rho}$ stands for the weight function with respect to which the Laguerre polynomials $L_n^{(\alpha)}(\rho)$ are orthogonal, i.e.,

$$\int_0^\infty L_n^{(\alpha)}(\rho) L_m^{(\alpha)}(\rho) \omega_\alpha(\rho) = \frac{\Gamma(n+\alpha+1)}{n!} \delta_{nm}. \tag{2.16}$$

Moreover, η is related to the principal hyperquantum number n and the dimension as

$$\eta = n + \frac{D-3}{2},$$

and $\mathcal{N}_{\eta,L}$ is the normalization constant. The latter is found imposing the normalization condition

$$\int_0^\infty |R_{\eta,L}(r)|^2 r^{D-1} dr = 1,$$

and its expression is given by

$$\mathcal{N}_{\eta,L} = \left(\frac{2\mu Z}{\eta} \right)^{D/2} \left(\frac{(\eta-L-1)!}{2\eta \left[(\eta+L)! \right]^3} \right)^{1/2}.$$

Summarizing, the eigenfunction of the D-dimensional hydrogenic atom is

$$\Psi_{\eta,L,\{\nu\}}(\mathbf{r}) = R_{\eta,L}(\rho)\mathcal{Y}_{\{\nu\}}(\Omega_{D-1}) = \mathcal{N}_{\eta,L}\sqrt{\frac{\omega_{2L+1}}{\rho^{D-2}}}L_{\eta-L-1}^{(2L+1)}(\rho)\mathcal{Y}_{\{\nu\}}(\Omega_{D-1}), \tag{2.17}$$

so that the normalized probability distribution of the system in the position space $P(\mathbf{r}) = |\Psi(\mathbf{r})|^2$ has the form

$$P(\mathbf{r}) = \mathcal{N}_{\eta,L}^2 \frac{\omega_{2L+1}(\rho)}{\rho^{D-2}}\left|L_{\eta-L-1}^{(2L+1)}(\rho)\right|^2\left|Y_{\{\nu\}}(\Omega_{D-1})\right|^2. \tag{2.18}$$

Note that for $D = 3$ we recover the well-known expression of the standard hydrogenic atom.

2.1.3. Electron distribution in momentum space

The wavefunctions in position and momentum spaces are related by means of the D-dimensional Fourier transform [51, 53], defined as

$$\psi(\mathbf{x}) = \frac{1}{(2\pi)^{D/2}}\int d\mathbf{p}\, e^{-i\mathbf{p}\cdot\mathbf{x}}\phi(\mathbf{p})$$

$$\phi(\mathbf{p}) = \frac{1}{(2\pi)^{D/2}}\int d\mathbf{x}\, e^{i\mathbf{p}\cdot\mathbf{x}}\psi(\mathbf{x}),$$

with $\mathbf{p} \equiv (p_1,\ldots,p_D)$ being the Cartesian momentum coordinates. It can be shown (see Ref. [51]) that if the wavefunction in position space is separable in radial and angular coordinates and, in particular, the angular part is described by the hyperspherical harmonics, i.e., $\psi(\mathbf{x}) = R(r)\mathcal{Y}_{\{\nu\}}(\Omega_{D-1})$, then the corresponding wavefunction in the momentum space is given by

$$\phi(\mathbf{p}) = S_l(p)\mathcal{Y}_{\{\nu\}}(\Omega_{D-1}^p).$$

In this expression, $\mathbf{p} \equiv (p,\theta_1^p,\ldots,\theta_{D-1}^p) \equiv (p,\Omega_{D-1}^p)$ are the hyperspherical coordinates in the momentum space and $l \equiv \nu_1$. The transformed radial part can be obtained from $R(r)$ as

$$S_l(p) = \frac{i^l}{p^{D/2-1}}\int_0^\infty dr\, r^{D/2}R(r)J_{D/2-l-1}(pr),$$

with $J_\alpha(z)$ being the Bessel functions.

Applying this result, one obtains that the D-dimensional hydrogen eigenfunction in momentum space $\Phi_{\eta,L,\{\nu\}}(\mathbf{p})$ has the form

$$\Phi_{\eta,L,\{\nu\}}(\mathbf{p}) = M_{\eta,L}(p)\mathcal{Y}_{\{\nu\}}(\Omega_{D-1}^p), \tag{2.19}$$

with the radial momentum eigenfunction reading

$$M_{\eta,L}(\tilde{p}) = \mathcal{K}_{\eta,L}\frac{(\eta\tilde{p})^{L-\frac{D-3}{2}}}{(1+\eta^2\tilde{p}^2)^{L+2}}C_{\eta-L-1}^{L+1}\left(\frac{1-\eta^2\tilde{p}^2}{1+\eta^2\tilde{p}^2}\right),$$

where $\tilde{p} = \frac{p}{Z\mu}$, $C_n^\lambda(z)$ are the Gegenbauer polynomials and the normalization constant $\mathcal{K}_{\eta,L}$ is

$$\mathcal{K}_{\eta,L} = \left(\frac{\eta}{Z\mu}\right)^{D/2}2^{2L+3}\left(\frac{\eta(\eta-L-1)!(L!)^2}{2\pi(\eta+L)!}\right)^{1/2}.$$

Thus, the corresponding probability distribution in momentum space $\gamma(\mathbf{p}) = \left|\Phi_{\eta,L,\{\nu\}}(\mathbf{p})\right|^2$ is expressed as

$$\gamma(\mathbf{p}) = \mathcal{K}_{\eta,L}^2\frac{(\eta\tilde{p})^{2L-D+3}}{(1+\eta^2\tilde{p}^2)^{2L+4}}\left|C_{\eta-L-1}^{L+1}\left(\frac{1-\eta^2\tilde{p}^2}{1+\eta^2\tilde{p}^2}\right)\right|^2\left|\mathcal{Y}_{\{\nu\}}(\Omega_{D-1}^p)\right|^2. \tag{2.20}$$

Here again, for D=3 this expression reduces to the corresponding momentum density of the three-dimensional hydrogenic atom [54].

2.2. The Fisher information in position space

In this section we calculate the Fisher information of a general D-dimensional hydrogenic system in position space. To do so, we apply the extension to the D-dimensional case of the translationally invariant Fisher information given in Eq. (2.1), i.e.,

$$I_r(D) = \int_{\mathbb{R}^D} \frac{[\nabla_D P(\mathbf{r})]^2}{P(\mathbf{r})} d\mathbf{r}, \qquad (2.21)$$

where the volume element in the D-dimensional space is $d\mathbf{r} = r^{D-1} dr d\Omega_{D-1}$. Taking into account the form of the hyperspherical harmonics (2.7) and its dependence with the angular coordinate θ_{D-1}, one can easily see that the probability distribution $P(\mathbf{r})$ is independent of this coordinate, i.e.,

$$P(\mathbf{r}) = \left|\Psi_{\eta,L,\{\nu\}}(r,\theta_1,\dots,\theta_{D-2},\theta_{D-1})\right|^2 = \left[\Psi_{\eta,L,\{\nu\}}(r,\theta_1,\dots,\theta_{D-2},0)\right]^2. \qquad (2.22)$$

As a consequence, the equation (2.21) can be rewritten as

$$I_r(D) = 4 \int_{\mathbb{R}^D} \left[\nabla_D \Psi_{\eta,L,\{\nu\}}(r,\theta_1,\dots,\theta_{D-2},0)\right]^2 d\mathbf{r}. \qquad (2.23)$$

We now make use of the separation of radial and angular coordinates and plug in the explicit expression of the multidimensional gradient (2.3) to obtain as a result

$$I_r(D) = I_R(D) + 4 \langle r^{-2} \rangle I_{\mathcal{Y}}(D),$$

with

$$I_R(D) = 4 \int_0^\infty \left[\frac{\partial}{\partial r} R(r)\right]^2 r^{D-1} dr \qquad (2.24)$$

$$\langle r^{-2} \rangle = \int_0^\infty r^{-2} R^2(r) r^{D-1} dr$$

$$I_{\mathcal{Y}}(D) = \sum_{i=1}^{D-2} \int_{\Omega_{D-1}} \left[\frac{1}{\prod_{k=1}^{i-1} \sin\theta_k} \frac{\partial}{\partial \theta_i} \mathcal{Y}_{\{\nu\}}(\theta_1,\dots,\theta_{D-2},0)\right]^2 d\Omega_{D-1}, \qquad (2.25)$$

where, for the sake of simplicity, we note $R(r) \equiv R_{\eta,L}(r)$. Here, we have used the orthonormalization condition (2.9) of the hyperspherical harmonics and the definition of the expectation value of a general radial function $f(r)$

$$\langle f(r) \rangle = \int_{\mathbb{R}^D} f(r) P(\mathbf{r}) d\mathbf{r} = \int_0^\infty f(r) R^2(r) r^{D-1} dr, \qquad (2.26)$$

for $f(r) = r^{-2}$. In the following two subsections, we are going to show that the radial integral $I_R(D)$ has the value

$$I_R(D) = \frac{(2Z\mu)^2}{\eta^3} \left\{\eta - \frac{2}{2L+1} \left[L(L+1) - \frac{1}{4}(D-1)(D-3)\right]\right\} \qquad (2.27)$$

and that the angular component $I_{\mathcal{Y}}(D)$ is given by

$$I_{\mathcal{Y}}(D) = L(L+1) - \frac{(D-1)(D-3)}{4} - \frac{|\nu_{D-1}|(2L+1)}{2}. \qquad (2.28)$$

Since the expectation value $\langle r^{-2} \rangle$ reads

$$\langle r^{-2} \rangle = \frac{(2Z\mu)^2}{2\eta^3} \frac{1}{2L+1}, \qquad (2.29)$$
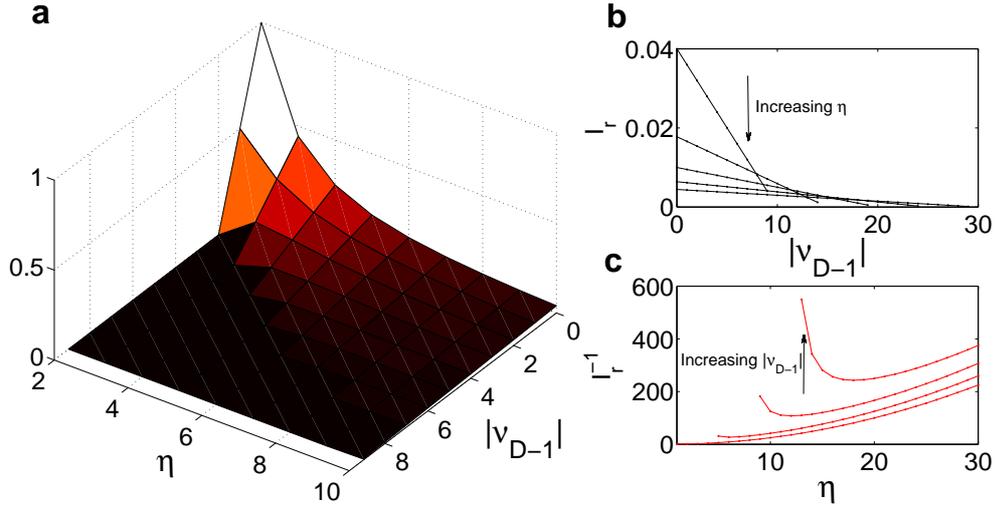
Figure 2.2.: a: Fisher information of the D-dimensional hydrogen atom ($Z = 1$) varying the grand principal and magnetic quantum numbers η and $|\nu_{D-1}|$, respectively. Note that for each value of $\eta = 2, 3, \ldots$ we consider all the possible values $|\nu_{D-1}| = 0, 1, \ldots, \eta - 1$. **b:** For several fixed values of η, there is a linear variation of the Fisher information with the absolute value of ν_{D-1}. **c:** For different $|\nu_{D-1}|$, the dependence of the inverse of Fisher information with the principal quantum number is depicted. For $\nu_{D-1} = 0$, the dependence is of the form η^2, while for $\nu_{D-1} \neq 0$ there exists a minimum (maximum of the Fisher information) for a value of $\eta \neq 1$.

one finds the following simple expression for the Fisher information of the D-dimensional hydrogenic system in the configuration space:

$$I_r(D) = \frac{(2Z\mu)^2}{\eta^3} \left(\eta - |\nu_{D-1}| \right), \tag{2.30}$$

valid for $D \geq 2$. Remark that it depends only of the grand principal quantum number η and the grand magnetic quantum number ν_{D-1}. It is observed that the Fisher information, as the ionization energy, behaves as η^{-2} with respect to the generalized principal quantum number η when $\nu_{D-1} = 0$. For values of $|\nu_{D-1}|$ different from 0, the dependence with the quantum number η is more complicated. The Fisher information decreases proportionally with the absolute value of ν_{D-1}, which corresponds to the magnetic quantum number m in the three-dimensional case. All these features can be observed in Fig. 2.2.

2.2.1. Radial contribution

Here, we shall show that the radial integral $I_R(D)$ (2.24) has actually the analytical value of Eq. (2.27) in terms of the corresponding quantum numbers. Noting $\frac{\partial}{\partial r} R(r) \equiv R'(r)$, the integration by parts leads us to the expression

$$I_R(D) = 4 \int_0^\infty r^{D-1} \left[R'(r) \right]^2 dr = -4(D-1) \int_0^\infty r^{D-2} R(r) R'(r) dr - 4 \int_0^\infty r^{D-1} R(r) R''(r) dr.$$

We make use now of the radial Schrödinger equation (2.12) that, in terms of the derivatives of $R(r)$, can be rewritten as

$$R''(r) = a_1(r) R'(r) + a_2(r) R(r),$$

with

$$a_1(r) = \frac{1 - D}{r} \tag{2.31}$$

$$a_2(r) = \frac{l(l + D - 2)}{r^2} - \frac{2Z\mu}{r} - 2E\mu. \tag{2.32}$$

Thus, denoting $R \equiv R(r)$ and $a_{1,2} \equiv a_{1,2}(r)$, the radial Fisher information yields

$$
\begin{aligned}
I_R(D) &= -4(D-1)\int_0^\infty r^{D-2}RR'dr - 4\int_0^\infty r^{D-1}R\left[a_1R' + a_2R\right]dr \\
&= -4\int_0^\infty r^{D-1}\left[(D-1) + a_1\right]RR'dr - 4\int_0^\infty r^{D-1}a_2R^2dr,
\end{aligned}
$$

and the integration by parts in the first term and the use of the expectation value of a radial function given by Eq. (2.26) leads to

$$
\begin{aligned}
I_R(D) &= \int_0^\infty \left[\frac{2(D-1)(D-2)}{r^2} + (D-1)\frac{a_1}{r} + 2a_1' - 4a_2\right]R^2r^{D-1}dr \\
&= 2(D-1)(D-2)\left\langle r^{-2}\right\rangle + 2(D-1)\left\langle \frac{a_1}{r}\right\rangle + 2\left\langle a_1'\right\rangle - 4\left\langle a_2\right\rangle.
\end{aligned}
$$

The explicit expression of a_1 and a_2, given by Eqs. (2.31) and (2.32), respectively, allows us to calculate the desired expectation values in terms of the known ones of the form $\langle r^\alpha \rangle$ as

$$
\begin{aligned}
\left\langle \frac{a_1}{r}\right\rangle &= (1-D)\left\langle r^{-2}\right\rangle \\
\left\langle a_1'\right\rangle &= (D-1)\left\langle r^{-2}\right\rangle \\
\left\langle a_2\right\rangle &= l(l+D-2)\left\langle r^{-2}\right\rangle - (2Z\mu)\left\langle r^{-1}\right\rangle - 2E\mu.
\end{aligned}
$$

Inserting these values into the radial integral $I_R(D)$, we obtain

$$
I_R(D) = 4Z\mu\left\langle r^{-1}\right\rangle - 4l(l+D-2)\left\langle r^{-2}\right\rangle,
$$

where, to eliminate the energy E we have made use of the Virial theorem

$$
E = -\frac{Z}{2}\left\langle r^{-1}\right\rangle.
$$

Thus, since $\left\langle r^{-1}\right\rangle = \frac{Z\mu}{\eta^2}$ and $\left\langle r^{-2}\right\rangle$ has the value given in (2.29), it is straightforward to obtain the expected expression (2.27) for the radial part of the D-dimensional position Fisher information of a hydrogenic system.

2.2.2. Angular contribution

Let us now compute the angular integral $I_{\mathcal{Y}}(D)$ defined by Eq. (2.25). To do that, according to Eq. (2.7) we express the involved hyperspherical harmonics in terms of the partial harmonics as

$$
\mathcal{Y}_{\{\nu\}}(\theta_1,\ldots,\theta_{D-2},0) = \frac{1}{\sqrt{2\pi}}\prod_{k=1}^{D-2}Y_{\nu_k,\nu_{k+1}}^{(k)}(\theta_k).
$$

Introducing this and the definition of the solid angle element (2.10) in the Eq. (2.25), we integrate the θ_{D-1} angle and obtain, after some algebraic manipulation, that the integral $I_{\mathcal{Y}}(D)$ can be decomposed into three types of integrals, i.e.,

$$
\begin{aligned}
I_{\mathcal{Y}}(D) &= \sum_{i=1}^{D-2}\int_0^\pi \left[\frac{\partial}{\partial\theta_i}Y_{\nu_i,\nu_{i+1}}^{(i)}(\theta_i)\right]^2(\sin\theta_i)^{D-i-1}d\theta_i \\
&\quad \times \prod_{j<i}\int_0^\pi \left[Y_{\nu_j,\nu_{j+1}}^{(j)}(\theta_j)\right]^2(\sin\theta_j)^{D-j-3}d\theta_j \\
&\quad \times \prod_{k>i}\int_0^\pi \left[Y_{\nu_k,\nu_{k+1}}^{(k)}(\theta_k)\right]^2(\sin\theta_k)^{D-k-1}d\theta_k.
\end{aligned}
$$

Let us go through each of these terms one by one. The last set of integrals are exactly one due to the normalization of the partial harmonics given in (2.8). The first integral can be solved by integrating by parts, yielding

$$
\int_0^\pi \left[\frac{\partial}{\partial \theta_i} Y_{\nu_i,\nu_{i+1}}^{(i)}(\theta_i) \right]^2 (\sin\theta_i)^{D-i-1} d\theta_i = -\int_0^\pi \frac{\partial}{\partial \theta_i} \left[(\sin\theta_i)^{D-i-1} \frac{\partial}{\partial \theta_i} Y_{\nu_i,\nu_{i+1}}^{(i)}(\theta_i) \right] Y_{\nu_i,\nu_{i+1}}^{(i)}(\theta_i) d\theta_i
$$

$$
= \nu_i(\nu_i + D - i - 1) - \nu_{i+1}(\nu_{i+1} + D - i - 2) \int_0^\pi (\sin\theta_i)^{D-i-3} \left[Y_{\nu_i,\nu_{i+1}}^{(i)}(\theta_i) \right]^2 d\theta_i,
$$

where we have used the differential equation (2.6) for which the partial harmonics are solutions. Thus, to calculate the result of the angular part of the Fisher information $I_{\mathcal{Y}}(D)$ we only have to evaluate the integral

$$
\int_0^\pi \left[Y_{\nu_j,\nu_{j+1}}^{(j)}(\theta_j) \right]^2 (\sin\theta_j)^{D-j-3} d\theta_j = \frac{2\nu_j + D - j - 1}{2\nu_{j+1} + D - j - 2}. \tag{2.33}
$$

This task is performed by writing the partial harmonics in terms of the associated Legendre functions $P_n^m(z)$ [55] and using the expression

$$
\int_{-1}^1 \frac{1}{1-z^2} \left[P_n^m(z) \right]^2 dz = \frac{(n+m)!}{m(n-m)!}. \tag{2.34}
$$

The final result yields

$$
\begin{aligned}
I_{\mathcal{Y}}(D) &= \sum_{i=1}^{D-2} \left(\nu_i(\nu_i + D - i - 1) - \frac{\nu_{i+1}(\nu_{i+1} + D - i - 2)(2\nu_i + D - i - 1)}{2\nu_{i+1} + D - i - 2} \right) \prod_{j<i} \frac{2\nu_j + D - j - 1}{2\nu_{j+1} + D - j - 2} \\
&= (2\nu_1 + D - 2) \sum_{i=1}^{D-2} \left(\frac{\nu_i(\nu_i + D - i - 1)}{2\nu_i + D - i - 1} - \frac{\nu_{i+1}(\nu_{i+1} + D - i - 2)}{2\nu_{i+1} + D - i - 2} \right) \\
&= \nu_1(\nu_1 + D - 2) - \frac{(2\nu_1 + D - 2)|\nu_{D-1}|}{2},
\end{aligned}
$$

that can be expressed as (2.28) substituting $\nu_1 \equiv l = L - (D-3)/2$.

2.3. The Fisher information in momentum space

Here we calculate the Fisher information of the D-dimensional hydrogenic system in momentum space in a parallel way to the position space described in the previous section. This measure is defined as

$$
I_p(D) = \int_{\mathbb{R}^D} \frac{\left[\nabla_D \gamma(\mathbf{p}) \right]^2}{\gamma(\mathbf{p})} d\mathbf{p}, \tag{2.35}
$$

where $\gamma(\mathbf{p}) = \left| \Phi_{\eta,L,\{\nu\}}(\mathbf{p}) \right|^2$ and $d\mathbf{p} = p^{D-1} dp d\Omega_{D-1}^p$ are the hydrogenic probability distribution given in (2.20) and volume element of the D-dimensional momentum space, respectively. Here, the gradient operator has the same formal expression as the one given in (2.3) but changing $\mathbf{r}$ by $\mathbf{p}$. Since the angular dependence is again given by the hyperspherical harmonics, once more the probability distribution is independent of the coordinate θ_{D-1}^p, i.e.,

$$
\gamma(\mathbf{p}) = \left| \Phi_{\eta,L,\{\nu\}}(p, \theta_1^p, \ldots, \theta_{D-1}^p) \right|^2 = \left[\Phi_{\eta,L,\{\nu\}}(p, \theta_1^p, \ldots, \theta_{D-2}^p, 0) \right]^2,
$$

so that one can rewrite the Fisher Information in momentum space as

$$
I_p(D) = 4 \int_{\mathbb{R}^D} \left[\nabla_D \Phi_{\eta,L,\{\nu\}}(p, \theta_1, \ldots, \theta_{D-2}, 0) \right]^2 d\mathbf{p}.
$$
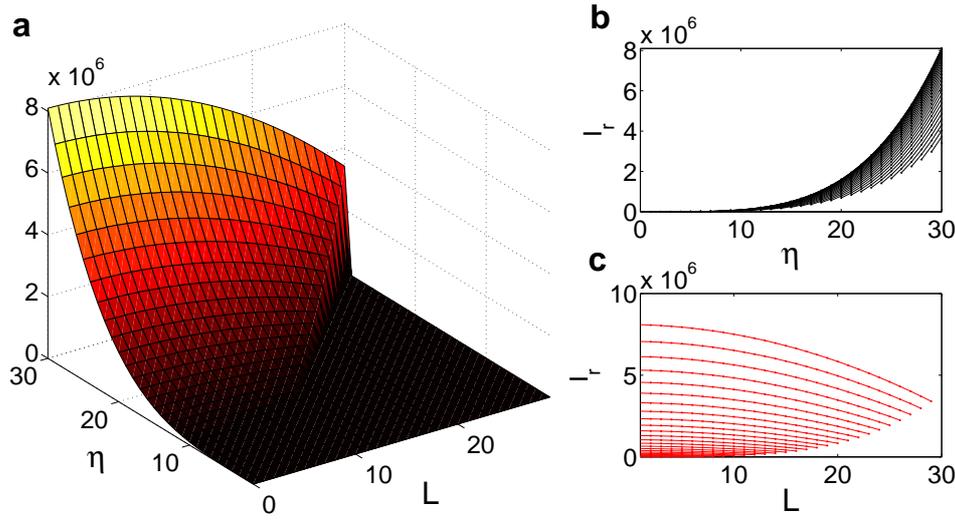
Figure 2.3.: a: Fisher information in momentum space of the D-dimensional hydrogen atom ($Z = 1$) varying the grand principal and orbital quantum numbers η and L, respectively, for $\nu_{D-1} = 0$. Note that, for each value of η, we have $L = 0, \ldots, \eta - 1$. **b:** For different values of L and $\nu_{D-1} = 0$, variation of the Fisher information with η. **c:** Again for $\nu_{D-1} = 0$, the dependence of the Fisher information in momentum space with the generalized orbital quantum number for fixed values of η.

Exploiting the separation of variables exposed in equation (2.19) allows us to write

$$I_p(D) = 4J_P(D) + 4 \left\langle p^{-2} \right\rangle I_{\mathcal{Y}}(D).$$

where we denote

$$J_P(D) = \int_0^\infty \left[\frac{\partial}{\partial p} M(p) \right]^2 p^{D-1} dp, \tag{2.36}$$

whose solution will be found in the next section, and where the expectation value $\left\langle p^{-2} \right\rangle$ has the well-known expression

$$\left\langle p^{-2} \right\rangle = \int_0^\infty p^{-2} M^2(p) p^{D-1} dp = \left(\frac{\eta}{Z\mu} \right)^2 \frac{8\eta - 3(2L+1)}{2L+1}, \tag{2.37}$$

where we have used the notation $M(p) \equiv M_{\eta,L}(p)$. The angular integral $I_{\mathcal{Y}}(D)$ has been shown to be reproduced by (2.28) in the previous section. Gathering together the radial integral $J_P(D)$, the expectation value $\left\langle p^{-2} \right\rangle$ and the angular integral $I_{\mathcal{Y}}(D)$, one finally obtains the following expression for the Fisher information of a D-dimensional hydrogenic system in momentum space:

$$I_p(D) = 2 \left(\frac{\eta}{Z\mu} \right)^2 \left[5\eta^2 - 3L(L+1) - |\nu_{D-1}|(8\eta - 3(2L+1)) + 1 \right], \tag{2.38}$$

valid for $D \geq 2$. In the Fig. 2.3, the case of the hydrogen ($Z = 1$) is represented. From (2.38) one can easily see that the Fisher information in momentum space has again a linear dependence with the absolute value of grand magnetic quantum number $|\nu_{D-1}|$. Thus, we take the case $\nu_{D-1} = 0$ in Fig. 2.3 and study the more complicated dependence on the quantum numbers η and L. It is evident that the Fisher information in momentum space decreases as L increases, increasing on the other hand with the generalized principal quantum number. Thus, opposite to the case of position space, the extreme value of this measure is not obtained for the ground state of the atom (minimum possible value of η), but for the highly excited states with low orbital quantum numbers.

2.3.1. Radial contribution

Let us now evaluate the radial integral $J_P(D)$ given by Eq. (2.36). Here we shall prove that this integral has the value

$$J_P(D) = \left(\frac{\eta}{Z\mu}\right)^2 \left[\frac{(2L - D + 3)(2L + D - 1)(6L - 8\eta + 3)}{2L + 1} + 2\left(1 + 5\eta^2 - 3L(L + 1)\right)\right]. \qquad (2.39)$$

To do so, we start by making the change of variable $x = \frac{\eta}{Z\mu}p$ so that

$$J_P(D) = \left(\frac{Z\mu}{\eta}\right)^{D-2} \int_0^\infty \left[\frac{\partial}{\partial x}M(x)\right]^2 x^{D-1}dx,$$

with

$$M_{\eta,L}(x) = \mathcal{K}_{\eta,L}\frac{x^{L-\frac{D-3}{2}}}{(1 + x^2)^{L+2}}C_{\eta-L-1}^{L+1}\left(\frac{1 - x^2}{1 + x^2}\right).$$

A further change of variable $x \to y$: $y = \frac{x^2-1}{x^2+1}$, so that $dx = (1 + y)^{-1/2}(1 - y)^{-3/2}dy$, allows us to write

$$J_P(D) = \left(\frac{Z\mu}{\eta}\right)^{D-2} \int_{-1}^{+1} \left[\frac{\partial}{\partial y}M(y)\right]^2 (1 + y)^{D/2}(1 - y)^{-D/2+2}dy,$$

with

$$M_{\eta,L}(y) = \frac{\mathcal{K}_{\eta,L}(-1)^{\eta-L-1}}{2^{L+2}}(1 + y)^{\frac{L}{2}-\frac{D-3}{4}}(1 - y)^{\frac{L}{2}+\frac{D+5}{4}}C_{\eta-L-1}^{L+1}(y),$$

where the parity of the Gegenbauer polynomials $C_m^\lambda(-y) = (-1)^m C_m^\lambda(y)$ has been used. With the notation $\omega_\lambda(y) = (1 - y^2)^{\lambda-1/2}$ for the weight function of the Gegenbauer polynomials $C_m^\lambda(y)$ and after some algebraic manipulation, $J_P(D)$ can be decomposed into six non-zero integrals,

$$J_P(D) = \left(\frac{Z\mu}{\eta}\right)^{D-2} \frac{\mathcal{K}_{\eta,L}^2}{2^{2L+4}} \left[J_{P_1} + J_{P_2} + J_{P_3} + J_{P_4} + J_{P_5} + J_{P_6}\right].$$

The explicit expression of these J_{P_i} one has to evaluate is

$$\begin{aligned}
J_{P_1} &= (2L - D + 3)^2 \int_{-1}^1 \omega_{L+1}(y)\left[C_{\eta-L-1}^{L+1}(y)\right]^2 (1 + y)^{-1}dy \\
J_{P_2} &= \left[\frac{(D + 1)^2}{4} - (2L - D + 3)^2\right] \int_{-1}^1 \omega_{L+1}(y)\left[C_{\eta-L-1}^{L+1}(y)\right]^2 dy \\
J_{P_3} &= \left[L(D - 3L - 11) + 2D - 10\right] \int_{-1}^1 \omega_{L+1}(y)\left[C_{\eta-L-1}^{L+1}(y)\right]^2 y^2 dy \\
J_{P_4} &= 4(L + 1)^2 \int_{-1}^1 \omega_{L+2}(y)\left[C_{\eta-L-2}^{L+2}(y)\right]^2 (1 + 3y^2)dy \\
J_{P_5} &= -8(2L - D + 3)(L + 1) \int_{-1}^1 \omega_{L+1}(y)C_{\eta-L-1}^{L+1}(y)C_{\eta-L-2}^{L+2}(y)ydy \\
J_{P_6} &= 2(6L - D + 11)(L + 1) \int_{-1}^1 \omega_{L+2}(y)C_{\eta-L-1}^{L+1}(y)C_{\eta-L-2}^{L+2}(y)ydy,
\end{aligned}$$

and their values are

$$
\begin{aligned}
J_{P_1} &= \mathcal{A}_{\eta,L}\frac{2\eta(2L-D+3)^2}{2L+1} \\
J_{P_2} &= \mathcal{A}_{\eta,L}\left[\frac{(D+1)^2}{4}-(2L-D+3)^2\right] \\
J_{P_3} &= \mathcal{A}_{\eta,L}\left[L(D-3L-11)+2D-10\right]\frac{\eta^2-1-L(L+1)}{2(\eta^2-1)} \\
J_{P_4} &= \mathcal{A}_{\eta,L}\left[\eta^2-(L+1)^2\right]\left[1+\frac{3}{2}\frac{\eta^2-3-L(L+3)}{\eta^2-1}\right] \\
J_{P_5} &= -\mathcal{A}_{\eta,L}4(2L-D+3)(\eta-L-1) \\
J_{P_6} &= \mathcal{A}_{\eta,L}(6L-D+11)(L+1)\frac{\eta^2-(L+1)^2}{2(\eta^2-1)},
\end{aligned}
$$

with

$$
\mathcal{A}_{\eta,L}=\frac{\pi(\eta+L)!}{2^{2L+1}\eta(\eta-L-1)!(L!)^2}.
$$

All the integrals appearing have be calculated by making intensive use of the recurrence and orthogonality relations verified by the Gegenbauer polynomials, i.e.,

$$
yC_n^\lambda(y)=C_{n+1}^\lambda(y)-\frac{2\lambda+n-1}{2\lambda-2}C_{n+1}^{\lambda-1}(y),
$$

$$
2(\lambda+n)yC_n^\lambda(y)=(n+1)C_{n+1}^\lambda(y)+(2\lambda+n-1)C_{n-1}^\lambda(y)
$$

and

$$
\int_{-1}^1\omega_\lambda(y)C_m^\lambda(y)C_n^\lambda(y)dy=\frac{\pi2^{1-2\lambda}\Gamma(n+2\lambda)}{n!(n+\lambda)\Gamma(\lambda)^2}\delta_{mn},
$$

respectively. Note that, in particular for the first integral J_{P_1}, the expression of the Gegenbauer polynomials in terms of the associated Legendre functions [55] and the relation (2.34) are needed. It can be seen that, eventually, the result (2.39) is obtained.

2.4. Alternative method and application to the case D=3

In another work [56], an alternative way of finding the position and momentum Fisher information in terms of the radial expectation values $\langle r^k\rangle$ and $\langle p^k\rangle$, with $k=-2,2$ has been proposed. Moreover, an uncertainty Fisher information relation is obtained for multidimensional single-particle systems with general central potentials. We outline here the alternative derivation of the expressions (2.30) and (2.38) for the Fisher informations and we apply them to the real ($D=3$) hydrogenic atoms.

Let us start with the position space. The momentum expectation value $\langle p^2\rangle=\langle\nabla_D^2\rangle$ is given by

$$
\langle p^2\rangle=\int_{\mathbb{R}^D}\left|\nabla_D\Psi_{\eta,L,\{\nu\}}(r,\theta_1,\dots,\theta_{D-1})\right|^2d\mathbf{r}. \tag{2.40}
$$

On the other hand, as we stated in Section 2.2, given that in a central potential the angular part of the wavefunction is described by the hyperspherical harmonics (2.7), and due to the dependence of these functions with the angular coordinate θ_{D-1}, the probability distribution in position space can be written as in Equation (2.22). As a consequence, the Fisher information can be expressed as (2.23). According to the form of the multidimensional gradient (2.3), the expectation value (2.40) can be decomposed as

$$
\langle p^2\rangle=\int_{\mathbb{R}^D}\left|\nabla_D\Psi_{\eta,L,\{\nu\}}(r,\theta_1,\dots,\theta_{D-2},0)\right|^2d\mathbf{r}+K(D),
$$

with

$$
\begin{aligned}
K(D) &= \int_{\mathbb{R}^D} \left| \frac{1}{r} \prod_{k=1}^{D-2} (\sin\theta_k)^{-1} \frac{\partial}{\partial\theta_{D-1}} \Psi_{\eta,L,\{\nu\}}(r,\theta_1,\ldots\theta_{D-1}) \right|^2 d\mathbf{r} \\
&= \left\langle r^{-2} \right\rangle \prod_{k=1}^{D-2} \int_0^\pi \left| Y_{\nu_k,\nu_{k+1}}^{(k)}(\theta_k) \right|^2 (\sin\theta_k)^{D-k-3} d\theta_k \frac{1}{2\pi} \int_0^{2\pi} \left| \frac{\partial}{\partial\theta_{D-1}} e^{i\nu_{D-1}\theta_{D-1}} \right|^2 d\theta_{D-1} \\
&= \left\langle r^{-2} \right\rangle \frac{|\nu_{D-1}|}{2}(2L+1),
\end{aligned}
$$

where the radial expectation value definition (2.26) and the integral (2.33) have been used. As a result, the Fisher information can be expressed as

$$
I_r(D) = 4\left\langle p^2 \right\rangle - 2K(D).
$$

The combination of these results leads to the following relation between the Fisher information and the radial expectation values $\left\langle r^{-2} \right\rangle$ and $\left\langle p^2 \right\rangle$,

$$
I_r(D) = 4\left\langle p^2 \right\rangle - 2|\nu_{D-1}|(2L+1)\left\langle r^{-2} \right\rangle. \tag{2.41}
$$

The application of the same procedure in momentum space allows to obtain that

$$
I_p(D) = 4\left\langle r^2 \right\rangle - 2|\nu_{D-1}|(2L+1)\left\langle p^{-2} \right\rangle. \tag{2.42}
$$

When applied to the hydrogenic case, these expressions give the same results as the ones obtained in the previous sections by direct integration.

Finally, it is worth noting that these results, when $D = 3$ is taken, coincide with the values obtained by other means [57, 58], i.e.,

$$
\begin{aligned}
I_r(D = 3) &= \frac{4Z^2\mu^2}{n^3}(n - |m|) \\
I_p(D = 3) &= \frac{2n^2}{Z^2\mu^2}\left[5n^2 + 1 - 3l(l+1) - |m|(8n - 6l - 3)\right].
\end{aligned}
$$

One observes that the Fisher information of the hydrogenic system in position space does not depend on the orbital quantum number l (as in the momentum space case), but only on the principal and magnetic quantum numbers n and m, respectively.

2.5. Summary and conclusions

The translationally invariant Fisher information, which is an information-theoretic measure of the localization of the quantum-mechanical distribution density all over the space, has been determined in a closed and compact form for D-dimensional hydrogenic systems. This has been done for both position and momentum spaces, and the corresponding expressions have been found to depend on the dimension parameter D, the nuclear charge Z and the D quantum numbers which fully describe the physical state under consideration.

Most of the results presented in this chapter are published in Refs. [57, 59].

3. Parameter-based Fisher Information of orthogonal polynomials

In 2005, J.S. Dehesa and J. Sánchez-Ruiz [31] exactly derived the locality Fisher information of a large class of probability distributions, the Rakhmanov densities, defined by

$$\rho_n(x) = \frac{1}{d_n^2} p_n^2(x)\omega(x)\chi_{[a,b]}(x),$$

where $\chi_{[a,b]}(x)$ is the characteristic function for the interval $[a,b]$, and $\{p_n(x)\}$ denotes a sequence of real polynomials orthogonal with respect to the nonnegative definite weight function $\omega(x)$ on the interval $[a,b] \subseteq \mathbb{R}$, that is,

$$\int_a^b p_n(x)p_m(x)\omega(x)dx = d_n^2\delta_{n,m} \tag{3.1}$$

with $\deg p_n(x) = n$. As first pointed out by E.A. Rakhmanov [60] (see also [61]), these distributions play a fundamental role in the analytic theory of orthogonal polynomials. In particular, it has been shown that they govern the asymptotic behavior of the ratio $p_{n+1}(x)/p_n(x)$ as $n \to \infty$. On the other hand, the Rakhmanov densities of the classical orthogonal polynomials of a real continuous variable describe the quantum-mechanical probability distributions of ground and excited states of numerous physical systems with an exactly solvable Schrödinger equation, particularly the most common prototypes (harmonic oscillator, hydrogen atom,...), in position and momentum spaces. These two fundamental and applied reasons have motivated an increasing interest for the determination of the spreading of the classical orthogonal polynomials $\{p_n(x)\}$ throughout its interval of orthogonality by means of the information-theoretic measures of their corresponding Rakhmanov densities $\rho_n(x)$ [16, 29, 31, 32, 57, 59, 62, 63].

The Shannon entropy of these densities has already been examined numerically [32]. On the theoretical side, let us point out that its asymptotics ($n \to \infty$) is well known for all classical orthogonal polynomials, but its exact value for every fixed n is only known for Chebyshev polynomials [19] and some Gegenbauer polynomials [30]. To this respect, see Ref. [29], which reviews the knowledge up to 2001. The variance and Fisher information of the Rakhmanov densities have also been found in a closed and compact form for all classical orthogonal polynomials [16, 31]. For other functionals of these Rakhmanov densities, see Ref. [28].

In this chapter we shall calculate the Fisher information of the real and continuous classical orthogonal polynomials (Gegenbauer, Grosjean, Jacobi and Laguerre) with respect to the parameter(s) of the polynomials. We start collecting some basic properties of these classical orthogonal polynomials which will be used later on. Then, the Fisher information with respect to a parameter is fully determined for Jacobi and Laguerre polynomials first, and then for Gegenbauer and Grosjean polynomials. Finally, conclusions and some open problems are given.

3.1. Some properties of the parameter-dependent classical orthogonal polynomials

Let $\{\tilde{y}_n(x;\theta)\}_{n\in\mathbb{N}_0}$ stand for the sequence of polynomials orthonormal with respect to the nonnegative definite weight function $\omega(x;\theta)$ on the real support (a,b), so that

$$\int_a^b \tilde{y}_n(x;\theta)\tilde{y}_m(x;\theta)\omega(x;\theta)dx = \delta_{nm}, \tag{3.2}$$

with $\deg \tilde{y}_n = n$. Here, in particular, we shall consider the classical families of Laguerre $L_n^{(\alpha)}(x)$, $\alpha > -1$, and Jacobi $J_n^{(\alpha,\beta)}(x)$, $\alpha,\beta > -1$, polynomials. The normalized-to-unity density functions $\tilde{\rho}_n(x;\theta)$, defined as

$$\tilde{\rho}_n(x;\theta) = \tilde{y}_n^2(x;\theta)\omega(x;\theta) \tag{3.3}$$

are called Rakhmanov densities [60, 61]. Here, we gather various properties of the parameter-dependent classical orthogonal polynomials in a real and continuous variable (i.e., Laguerre and Jacobi) in the form of two lemmas, which shall be used later on.

The weight function of these polynomials can be always written as

$$\omega(x;\theta) = h(x)\left[t(x)\right]^\theta.$$

In particular,

$$\omega_L(x;\alpha) = e^{-x}x^\alpha \quad \Longrightarrow \quad h_L(x) = e^{-x} \quad \text{and} \quad t_L(x) = x$$

for the Laguerre polynomials, $L_n^{(\alpha)}(x)$, and

$$\omega_J(x;\alpha) = (1-x)^\alpha(1+x)^\beta \quad \Longrightarrow \quad h_J(x) = (1+x)^\beta \quad \text{and} \quad t_J(x) = 1-x$$

for the Jacobi, $P_n^{(\alpha,\beta)}(x)$. Note that in this definition we consider the parameter of interest to be the first one, i.e., α. When considering the second one, we take

$$\omega_J(x;\beta) = (1-x)^\alpha(1+x)^\beta \quad \Longrightarrow \quad h_J(x) = (1-x)^\alpha \quad \text{and} \quad t_J(x) = 1+x.$$

Lemma 3.1.1 *The derivative of the orthonormal polynomial $\tilde{y}_n(x;\theta)$ with respect to the parameter θ is given by*

$$\frac{\partial}{\partial\theta}\tilde{y}_n(x;\theta) = \sum_{k=0}^n \tilde{A}_k(\theta)\tilde{y}_k(x;\theta) \tag{3.4}$$

with

$$\tilde{A}_k(\theta) = \frac{d_k(\theta)}{d_n(\theta)}A_k(\theta) \quad \text{for} \quad k = 0,1,\ldots,n-1 \tag{3.5}$$

$$\tilde{A}_n(\theta) = A_n(\theta) - \frac{1}{d_n(\theta)}\frac{\partial}{\partial\theta}d_n(\theta), \tag{3.6}$$

where $d_m^2(\theta)$ denotes, according to Eq. (3.1), the normalization constant of the orthogonal polynomial $p_m(x) = y_m(x;\theta)$, and $A_k(\theta)$ with $k = 0,1,\ldots,m$ are the expansion coefficients of the derivative of $y_m(x;\theta)$ in terms of the system $\{y_m(x;\theta)\}$, i.e.,

$$\frac{\partial}{\partial\theta}y_m(x;\theta) = \sum_{k=0}^m A_k(\theta)y_k(x;\theta). \tag{3.7}$$

Both quantities $d_n(\theta)$ and $A_k(\theta)$ are known in the literature for the Laguerre and Jacobi cases. Indeed, the norms for the Laguerre $L_n^{(\alpha)}(x)$ and the Jacobi $P_n^{(\alpha,\beta)}(x)$ polynomials [64] are

$$\left[d_n^{(L)}(\alpha)\right]^2 = \frac{\Gamma(n+\alpha+1)}{n!}, \tag{3.8}$$

$$\left[d_n^{(J)}(\alpha,\beta)\right]^2 = \frac{2^{\alpha+\beta+1}\Gamma(n+\alpha+1)\Gamma(n+\beta+1)}{n!(2n+\alpha+\beta+1)\Gamma(n+\alpha+\beta+1)}, \tag{3.9}$$

respectively. On the other hand, the expansion coefficients in Eq. (3.7) are known to have the form [65, 66, 67]

$$A_k^{(L)} = \frac{1}{n-k} \quad \text{for} \quad k = 0, 1, \ldots, n-1 \quad \text{and} \quad A_n^{(L)} = 0 \tag{3.10}$$

for the Laguerre polynomials $L_n^{(\alpha)}(x)$ and

$$A_k^{(J_\alpha)} = \frac{\alpha+\beta+1+2k}{(n-k)(\alpha+\beta+1+n+k)}\frac{(\beta+k+1)_{n-k}}{(\alpha+\beta+k+1)_{n-k}}; \quad k = 0, 1, \ldots, n-1, \tag{3.11}$$

$$A_n^{(J_\alpha)} = \sum_{k=0}^{n-1}\frac{1}{\alpha+\beta+1+n+k} = \psi(1+\alpha+\beta+2n) - \psi(1+\alpha+\beta+n) \tag{3.12}$$

for the Jacobi expansion of $\frac{\partial}{\partial\alpha}P_n^{(\alpha,\beta)}(x)$, and

$$A_k^{(J_\beta)} = (-1)^{n-k}\frac{\alpha+\beta+1+2k}{(n-k)(\alpha+\beta+1+n+k)}\frac{(\alpha+k+1)_{n-k}}{(\alpha+\beta+k+1)_{n-k}}; \quad k = 0, 1, \ldots, n-1, \tag{3.13}$$

$$A_n^{(J_\beta)} = \sum_{k=0}^{n-1}\frac{1}{\alpha+\beta+1+n+k} = \psi(1+\alpha+\beta+2n) - \psi(1+\alpha+\beta+n) \tag{3.14}$$

for $\frac{\partial}{\partial\beta}P_n^{(\alpha,\beta)}(x)$. The symbol $\psi(x) = \frac{\Gamma'(x)}{\Gamma(x)}$ denotes here the well-known digamma function.

Using Eqs. (3.8) and (3.10) in Lemma 3.1.1 allows us to derive the following expression for the expansion coefficients $\tilde{A}_k(\alpha)$ for the orthonormal Laguerre polynomials $\tilde{L}_n^{(\alpha)}(x)$

$$\tilde{A}_k^{(L)} = \frac{1}{n-k}\left[\frac{(k+1)_{n-k}}{(k+\alpha+1)_{n-k}}\right]^{1/2}; \quad k = 0, 1, \ldots, n-1 \tag{3.15}$$

$$\tilde{A}_n^{(L)} = -\frac{\psi(n+\alpha+1)}{2}. \tag{3.16}$$

In a similar way, this Lemma, together with the specific values for the Jacobi polynomials (3.9) and (3.12)-(3.14), has allowed us to find the expressions

$$\tilde{A}_k^{(J_\alpha)} = \left[\frac{(k+\beta+1)_{n-k}(k+1)_{n-k}}{(k+\alpha+1)_{n-k}(k+\alpha+\beta+1)_{n-k}}\frac{2n+\alpha+\beta+1}{2k+\alpha+\beta+1}\right]^{1/2} \tag{3.17}$$

$$\times\frac{2k+\alpha+\beta+1}{(n-k)(n+k+\alpha+\beta+1)}; \quad k = 0, 1, \ldots, n-1$$

$$\tilde{A}_n^{(J_\alpha)} = \frac{1}{2}\Big[2\psi(2n+\alpha+\beta+1) - \psi(n+\alpha+\beta+1) - \psi(n+\alpha+1)$$

$$- \ln 2 + \frac{1}{2n+\alpha+\beta+1}\Big] \tag{3.18}$$

and

$$\tilde{A}_k^{(J_\beta)} = \left[\frac{(k+\alpha+1)_{n-k}(k+1)_{n-k}}{(k+\beta+1)_{n-k}(k+\alpha+\beta+1)_{n-k}} \frac{2n+\alpha+\beta+1}{2k+\alpha+\beta+1} \right]^{1/2} \tag{3.19}$$

$$\times (-1)^{n-k} \frac{2k+\alpha+\beta+1}{(n-k)(n+k+\alpha+\beta+1)}; \qquad k=0,1,\dots,n-1$$

$$\tilde{A}_n^{(J_\beta)} = \frac{1}{2} \left[2\psi(2n+\alpha+\beta+1) - \psi(n+\alpha+\beta+1) - \psi(n+\beta+1) \right.$$

$$\left. - \ln 2 + \frac{1}{2n+\alpha+\beta+1} \right] \tag{3.20}$$

for the expansion coefficients of the derivative of the Jacobi polynomials $P_n^{(\alpha,\beta)}(x)$ with respect to the parameters α and β, respectively.

Lemma 3.1.2 *The parameter-dependent classical orthonormal polynomials $\tilde{y}_n(x;\theta)$ satisfy*

(a) $\displaystyle \int_a^b \frac{\partial \omega(x;\theta)}{\partial \theta} [\tilde{y}_n(x;\theta)]^2 \, dx = -2\tilde{A}_n(\theta)$

(b) $\displaystyle \int_a^b \frac{\partial \omega(x;\theta)}{\partial \theta} \tilde{y}_n(x;\theta)\tilde{y}_k(x;\theta) dx = -\tilde{A}_k(\theta) \quad k=0,1,\dots,n-1$

(c) $\displaystyle \int_a^b \frac{\partial^2 \omega(x;\theta)}{\partial \theta^2} [\tilde{y}_n(x;\theta)]^2 \, dx = 2\sum_{k=0}^n (\tilde{A}_k(\theta))^2 + 2(\tilde{A}_n(\theta))^2 - 2\frac{\partial \tilde{A}_n(\theta)}{\partial \theta}.$

To prove the integrals (a) and (b) we have to derive with respect to the parameter θ the orthonormalization condition (3.2) for $m=n$ and $m=k\neq n$, respectively. Then, one has to use the Lemma 3.1.1 and again Eq. (3.2), and the results follow. The integral (c) is obtained by deriving the integral (a) with respect to θ and taking into account the values of the two previous, i.e., (a) and (b).

3.2. Parameter-based Fisher information of Jacobi and Laguerre polynomials

The distribution of the orthonormal polynomials $\tilde{y}_n(x;\theta)$ on their orthonormality interval and the spreading of the associated Rakhmanov densities can be most appropriately estimated by means of their information-theoretic measures, the Shannon entropy [39] and the Fisher information [33]. The former has been theoretically [29, 62] and numerically [32] examined for general orthogonal polynomials. In the latter case, the Fisher information associated with translations of the variable (i.e., the locality Fisher information) has been analyzed both analytically [31] and numerically [63]. Here we extend this study by means of the computation of a more general concept, the parameter-based Fisher information of the polynomials $\tilde{y}_n(x;\theta)$. This quantity is defined as the Fisher information of the associated Rakhmanov density (3.3) with respect to the parameter θ, i.e., according to Eq. (1.1) and after some manipulation,

$$I_n(\theta) = 4 \int_a^b \left\{ \frac{\partial}{\partial \theta} [\tilde{\rho}_n(x;\theta)]^{1/2} \right\}^2 dx. \tag{3.21}$$

Theorem 3.2.1 *The parameter-based Fisher information $I_n(\theta)$ of the parameter-dependent classical orthonormal polynomials $\tilde{y}_n(x;\theta)$ (i.e., Jacobi and Laguerre) defined by Eq. (3.21) has the value*

$$I_n(\theta) = 2\sum_{k=0}^{n-1} \left[\tilde{A}_k(\theta) \right]^2 - 2\frac{\partial \tilde{A}_n(\theta)}{\partial \theta}, \tag{3.22}$$

where $\tilde{A}_k(\theta)$, $k = 0, 1, \ldots, n$ are the expansion coefficients of the derivative with respect to θ of $\tilde{y}_n(x;\theta)$ in terms of the polynomials $\{\tilde{y}_k(x;\theta)\}_{k=0}^n$, which are given by Lemma 3.1.1. See Eqs. (3.15)-(3.16) and (3.17)-(3.20) for the Laguerre and Jacobi families, respectively.

Remark Let us underline that the Fisher information with respect to a parameter in the cases of orthogonal, monic orthogonal and orthonormal polynomials has the same value. This is because of the definition of the Rakhmanov densities (3.3) and their probabilistic character.

Proof To prove this theorem we start taking the derivative with respect to θ of $[\tilde{\rho}_n(x;\theta)]^{1/2}$ and using Lemma 3.1.1 to obtain

$$\frac{\partial}{\partial \theta} [\tilde{\rho}_n(x;\theta)]^{1/2} = [\omega(x;\theta)]^{1/2} \sum_{k=0}^n \tilde{A}_k(\theta)\tilde{y}_k(x;\theta) + \frac{\partial [\omega(x;\theta)]^{1/2}}{\partial \theta} \tilde{y}_n(x;\theta).$$

Introducing this expression into Eq. (3.21) leads to

$$I_n(\theta) = J_1 + J_2 + J_3,$$

where

$$J_1 = 4 \int_a^b \omega(x;\theta) \left(\sum_{k=0}^n \tilde{A}_k(\theta)\tilde{y}_k(x;\theta) \right)^2 dx,$$

$$J_2 = 4 \int_a^b \left(\frac{\partial [\omega(x;\theta)]^{1/2}}{\partial \theta} \right)^2 [\tilde{y}_n(x;\theta)]^2 dx,$$

and

$$J_3 = 8 \sum_{k=0}^n \tilde{A}_k(\theta) \int_a^b [\omega(x;\theta)]^{1/2} \frac{\partial [\omega(x;\theta)]^{1/2}}{\partial \theta} \tilde{y}_n(x;\theta)\tilde{y}_k(x;\theta) dx.$$

Now we take into account that the weight function of the parameter-dependent families of classical orthonormal polynomials in a real and continuous variable (i.e., Laguerre and Jacobi) has the form $\omega(x;\theta) = h(x) [t(x)]^\theta$, so that

$$\left\{ \frac{\partial [\omega(x;\theta)]^{1/2}}{\partial \theta} \right\}^2 = \frac{1}{4}\omega(x;\theta) [\ln t(x)]^2 = \frac{1}{4} \frac{\partial^2 \omega(x;\theta)}{\partial \theta^2},$$

and

$$[\omega(x;\theta)]^{1/2} \frac{\partial [\omega(x;\theta)]^{1/2}}{\partial \theta} = \frac{1}{2}\omega(x;\theta) \ln t(x) = \frac{1}{2} \frac{\partial \omega(x;\theta)}{\partial \theta}.$$

The use of these two expressions in the integrals J_2 and J_3 together with Lemma 3.1.2 and the consideration of the orthonormalization condition (3.2) in J_1 yield

$$J_1 = 4 \sum_{k=0}^n \left[\tilde{A}_k(\theta) \right]^2,$$

$$J_2 = 2 \sum_{k=0}^n \left[\tilde{A}_k(\theta) \right]^2 + 2 \left[\tilde{A}_n(\theta) \right]^2 - 2\frac{\partial \tilde{A}_n(\theta)}{\partial \theta},$$

and

$$J_3 = -4 \sum_{k=0}^n \left[\tilde{A}_k(\theta) \right]^2 - 4 \left[\tilde{A}_n(\theta) \right]^2,$$

so that they lead to Eq. (3.22). ∎

Corollary 3.2.1.1 *The Fisher information with respect to the parameter* α, $I_n^{(L)}(\alpha)$, *of the Laguerre polynomial* $\tilde{L}_n^{(\alpha)}(x)$ *is given by*

$$
\begin{aligned}
I_n^{(L)}(\alpha) &= 2\sum_{k=0}^{n-1}\left[\tilde{A}_k^{(L)}\right]^2 - 2\frac{\partial \tilde{A}_n^{(L)}}{\partial \alpha} \\
&= \psi^{(1)}(n+\alpha+1) + \frac{2n}{n+\alpha}\,{}_4F_3\left(\begin{array}{cccc|c} 1 & 1 & 1 & 1-n & \\ & & & & 1 \\ 2 & 2 & 1-\alpha-n & & \end{array}\right),
\end{aligned}
\tag{3.23}
$$

where $\psi^{(1)}(x) = \frac{d}{dx}\psi(x)$ *is the trigamma function.*

Corollary 3.2.1.2 *The Fisher information with respect to the parameter* α, $I_n^{(J_\alpha)}(\alpha,\beta)$, *of the Jacobi polynomial* $\tilde{P}_n^{(\alpha,\beta)}(x)$ *is given by*

$$
\begin{aligned}
I_n^{(J_\alpha)}(\alpha,\beta) &= 2\sum_{k=0}^{n-1}\left[\tilde{A}_k^{(J_\alpha)}\right]^2 - 2\frac{\partial \tilde{A}_n^{(J_\alpha)}}{\partial \alpha} \\
&= 2\frac{\Gamma(n+\beta+1)n!(2n+\alpha+\beta+1)}{\Gamma(n+\alpha+1)\Gamma(n+\alpha+\beta+1)} \\
&\quad \times \sum_{k=0}^{n-1}\frac{\Gamma(k+\alpha+1)\Gamma(k+\alpha+\beta+1)(2k+\alpha+\beta+1)}{\Gamma(k+\beta+1)k!(n-k)^2(n+k+\alpha+\beta+1)^2} \\
&\quad -2\psi^{(1)}(2n+\alpha+\beta+1) + \psi^{(1)}(n+\alpha+\beta+1) \\
&\quad +\psi^{(1)}(n+\alpha+1) + \frac{1}{(2n+\alpha+\beta+1)^2},
\end{aligned}
\tag{3.24}
$$

and the Fisher information with respect to the parameter β, $I_n^{(J_\beta)}(\alpha,\beta)$, *of the Jacobi polynomial* $\tilde{P}_n^{(\alpha,\beta)}(x)$ *is given by*

$$
\begin{aligned}
I_n^{(J_\beta)}(\alpha,\beta) &= 2\sum_{k=0}^{n-1}\left[\tilde{A}_k^{(J_\beta)}\right]^2 - 2\frac{\partial \tilde{A}_n^{(J_\beta)}}{\partial \beta} \\
&= 2\frac{\Gamma(n+\alpha+1)n!(2n+\alpha+\beta+1)}{\Gamma(n+\beta+1)\Gamma(n+\alpha+\beta+1)} \\
&\quad \times \sum_{k=0}^{n-1}\frac{\Gamma(k+\beta+1)\Gamma(k+\alpha+\beta+1)(2k+\alpha+\beta+1)}{\Gamma(k+\alpha+1)k!(n-k)^2(n+k+\alpha+\beta+1)^2} \\
&\quad -2\psi^{(1)}(2n+\alpha+\beta+1) + \psi^{(1)}(n+\alpha+\beta+1) \\
&\quad +\psi^{(1)}(n+\beta+1) + \frac{1}{(2n+\alpha+\beta+1)^2}.
\end{aligned}
\tag{3.25}
$$

Both corollaries follow from Theorem 3.2.1 in a straightforward manner by taking into account the expressions (3.15)-(3.20) for the expansion coefficients $\tilde{A}_k$ of the corresponding families.

3.3. Parameter-based Fisher information of the Gegenbauer and Grosjean polynomials

In this section we describe the Fisher information of two important subfamilies of the Jacobi polynomials $P_n^{(\alpha,\beta)}(x)$: the ultraspherical or Gegenbauer polynomials [29, 64, 68], which have $\alpha = \beta = \lambda - 1/2$, and the Grosjean polynomials of the first and second kind [69, 70, 71], which have $\alpha + \beta = \pm 1$, respectively. Let us remark that the parameter-based Fisher information for

these subfamilies cannot be obtained from the expressions of the similar quantity for the Jacobi polynomials (given by corollary 3.2.1.2) by means of a mere substitution of the parameters, because it depends on the derivative with respect to the parameter(s) and now α and β are correlated.

The Gegenbauer polynomials $C_n^{(\lambda)}(x)$ are Jacobi-like polynomials satisfying the orthogonality condition (3.1) with the weight function

$$\omega_C(x;\lambda) = (1 - x^2)^{\lambda - \frac{1}{2}} \quad \text{for} \quad \lambda > -\frac{1}{2},$$

and the normalization constant

$$\left[d_n^{(C)}(\lambda) \right]^2 = \frac{\pi 2^{1-2\lambda} \Gamma(n + 2\lambda)}{n!(n + \lambda)\Gamma^2(\lambda)}$$

so that they can be expressed as

$$C_n^{(\lambda)}(x) = \frac{(2\lambda)_n}{(\lambda + \frac{1}{2})_n} P_n^{(\lambda - \frac{1}{2}, \lambda - \frac{1}{2})}(x).$$

It is known [66] that the expansion (3.7) for the derivative of $C_n^{(\lambda)}(x)$ with respect to the parameter λ has the coefficients

$$A_k^{(C)}(\lambda) = \frac{2\left(1 + (-1)^{n-k}\right)(k + \lambda)}{(k + n + 2\lambda)(n - k)} \quad \text{for} \quad k = 0, 1, \ldots, n - 1$$

$$A_n^{(C)}(\lambda) = \sum_{k=0}^{n-1} \frac{2(k + 1)}{(2k + 2\lambda + 1)(k + 2\lambda)} + \frac{2}{k + n + 2\lambda} = \psi(n + \lambda) - \psi(\lambda).$$

Then, according to Lemma 3.1.1, the expansion (3.4) for the derivative of the orthonormal Gegenbauer polynomials has the following coefficients

$$\tilde{A}_k^{(C)}(\lambda) = \left[\frac{\Gamma(k + 2\lambda)n!(n + \lambda)}{\Gamma(n + 2\lambda)k!(k + \lambda)} \right]^{1/2} \frac{2\left(1 + (-1)^{n-k}\right)(k + \lambda)}{(k + n + 2\lambda)(n - k)} \quad \text{for} \quad k = 0, 1, \ldots, n - 1$$

$$\tilde{A}_n^{(C)}(\lambda) = \psi(n + \lambda) - \psi(n + 2\lambda) + \ln 2 + \frac{1}{2(n + \lambda)}.$$

Theorem 3.2.1 provides, according to Eq. (3.22), the following value for the Fisher information of the Gegenbauer polynomials $C_n^{(\lambda)}(x)$ with respect to the parameter λ:

$$I_n^{(C)}(\lambda) = \frac{16n!(n + \lambda)}{\Gamma(n + 2\lambda)} \sum_{k=0}^{n-1} \frac{\left(1 + (-1)^{n-k}\right)\Gamma(k + 2\lambda)(k + \lambda)}{k!(k + n + 2\lambda)^2(n - k)^2}$$

$$-2\psi^{(1)}(n + \lambda) + 4\psi^{(1)}(n + 2\lambda) + \frac{1}{(n + \lambda)^2}.$$

Let us now perform the same task for the Grosjean polynomials of the first and second kind, which are the monic Jacobi polynomials $\hat{P}_n^{(\alpha,\beta)}(x)$ with $\alpha + \beta = -1, +1$, respectively. Hence, we have [69, 70]

$$G_n^{(\alpha)}(x) = c_n P_n^{(\alpha,-1-\alpha)}(x) \qquad -1 < \alpha < 0,$$

and

$$g_n^{(\alpha)}(x) = e_n P_n^{(\alpha,1-\alpha)}(x) \qquad -1 < \alpha < 2,$$

for the Grosjean polynomials of first and second kind, respectively, with the values

$$c_n = 2^n \binom{2n - 1}{n}^{-1} \quad \text{and} \quad e_n = 2^n \binom{2n + 1}{n}^{-1}.$$

The Grosjean polynomials of the first kind $G_n^{(\alpha)}(x)$ satisfy the orthogonality condition (3.1) with respect to the weight function

$$\omega_G(x;\alpha) = \left(\frac{1-x}{1+x}\right)^\alpha \frac{1}{1+x},$$

and with normalization constant

$$\left[d_n^{(G)}(\alpha)\right]^2 = \frac{2^{2n-1}\Gamma^2(n)}{\Gamma^2(2n)}\Gamma(n+\alpha+1)\Gamma(n-\alpha).$$

These polynomials, together with the Chebyshev of the first, second, third and fourth kind, are the only Jacobi polynomials for which the associated ones are again Jacobi polynomials [69]. The expansion (3.7) for the derivative of $G_n^{(\alpha)}(x)$ with respect to the parameter α can be obtained as

$$\frac{\partial G_n^{(\alpha)}(x)}{\partial \alpha} = \frac{\partial \hat{P}_n^{(\alpha,-1-\alpha)}(x)}{\partial \alpha} = \frac{\partial \hat{P}_n^{(\alpha,\beta)}(x)}{\partial \alpha}\bigg|_{\beta=-1-\alpha} - \frac{\partial \hat{P}_n^{(\alpha,\beta)}(x)}{\partial \beta}\bigg|_{\beta=-1-\alpha} = \sum_{k=0}^{n-1} A_k^{(G)}(\alpha)G_n^{(\alpha)}(x)$$

with

$$A_k^{(G)}(\alpha) = \frac{2^{n-k+1}k}{n^2-k^2}\frac{\Gamma(2k)\Gamma(n+1)}{\Gamma(2n)\Gamma(k+1)}\left[(k-\alpha)_{n-k}-(-1)^{n-k}(k+\alpha+1)_{n-k}\right]$$

for $k = 0, 1, \ldots, n-1$ and $A_n^{(G)}(\alpha) = 0$. Then, Lemma 3.1.1 provides the expansion (3.4) for the derivative of the orthonormal Grosjean polynomials with the coefficients

$$\tilde{A}_k^{(G)}(\alpha) = \frac{2n}{n^2-k^2}\frac{(k-\alpha)_{n-k}-(-1)^{n-k}(k+\alpha+1)_{n-k}}{\left[(k+\alpha+1)_{n-k}(k-\alpha)_{n-k}\right]^{1/2}} \quad \text{for} \quad k = 0, 1, \ldots, n-1,$$

$$\tilde{A}_n^{(G)}(\alpha) = \frac{1}{2}\left[\psi(n-\alpha)-\psi(n+\alpha+1)\right].$$

Finally, Eq. (3.22) of Theorem 3.2.1 allows us to find the following value for the Fisher information of the Grosjean polynomials of the first kind:

$$I_n^{(G)}(\alpha) = 8n^2 \sum_{k=0}^{n-1} \frac{1}{(n^2-k^2)^2}\frac{\left[(k-\alpha)_{n-k}-(-1)^{n-k}(k+\alpha+1)_{n-k}\right]^2}{(k+\alpha+1)_{n-k}(k-\alpha)_{n-k}}$$
$$+\psi^{(1)}(n-\alpha)+\psi^{(1)}(n+\alpha+1).$$

On the other hand, the Grosjean polynomials of the second kind $g_n^{(\alpha)}(x)$ satisfy the orthogonality property (3.1) with respect to the weight function

$$\omega_g(x;\alpha) = \left(\frac{1-x}{1+x}\right)^\alpha (1+x),$$

and the normalization constant

$$\left[d_n^{(g)}(\alpha)\right]^2 = \frac{2^{2n+1}\Gamma^2(n)}{\Gamma^2(2n+2)}\Gamma(n+\alpha+1)\Gamma(n-\alpha+2).$$

Moreover, the derivative of these polynomials with respect to the parameter α can be again expanded in the form (3.4) as

$$\frac{\partial g_n^{(\alpha)}(x)}{\partial \alpha} = \frac{\partial \hat{P}_n^{(\alpha,1-\alpha)}(x)}{\partial \alpha} = \frac{\partial \hat{P}_n^{(\alpha,\beta)}(x)}{\partial \alpha}\bigg|_{\beta=1-\alpha} - \frac{\partial \hat{P}_n^{(\alpha,\beta)}(x)}{\partial \beta}\bigg|_{\beta=1-\alpha} = \sum_{k=0}^{n-1} A_k^{(g)}(\alpha)g_n^{(\alpha)}(x),$$

with

$$A_k^{(g)}(\alpha) = \frac{2^{n-k+1}(k+1)}{(n-k)(n+k+2)} \frac{\Gamma(2k+2)\Gamma(n+1)}{\Gamma(2n+2)\Gamma(k+1)} \left[(k+2-\alpha)_{n-k} - (-1)^{n-k}(k+\alpha+1)_{n-k} \right]$$

for $k = 0, 1, \ldots, n-1$ and $A_n^{(g)}(\alpha) = 0$. Then, Lemma 3.1.1 is able to provide the analogous expansion (3.4) for the orthonormal polynomials with the coefficients

$$\tilde{A}_k^{(g)}(\alpha) = \frac{2(k+1)}{(n-k)(n+k+2)} \frac{(k+2-\alpha)_{n-k} - (-1)^{n-k}(k+\alpha+1)_{n-k}}{\left[(k+\alpha+1)_{n-k}(k+2-\alpha)_{n-k} \right]^{1/2}};$$
$$\text{for} \quad k = 0, 1, \ldots, n-1,$$
$$\tilde{A}_n^{(g)}(\alpha) = \frac{1}{2} \left[\psi(n+2-\alpha) - \psi(n+\alpha+1) \right].$$

Finally, we obtain by means of Eq. (3.22) of Theorem 3.2.1 the Fisher information of the Grosjean polynomials of the second kind, which turns out to have the value

$$I_n^{(g)}(\alpha) = 8 \sum_{k=0}^{n-1} \frac{(k+1)^2}{(n-k)^2(n+k+2)^2} \frac{\left[(k+2-\alpha)_{n-k} - (-1)^{n-k}(k+\alpha+1)_{n-k} \right]^2}{(k+\alpha+1)_{n-k}(k+2-\alpha)_{n-k}}$$
$$+ \psi^{(1)}(n+2-\alpha) + \psi^{(1)}(n+\alpha+1).$$

3.4. Summary and conclusions

In summary, we have calculated the parameter-based Fisher information for the classical orthogonal polynomials of a continuous and real variable with a parameter dependence; namely, the Jacobi and Laguerre polynomials. Then we have evaluated the corresponding Fisher information for the two most relevant parameter-dependent Jacobi polynomials $P_n^{(\alpha,\beta)}(x)$: the Gegenbauer ($\alpha = \beta = \lambda - 1/2$) and the Grosjean ($\alpha + \beta = \pm 1$) families.

As we already pointed out, the Fisher information is a measure of the error when estimating the considered parameter. In practice, this can be understood as follows: Let us consider a probability distribution (here the Rakhmanov density) with two different but close values of the parameter. If those distributions are very similar the error associated to a measure of this parameter will be very large and, as a consequence of the Cramer-Rao inequality (1.2), the value of the Fisher information will be small. Thus, we can consider the Fisher information in this sense to be a measure of the distinguishability of a probability distribution with respect to the neighboring ones when varying a given parameter. This can also be seen from the relation between the Fisher information and the so-called Kullback-Leibler divergence (1.5). This relative entropy between two distributions, that was given in Eq. (1.6), measures the difference in information when using a distribution $q(y)$ different from the reference one $p(y)$.

This outlined use of the Fisher information as a measure of distinguishability of the probability distributions can be seen, e.g., in Fig. 3.1 for the Rakhmanov densities associated to the Laguerre polynomials. The Fisher information in this case increases with the degree n and decreases with the parameter α. In Figs. 3.1b and c, two limiting cases are depicted, with large value of n and small of α and viceversa. One can see that, as expected, the distributions are in the first case qualitatively different, corresponding to a large value of the Fisher information, while in the latter case the opposite behavior is found. Quantitatively, the Kullback-Leibler divergence is found to be $D\left[\tilde{\rho}_9(x; 0.1) \| \tilde{\rho}_9(x; 1.1) \right] = 0.95$ and $D\left[\tilde{\rho}_0(x; 9.5) \| \tilde{\rho}_0(x; 10.5) \right] = 0.048$, respectively. The same features are observed in Fig. 3.2 for the Rakhmanov densities of the Gegenbauer polynomials. Here, there is again a decreasing value of the Fisher information for increasing λ, while it decreases with the degree of the polynomial n (except for small values of λ, where there is a sudden increase followed
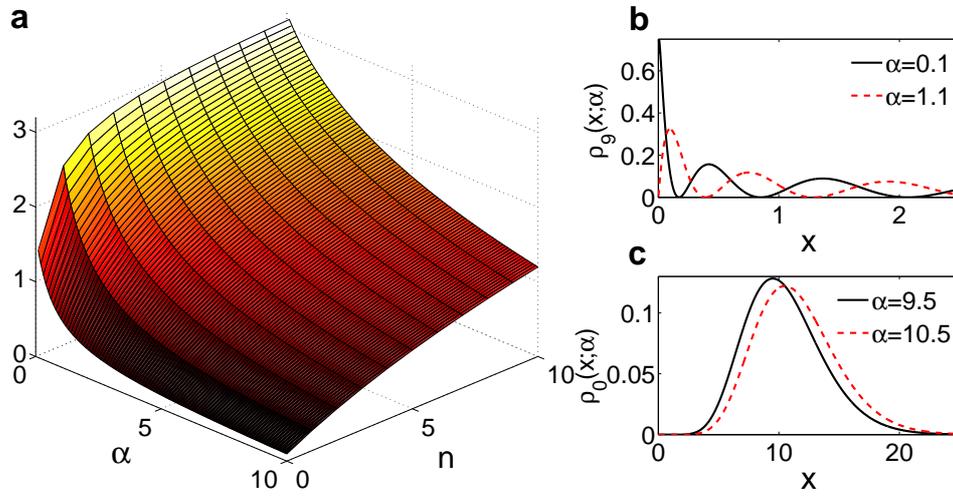
Figure 3.1.: a: Fisher information of the Rakhmanov density associated to the orthonormal Laguerre polynomials $\tilde{L}_n^{(\alpha)}(x)$; dependence with n and α. **b:** Distributions for $n = 9$ and $\alpha = 0.1, 1.1$, where the Fisher information has the largest value. One observes that the two distributions are qualitatively different. **c:** Conversely, the Fisher information has a very low value for $n = 0$ and $\alpha = 9.5, 10.5$, and the distributions can be seen to be, in fact, qualitatively similar.
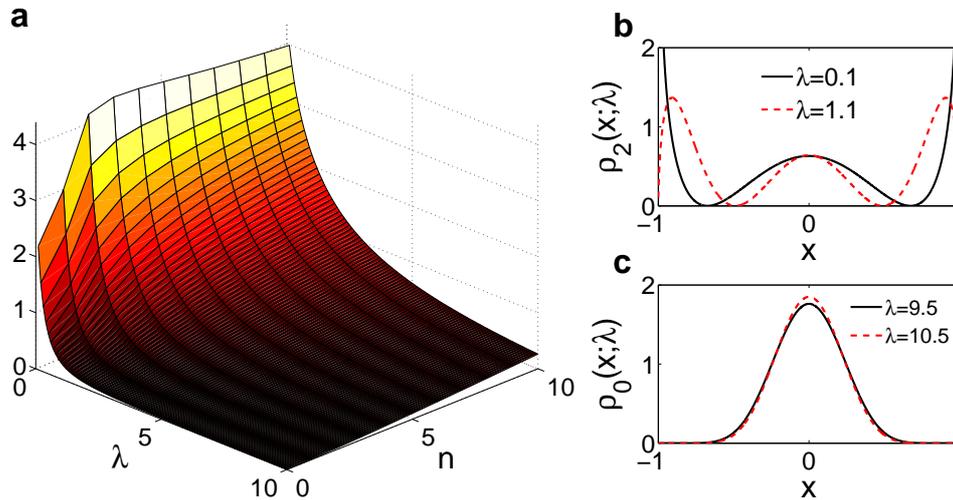
Figure 3.2.: a: Fisher information of the Rakhmanov density associated to the orthonormal Gegenbauer polynomials $\tilde{C}_n^{(\lambda)}(x)$; dependence with n and λ. **b:** Distributions for $n = 2$ and $\lambda = 0.1, 1.1$, where the Fisher information has the largest value. One observes that the two distributions are qualitatively different. **c:** Conversely, the Fisher information has a very low value for $n = 0$ and $\lambda = 9.5, 10.5$, and the distributions can be seen to be, in fact, qualitatively similar.

by a plateau of the Fisher information). Again, an evaluation of the Kullback-Leibler divergence can be done, obtaining $D\left[\tilde{\rho}_2(x;0.1)\|\tilde{\rho}_2(x;1.1)\right] = 0.85$ and $D\left[\tilde{\rho}_0(x;9.5)\|\tilde{\rho}_0(x;10.5)\right] = 0.0025$, for the distributions depicted in Figs. 3.2b and c, respectively.

This work, together with Ref. [31], opens the way for the developement of the Fisher estimation theory of the Rakhmanov density for continuous and discrete orthogonal polynomials in and beyond the Askey scheme. This fundamental task in approximation theory includes the determination of the spreading of the orthogonal polynomials throughout its orthogonality domain by means of the Fisher information with a locality property. All these mathematical questions have a straightforward application to quantum systems because their wavefunctions are often controlled by orthogonal polynomials, so that the probability densities which describe the quantum-mechanical states of these physical systems are just the Rakhmanov densities of the corresponding orthogonal polynomials. In particular, they correspond to the ground and excited states of the physical systems with an exactly solvable spherically symmetric potential [64], including the most common prototypes (harmonic oscillator and hydrogen atom), in both position and momentum spaces.

Most of the results presented in this chapter can be found published in Ref. [72].

Part II.

Collective Rydberg excitations of an atomic gas confined in a ring lattice

4. Introduction

Nowadays, the laser and evaporative cooling of atoms to temperatures below one micro-Kelvin are well-established experimental techniques, that have opened a doorway to a wide range of new experiments with ultracold atoms. In particular, the achievement in 1995 of the Bose-Einstein condensation in atomic gases of rubidium, sodium and lithium [73, 74, 75], that had been theoretically predicted more than 80 years ago, can be set as the starting point of this new development. Fermionic gases were also brought to degeneracy only a few years later [76].

Ultracold atoms provide a unique toolbox to study many-particle physics under very clean and well-defined conditions. The reasons for this are rooted in: (i) the precise control that can be achieved over the interactions in cold gases using Feshbach resonances, and (ii) the possibility of generating strong external trapping potentials for cold atoms through optical, magnetic or electric fields. These features allow to study the dynamics of phase transitions as well as the preparation of strongly correlated quantum states (see [77] for a complete overview in this topic).

While so far the majority of experiments in ultracold gases is carried out with ground state atoms, during the recent years an increasing amount of experimental and theoretical efforts have been dedicated to the study of atoms excited to Rydberg states [78]. This is due to the unique properties of these highly excited states. In particular, Rydberg atoms can interact via dipole-dipole or van-der-Waals forces with interaction strengths that can be of the order of several tens of MHz at a distance of several micrometers. As a consequence, the corresponding quantum dynamics takes place on a microsecond timescale, which is orders of magnitude faster than the atoms' external dynamics. Such scenario is usually referred to as 'frozen gas' [79, 80] and the evolution of Rydberg excitations is usually described by a spin model [81, 82], where the spin up/down state represents a Rydberg/ground state atom. Unlike in a typical solid state system, there are no significant dissipative processes which make the system assume its ground state over the typical experimental timescale. Therefore, in this kind of systems one can regard the dynamics as fully coherent [83, 84] and the time evolution of quantities like the mean number of Rydberg excitations is expected to depend crucially on the initial state.

The most intriguing manifestation of the strong interaction among Rydberg states is the blockade mechanism [85, 86], which prevents the excitation of a Rydberg atom in the vicinity of an already excited one. This effect has been thoroughly studied in the context of quantum information processing since it is a natural implementation of a state dependent interaction which is essential to devise two-qubit gates. In the context of gases, a first experimental indication of the strong Rydberg-Rydberg interaction was the non-linear behavior of the number of excited atoms as a function of increasing laser power and atomic density [87, 88]. Later, it was shown that, in the case of a dense gas, the Rydberg blockade gives rise to the formation of coherent collective excitations - so-called 'superatoms' [89, 90]. Very recently, the power of Rydberg states to establish a controlled interaction of single atoms confined in distant traps has been demonstrated in a series of impressive experiments [91, 92, 93, 94].

Strongly supported by these results, nowadays highly excited atoms are believed to have a manifold of applications ranging far beyond traditional atomic physics. On the theory side, it has been shown that the long-ranged character of the interaction can be employed to manipulate whole atomic ensembles by just a single control atom [95]. Moreover, exploiting the properties of atoms in Rydberg states permits the study of spin systems at criticality [82], the quantum simulation of complex spin models [96], the investigation of the thermalization of strongly interacting many-particle

systems [97] and also the implementation of quantum information protocols [98].

In the present work, we study the excitation properties of a Rydberg gas in a particularly structured and symmetric scenario (see Chapter 6). In our setup, ground state atoms are homogeneously distributed over a ring lattice and at most a single Rydberg atom per site can be excited via a laser. In Chapter 5, some preliminary concepts needed for the understanding of this part of the thesis are introduced, such as the atom-light interaction or the Rydberg atoms. That chapter can, hence, be skipped by the reader who is familiar with quantum optics and Rydberg physics.

In the framework of the perfect blockade regime, in Chapter 7 we study the temporal evolution of the Rydberg excitation number, the formation of correlations in the Rydberg density and the entanglement properties in lattices with up to 25 sites. We demonstrate that the dynamics of this system is divided into short and long time domains and that in the latter the system acquires a steady state. We study the origin of this steady state which occurs as result of a purely coherent dynamics of a closed system in Chapter 8. This subject is closely related to the discussion about how and why a closed system which is prepared in a pure state actually thermalizes, i.e., assumes a state in which the mean values of macroscopic observables are stationary and can be calculated from the microcanonical ensemble. These questions are of fundamental interest [99, 100] and have been investigated in a number of systems [101, 102, 103, 104, 105].

We also show (Chapter 9) that the setup mentioned above allows to create and explore collective many-particle states that are entangled and extend over the entire lattice, e.g., spin waves, on a microsecond timescale. Finding simple ways for creating entangled many-particle states is of importance, since such states have a number of applications, e.g., they serve as resource for the creation of single-photon light sources [106], for improving precision quantum measurements [107] and for measurement-based quantum information processing. We finally show that the system offers the possibility to study fermions in the presence of a disorder potential although no external atomic motion takes place.

Most of the results presented in this part can be found in the following publications:

- B. Olmos, R. González-Férez and I. Lesanovsky, "Collective Rydberg excitations of an atomic gas confined in a ring lattice", *Phys. Rev. A*, vol. 79, p. 043419, 2009.

- B. Olmos, R. González-Férez and I. Lesanovsky, "Fermionic collective excitations in a lattice gas of Rydberg atoms", *Phys. Rev. Lett.*, vol. 103, p. 185302, 2009.

- B. Olmos, M. Müller and I. Lesanovsky, "Thermalization of a strongly interacting 1D Rydberg lattice gas", *New J. Phys.*, vol. 12, p. 013024, 2010.

- B. Olmos, R. González-Férez and I. Lesanovsky, "Creating collective many-body states with highly excited atoms", *Phys. Rev. A, Accepted*, arXiv: 0812.4894, 2010.

5. Preliminary concepts

This chapter has an introductory character, since in it some preliminary concepts are presented. Throughout all this work we consider trapped atoms whose internal states (ground and excited) are coupled by laser light. Hence, the form of the interaction between a two-level atom and a laser field is derived. Then, we use the second quantization picture to obtain a Hamiltonian that describes the dynamics of this coupling in terms of creation and annihilation operators of ground and excited atoms. The excited level of the atoms that we consider here is a so-called Rydberg state. Hence, the properties of these Rydberg states are also reviewed in this chapter, paying special attention to the strong interaction between them and its consequences.

5.1. Interaction of a two-level atom and a monochromatic light field

We consider a single atom in a trap, represented by the external potential $U(\mathbf{R})$ with $\mathbf{R}$ being the center of mass coordinate. The Hamiltonian that drives the external dynamics of this system is given by the sum of the kinetic and potential energies, i.e.,

$$H_{\text{ext}} = \frac{\mathbf{P}^2}{2M} + U(\mathbf{R}),$$

where M is the mass of the atom and $\mathbf{P}$ represents its momentum. The eigenfunctions and eigenvalues of this Hamiltonian are $H_{\text{ext}}\phi_\lambda(\mathbf{R}) = \epsilon_\lambda \phi_\lambda(\mathbf{R})$, with λ denoting the mode of the trapping potential. We consider that the atom has only two internal levels $|g\rangle$ and $|r\rangle$. The energy of the state $|g\rangle$ is put to zero, so the energy of $|r\rangle$ corresponds to the gap between the two levels ω_a (in atomic units). The internal dynamics is then described by the Hamiltonian

$$H_0 = \omega_a |r\rangle \langle r|.$$

We introduce now a laser field as a plane wave with momentum $\mathbf{k}$ and frequency ω_l as

$$\mathbf{E}(\mathbf{r}, t) = E_0 \cos(\omega_l t - \mathbf{k} \cdot \mathbf{r})\hat{\varepsilon},$$

where E_0 is the amplitude of the light field and $\hat{\varepsilon}$ is the unit polarization vector. The laser is detuned $\Delta = \omega_a - \omega_l$ with respect to the transition $|g\rangle \to |r\rangle$ (see Fig. 5.1). We work here within the dipole approximation, i.e., we consider that the field does not vary over the extension of the atom. In that case, one can describe the interaction of this laser field with the atom by means of the Hamiltonian

$$H_{\text{laser}} = -\mathbf{r} \cdot \mathbf{E}(\mathbf{R}, t),$$
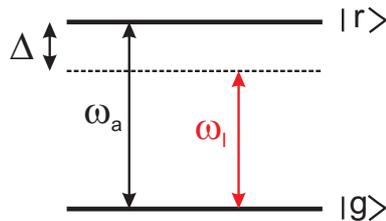
Figure 5.1.: Atom modeled as a two-level system. These states are coupled by means of a laser field with frequency ω_l in general not resonant with the energy gap ω_a, i.e., with a detuning $\Delta = \omega_a - \omega_l$.

where, as pointed out before, $\mathbf{R}$ is the external position of the center of mass of the atom and $\mathbf{r} \equiv (x, y, z)$ accounts for the relative coordinate of the electron. If we consider the laser to be linearly polarized in the direction $\hat{\varepsilon} = -\hat{z}$, then the laser Hamiltonian becomes

$$H_{\text{laser}} = E_0 z \cos(\omega_l t - \mathbf{k} \cdot \mathbf{R}).$$

The complete Hamiltonian that drives the dynamics of the two-level atom coupled to a monochromatic light field is thus given by the sum of the three terms,

$$H = H_{\text{ext}} + H_0 + H_{\text{laser}}.$$

We can rewrite this Hamiltonian as a matrix representing it in the basis composed of the two possible internal states of the atom $|g\rangle \equiv \begin{pmatrix} 0 \\ 1 \end{pmatrix}$ and $|r\rangle \equiv \begin{pmatrix} 1 \\ 0 \end{pmatrix}$ as

$$H = \begin{pmatrix} H_{\text{ext}} + \omega_a + E_0 \langle r | z | r \rangle \cos(\omega_l t - \mathbf{k} \cdot \mathbf{R}) & E_0 \langle r | z | g \rangle \cos(\omega_l t - \mathbf{k} \cdot \mathbf{R}) \\ E_0 \langle g | z | r \rangle \cos(\omega_l t - \mathbf{k} \cdot \mathbf{R}) & H_{\text{ext}} + E_0 \langle g | z | g \rangle \cos(\omega_l t - \mathbf{k} \cdot \mathbf{R}) \end{pmatrix},$$

where we have assumed H_{ext} to be independent of the internal state of the atom. The matrix elements $\langle r | z | r \rangle$ and $\langle g | z | g \rangle$ vanish since $|g\rangle$ and $|r\rangle$ are parity eigenstates and the cross terms $\langle r | z | g \rangle = \langle g | z | r \rangle$ are absorbed in the so-called Rabi frequency

$$\Omega_0 \equiv \frac{E_0}{2} \langle r | z | g \rangle, \tag{5.1}$$

so that

$$H = \begin{pmatrix} H_{\text{ext}} + \omega_a & 2\Omega_0 \cos(\omega_l t - \mathbf{k} \cdot \mathbf{R}) \\ 2\Omega_0 \cos(\omega_l t - \mathbf{k} \cdot \mathbf{R}) & H_{\text{ext}} \end{pmatrix}.$$

To eliminate the time-dependence of the Hamiltonian, we go now into a rotating frame by means of an unitary transformation

$$U = \begin{pmatrix} e^{-i\omega_l t} & 0 \\ 0 & 1 \end{pmatrix}.$$

This operation transforms the time-dependent Schrödinger equation such that

$$i\frac{\partial}{\partial t}\Psi = H\Psi \quad \rightarrow \quad i\frac{\partial}{\partial t}\tilde{\Psi} = \tilde{H}\tilde{\Psi},$$

with

$$\tilde{\Psi} = U^\dagger \Psi \qquad \tilde{H} = U^\dagger H U - i U^\dagger \frac{\partial}{\partial t} U,$$

so the Hamiltonian is transformed such that

$$\tilde{H} \approx H_{\text{ext}} + \Delta |r\rangle \langle r| + \left(\Omega_0 r e^{i\mathbf{k}\cdot\mathbf{R}} |r\rangle \langle g| + \Omega_0 r e^{-i\mathbf{k}\cdot\mathbf{R}} |g\rangle \langle r| \right) \tag{5.2}$$

where we have made the Rotating Wave Approximation (RWA) neglecting the terms oscillating with a frequency $2\omega_l$.

5.2. Second quantization

We are now interested in deriving the Hamiltonian that drives the dynamics of the atom-light interaction in terms of the creation and annihilation operators of the ground and excited-state atoms. To do so, we go to the second quantization picture, and introduce the field operators that annihilate a particle in a given internal state at $\mathbf{R}$ in the λ-th mode of the trapping potential as

$$\hat{\psi}(\mathbf{R}) = \left(\begin{array}{c} \sum_\lambda a_\lambda(1)\phi_\lambda(\mathbf{R}) \\ \sum_{\lambda'} a_{\lambda'}(2)\phi_{\lambda'}(\mathbf{R}) \end{array} \right) \equiv \left(\begin{array}{c} \hat{\psi}_1(\mathbf{R}) \\ \hat{\psi}_2(\mathbf{R}) \end{array} \right) = \hat{\psi}_1(\mathbf{R})\,|r\rangle + \hat{\psi}_2(\mathbf{R})\,|g\rangle\,.$$

The components of the field operators obey the commutation relation

$$\left[\hat{\psi}_k(\mathbf{R}), \hat{\psi}_{k'}^\dagger(\mathbf{R}')\right] = \delta_{kk'}\delta(\mathbf{R} - \mathbf{R}'),$$

given that the creation and annihilation operators satisfy the usual bosonic commutation relations

$$\left[a_\lambda(k), a_{\lambda'}^\dagger(k')\right] = \delta_{\lambda,\lambda'}\delta_{kk'}, \qquad \left[a_\lambda(k), a_{\lambda'}(k')\right] = \left[a_\lambda^\dagger(k), a_{\lambda'}^\dagger(k')\right] = 0,$$

and that the functions $\{\phi_\lambda\}$ form an orthogonal set. Here, we denote by $a_\lambda(1) \equiv r_\lambda$ and $a_\lambda(2) \equiv b_\lambda$ the annihilation operators of an atom in the excited and ground state, respectively, and $\phi_\lambda(\mathbf{R})$ are the eigenfunctions of H_{ext}. The Hamiltonian (5.2) can be rewritten in terms of these field operators as follows

$$\hat{H} = \int d\mathbf{R}\,\hat{\psi}^\dagger(\mathbf{R})\tilde{H}\hat{\psi}(\mathbf{R}) = \sum_\lambda \epsilon_\lambda \left(b_\lambda^\dagger b_\lambda + r_\lambda^\dagger r_\lambda\right) + \Delta \sum_\lambda r_\lambda^\dagger r_\lambda + \Omega_0 \sum_\lambda \left(b_\lambda^\dagger r_\lambda e^{i\mathbf{k}\cdot\mathbf{R}} + r_\lambda^\dagger b_\lambda e^{-i\mathbf{k}\cdot\mathbf{R}}\right),$$

where we have assumed that the external potential is independent of the internal state of the atom. Taking into account that we consider the atoms lying in the ground state of the trapping potential ($\lambda = 0$), and setting this ground state energy to zero ($\epsilon_0 = 0$), we obtain

$$\hat{H} = \Delta r^\dagger r + \Omega_0 \left(b^\dagger r e^{i\mathbf{k}\cdot\mathbf{R}} + r^\dagger b e^{-i\mathbf{k}\cdot\mathbf{R}}\right).$$

One can always find another unitary transformation U_2 to remove the dependence on the position of the atom such that

$$U_2^\dagger r U_2 = e^{-i\mathbf{k}\cdot\mathbf{R}}r, \qquad U_2^\dagger r^\dagger U_2 = e^{i\mathbf{k}\cdot\mathbf{R}}r^\dagger,$$

and, thus, the Hamiltonian yields

$$\hat{H} = \Delta r^\dagger r + \Omega_0 \left(b^\dagger r + r^\dagger b\right). \tag{5.3}$$

Note that the wavefunction acquires then a phase that one has to take into account in the case of more than one atom, e.g., when measuring correlations between several atoms in different positions. This Hamiltonian can be easily extended to its many-particle version, as will be done in Section 6.1.

5.3. Rydberg atom

A Rydberg atom is an atom in a state with very high principal quantum number $n \gg 1$ that, as a consequence, possesses exaggerated properties [78]. Historically, the first time that this concept appeared was in 1885, with Balmer's formula for the wavelengths of the visible lines of the hydrogen

$$\lambda = \frac{bn^2}{(n^2 - 4)^2}.$$
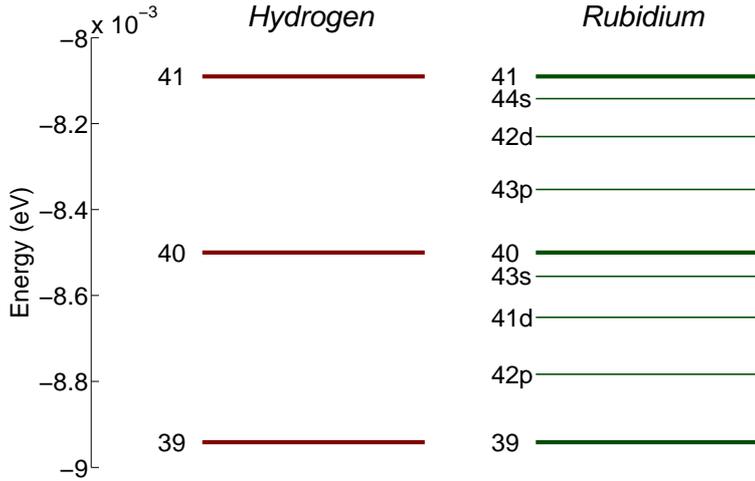
Figure 5.2.: Scheme of the spectra of the Rydberg states of a hydrogen and a rubidium atom. Due to the quantum defect the spectrum decays into degenerate n-manifolds (hydrogen-like) except for the low orbital quantum number states, that are energetically isolated from the rest.

We now know that this expression, with $b = 3645.6\,\mathring{A}$, gives the wavelengths of the transitions from the state of hydrogen with $n = 2$ to higher lying levels, as can be seen rewriting it as

$$\nu = \frac{1}{4b}\left(\frac{1}{4} - \frac{1}{n^2}\right).$$

With the theory of Bohr of the atomic structure of the hydrogen atom in 1913, the physical significance of the states with high principal quantum number n was understood for the first time. In his picture, the hydrogen atom was constituted by a proton and an electron describing orbits around it. The orbits allowed for the electron (in which it would not emit radiation) were given by multiples of the orbital momentum. With this simple model, in particular, an expression for the orbital radius of a hydrogen atom in a given state was obtained to be proportional to n^2,

$$r = a_0 n^2,$$

with $a_0 = 0.529\,\mathring{A}$ being the so-called Bohr radius. Also, it was found that the binding energy of the electron decreases as n^{-2}

$$W = -\frac{Ry}{n^2},$$

where $Ry = -13.6$ eV is the universal so-called Rydberg constant. The value of this constant had already been measured in the year 1890 by J.R. Rydberg when he began to classify the spectra of alkali atoms into sharp, principal and diffuse series of lines (s, p and d states, respectively, notation that survived until nowadays). As a consequence, from Bohr's theory one could physically understand a Rydberg atom as one whose valence electron is in a very large and loose orbit characterized by the quantum number n. We know now that this description is correct from the intuitive point of view but not complete. To actually obtain a description of the Rydberg atoms, quantum mechanics is necessary. The wavefunction ψ, solution of the Schrödinger equation

$$\left(-\frac{\nabla^2}{2} - \frac{1}{r}\right)\psi = W\psi, \tag{5.4}$$

will provide us the different properties of the corresponding system. The solution is of the form

$$\psi_{nlm}(\mathbf{r}) = CR_{nl}(r)Y_{lm}(\theta, \phi), \tag{5.5}$$

with C being the normalization constant, and where $Y_{lm}(\theta, \phi)$ stands for the so-called spherical harmonics. Note that the dependence of the wavefunction with the principal quantum number is encoded exclusively in the radial part $R_{nl}(r)$.

The description of the alkali Rydberg atoms is parallel to the hydrogen case, and the general form of the wavefunctions is very similar. The difference between the two cases is that in the alkali atom the positive core, although having a net charge of +1, is formed by a nucleus with charge $+Z$ and $Z - 1$ electrons, i.e., has structure and cannot be considered 'point-like' as the proton. In high angular momentum states $l \geq 4$, the basic properties of the two systems are the same, since the valence electron in this kind of orbit does not 'see' the inner structure of the core. On the other hand, when l takes low values, as in the case of the s, p or d states, the valence electron penetrates the inner core and, as a consequence, the corresponding wavefunctions of the alkali atoms differ from their hydrogen counterparts. Hence, the energy levels of an alkali Rydberg atom are accurately described by

$$E_{nl} = -\frac{Ry}{(n - \delta_l)^2} = -\frac{Ry}{n^{*2}},$$

where, δ_l stands for the so-called quantum defect, a function of the orbital quantum number and $n^* = n - \delta_l$ is the effective principal quantum number. In the following, when we mention n we will be actually referring to n^*. The quantum defect is negligible except in the case of low l, particularly high for s-states, so that the spectrum decomposes into degenerate manifolds with the same principal quantum number n except for these low-l states (see Fig. 5.2 to see the case of the rubidium atom). In this work, when we use Rydberg states, we shall focus on ns-states that are energetically well isolated from the rest.

Property	n dependence
Orbital radius	n^2
Binding energy	n^{-2}
Radiative lifetime	n^3
Energy level spacing	n^{-3}
Dipole matrix elements	n^2
Polarizability	n^7

Table 5.1.: Dependence of several features of Rydberg atoms with the (effective) principal quantum number n.

Other properties of these Rydberg states can be inferred from the wavefunction solution of the corresponding Schrödinger equation. In particular, their scaling with the principal quantum number n are given in Table 5.1, extracted from Ref. [78]. Let us highlight that the lifetime of these highly excited states is rapidly increasing with n, $\tau \propto n^\alpha$. The exponent α changes with the orbital quantum number l, being $\alpha = 3$ for s-states and $\alpha = 5$ for circular states, i.e., $l = n - 1$. To have an idea of the timescale we are referring to, the lifetime for Rb in the 43s state is approximately 90 μs [78]. Another interesting feature of these highly excited states is their large polarizability. It is obtained by the sum of the squared matrix elements between the state and the neighboring levels $\langle nl | r | n'l' \rangle$, that scales as n^2, divided by the energy difference between the levels, given roughly by n^{-3}. As a consequence the corresponding polarizability scales as n^7, which gives very large values that yield to very strong interactions between the Rydberg atoms.
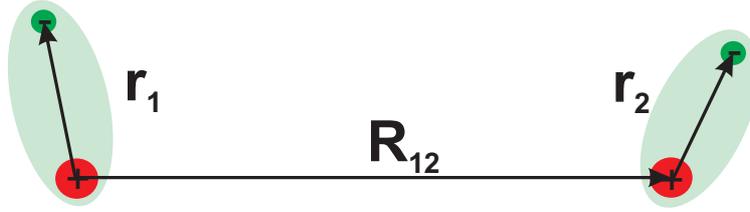
Figure 5.3.: Scheme of two Rydberg atoms separated by a large distance $\mathbf{R}_{12}$.
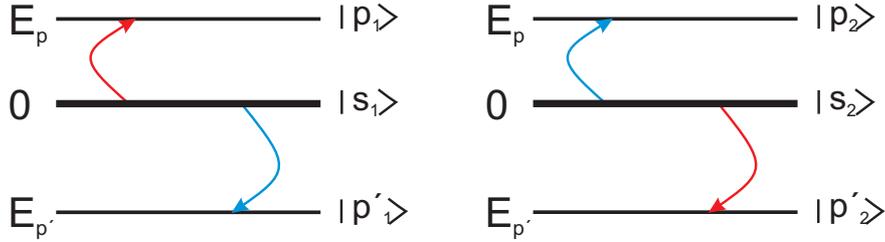
Figure 5.4.: Scheme of the spectrum of two Rydberg atoms in the s-state, whose energy is put to zero.

5.4. Interacting Rydberg atoms

The interaction energy between two Rydberg atoms separated by a very large internuclear distance $\mathbf{R}_{12} = R_{12}\hat{z}$ in comparison with the extension of the atoms (see Fig. 5.3) can be written as

$$V_{12}(\mathbf{R}_{12}) = \frac{1}{R_{12}^3} \left[\mathbf{r}_1 \cdot \mathbf{r}_2 - 3\left(\mathbf{r}_1 \cdot \hat{z}\right)\left(\mathbf{r}_2 \cdot \hat{z}\right) \right].$$

In order to analyze the interaction properties of the Rydberg atoms and obtain, in particular, the dependence of its strength with the principal quantum n, we make use of a simplified model. For more elaborate calculations, see Refs. [108, 109].

5.4.1. Simple model

Let us consider the situation where two atoms are in a certain ns state, as it is outlined in Fig. 5.4, i.e., the initial situation is $|S\rangle \equiv |s_1\rangle \otimes |s_2\rangle$. Given the form of the wavefunctions (5.5) and the properties of the spherical harmonics, it is easy to see that this state is only coupled by means of the interaction to the levels where both of the atoms are in a p-state (note that we put here the energy of the s-state to zero, so that $E_p > 0$ and $E_{p'} < 0$). Thus, those most strongly coupled to the initial one, $|S\rangle$, are

$$|P\rangle \equiv |p_1\rangle \otimes |p_2\rangle, \quad |P'\rangle \equiv |p'_1\rangle \otimes |p'_2\rangle, \quad |PP'\rangle \equiv \frac{1}{\sqrt{2}} \left[|p_1\rangle \otimes |p'_2\rangle + |p'_1\rangle \otimes |p_2\rangle \right].$$

We consider a regime in which $E_p + E_{p'} \ll 2E_p, E_{p'}$, i.e., the first two states $|P\rangle$ and $|P'\rangle$ are far detuned and thus we take the corresponding probabilities of transition to those to be negligible. Within this approximation, the Hamiltonian $H = H_1 + H_2 + V_{12}$ can be written in terms of the two most strongly coupled states $|S\rangle$ and $|PP'\rangle$

$$H \approx \begin{pmatrix} 0 & \frac{\alpha}{R_{12}^3} \\ \frac{\alpha}{R_{12}^3} & E_p + E_{p'} \end{pmatrix} \equiv \begin{pmatrix} 0 & V \\ V & \delta \end{pmatrix},$$
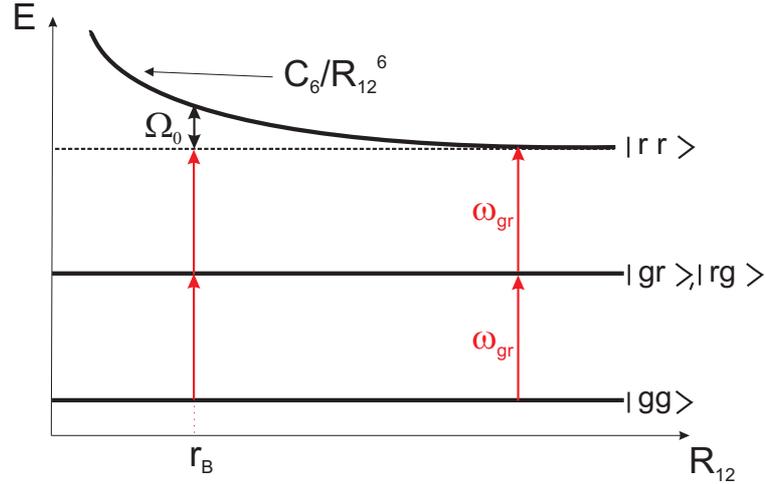
Figure 5.5.: Scheme of the Rydberg blockade mechanism. The ratio between the Rabi frequency Ω_0 and the van-der-Waals coefficient C_6 determines the blockade radius r_B from which no double excitation is accessible by the laser field.

where $\langle S | \mathbf{r}_1 \cdot \mathbf{r}_2 - 3 (\mathbf{r}_1 \cdot \hat{z}) (\mathbf{r}_2 \cdot \hat{z}) | PP' \rangle \equiv \alpha$. It can be easily diagonalized obtaining as a result the energies

$$E_\pm = \frac{\delta}{2} \left[1 \pm \sqrt{1 + \left(\frac{2V}{\delta} \right)^2} \right] \approx \frac{\delta}{2} \pm \frac{\delta}{2} \pm \frac{V^2}{\delta},$$

where we have considered that $\delta \gg V$. Hence, the two ns Rydberg atoms interact via the quickly decaying van-der-Waals potential

$$V_{\text{vdW}}(R_{12}) = -\frac{V^2}{\delta} \equiv -\frac{C_6}{R_{12}^6},$$

with the van-der-Waals coefficient being $C_6 = -\frac{\alpha^2}{E_p + E_{p'}} \propto n^{11}$. The dependence of C_6 with n can be obtained considering that in this simple model we do not take into account the specific angular configuration of the atoms, and thus $\alpha \sim \langle S | \mathbf{r}_1 \cdot \mathbf{r}_2 | PP' \rangle \propto n^4$, and that the energy separation is proportional to n^{-3}, as given in Table 5.1.

5.4.2. Rydberg blockade

Given the dependence of $C_6 \propto n^{11}$, one can see that the interaction between Rydberg states is very strong. For example, the van-der-Waals coefficient for the 43s state of rubidium is given by $C_6 = -2.45\,10^{-27}\,\text{MHz} \cdot \text{m}^6$ [108]. Hence, two of those Rydberg atoms placed $3\,\mu m$ apart interact with a strength of $3.35\,\text{MHz}$.

As a consequence of this strong interaction, the so-called blockade effect arises [85, 86]. Let us consider two atoms at a distance R_{12} from each other that are resonantly driven from the ground state $|g\rangle$ to a Rydberg state $|r\rangle$ via a laser field. The possible states of this two-body system are thus $|gg\rangle, |gr\rangle, |rg\rangle$ and $|rr\rangle$, as depicted in Fig. 5.5. Note that the energy needed to excite both states $|gr\rangle$ and $|rg\rangle$ is the same, ω_{gr}. When the interparticle distance is very large, as a consequence of the quickly decaying character of the van-der-Waals interaction, the atoms in the Rydberg state $|rr\rangle$ do not interact, and thus its energy is given by two times the single-excitation one, $2\omega_{gr}$. Hence, in this regime the laser can excite both atoms. As the interparticle distance becomes smaller the interaction becomes stronger and thus the energy of the doubly excited state is shifted, until the laser field is no longer capable of exciting it. In the simplest model, the so-called blockade radius, i.e., the distance at which we consider the laser out of resonance, can be estimated by equaling

the van-der-Waals interaction with the power-broadened linewidth of the laser given by its Rabi frequency (proportional to its intensity) [89], i.e., $r_{\mathrm{B}}^6 \propto C_6/\Omega_0$.

In summary, the effect of the interaction between the Rydberg states is a suppression of the excitation of more than one atom in a neighborhood defined by the ratio between the Rabi frequency of the laser and the interaction strength. As a consequence, within this blockade radius there can only be one excitation, which in the case of two atoms corresponds to a symmetric superposition of the two possible excited states, i.e., $\left[|gr\rangle + |rg\rangle\right]/\sqrt{2}$. Extending this to a gas of atoms yields to the concept of 'superatom' (see Refs. [89, 90]), that is nothing but a collective delocalized excitation in an area (for a 2D gas) or volume (3D) defined by the blockade radius r_B. This concept will be explained in more detail in the next section and used extensively throughout all this work.

6. Laser-driven atomic gas confined to a ring lattice

In this chapter we use the concepts introduced in the previous one to present the system that is the focus of our study, i.e., an atomic gas of atoms confined to a lattice whose internal states are coupled by means of a laser field. We consider also the interaction between the atoms and derive the Hamiltonian that drives the dynamics of this system. Finally, we explain how the symmetries of the setup can be exploited in order to simplify the problem.

6.1. The system and its Hamiltonian

We study a gas of bosonic ground-state atoms confined to a deep large spacing ring lattice with periodicity $a \approx \mu m$ (see Fig. 6.1). These ring lattices can be created approximatively starting from a large spacing standard rectangular lattice [110], removing then the atoms from the unwanted sites, thereby 'cutting out' a ring. It has been experimentally demonstrated that this is possible starting from magnetic arrays of microtraps on a chip and using a focused laser to address and rapidly empty individual traps [111]. Optical 2D lattices have been also shown to be a good candidate to create a ring lattice, where the individual sites are here addressed and emptied by the use of electron beams [112]. Near the lattice minima, the atomic motion approaches to that of the harmonic oscillator. For sufficiently large trap depths, the atoms are localized near the potential minima. Each site has thus an harmonic oscillator wavefunction associated with it, and for sufficiently strong potentials, there is very little overlap between the wavefunctions $\phi_k(\mathbf{x})$ in different wells. In other words, we consider the functions $\phi_k(\mathbf{x})$ of the atoms lying on the k-th site to be very narrow, i.e., localized with a width $\sigma \ll a$.

The internal (electronic) dynamics - in which we are interested here - takes place on a much shorter timescale than the external dynamics (hundreds of nanoseconds and milliseconds, respectively). Hence, we can assume the external dynamics of the atoms to be frozen, i.e., no hopping and thus no particle exchange between the lattice sites is present.

As in Sections 5.1 and 5.2, we consider only two internal electronic levels in each atom, which are denoted by $|g\rangle$ and $|r\rangle$. Here, $|g\rangle$ stands for the ground state and $|r\rangle$ for a highly excited (Rydberg) ns-state which - as we explained in Sec. 5.3 - is well isolated from any other electronic level. We assume that the atoms experience the same trapping potential independently of their internal state. This requirement is, however, not crucial as the typical timescale of the electronic excitation dynamics, which we are going to study, is much smaller than the dephasing time due to different trapping potentials experienced by $|g\rangle$ and $|r\rangle$. Experimentally these two levels are usually coupled by a two-photon transition (see Appendix A). Here, we assume, without any loss of generality, that they are coupled resonantly by a laser of Rabi frequency Ω_0 and detuning Δ.

The system can be considered, then, as an ensemble of two-level atoms lying in L independent harmonic traps. Hence, the coupling of these atoms with the laser field can be described (within the RWA) as an extension of the Hamiltonian derived in Sec. 5.2, i.e.,

$$H_L = \Omega_0 \sum_{k=1}^{L} \left(b_k^\dagger r_k + r_k^\dagger b_k \right) + \Delta \sum_{k=1}^{L} n_k, \tag{6.1}$$
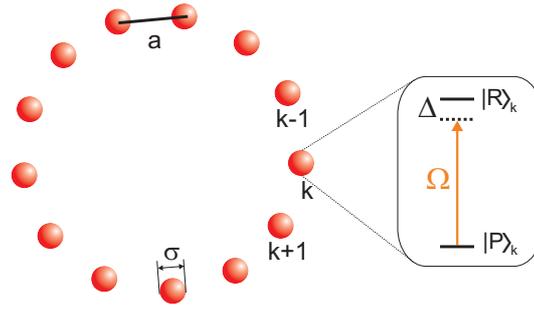
Figure 6.1.: Ring lattice with spacing a being much larger than the extension σ of the external wavefunctions (deep lattice). The internal atomic degrees of freedom at each site are described by the (collective) states $|P\rangle_k$ and $|R\rangle_k$, coupled by Ω.

where $b_k^\dagger$ and $r_k^\dagger$ (b_k and r_k) represent the creation (annihilation) of a ground and a Rydberg state, respectively, and $n_k = r_k^\dagger r_k$ stands for the number of atoms in state $|r\rangle$ at the k-th site. For the sake of simplicity, we will consider in the following the case where each lattice site is occupied by the same number of atoms, N_0. This is achieved, for example, if the system is initialized in a Mott-insulator state.

The interaction between the Rydberg atoms is given by the van-der-Waals potential $V(x) = -C_6/x^6$, that is quickly decaying with the distance x between excited atoms. Nevertheless, as C_6 scales with the eleventh power of the principal quantum number n, the interaction can strongly affect the excitation dynamics of atoms that are separated by several micrometers. This strong interaction gives rise to the so-called blockade effect [85, 86] (see Sections 5.3 and 5.4). We consider that the simultaneous excitation of two or more atoms to the Rydberg state on a single lattice site is blockaded. This is justified since one can always find a scenario (large enough n and/or deep enough lattice) in which the corresponding blockade radius is larger than the extension σ associated to the atoms in a site. Thus, on each lattice site k, only the two states

$$
\begin{aligned}
|P\rangle_k &= [|g\rangle_k]_1 \otimes \ldots [|g\rangle_k]_{N_0} \\
|R\rangle_k &= \frac{1}{\sqrt{N_0}} \mathcal{S}\left\{ [|r\rangle_k]_1 \otimes [|g\rangle_k]_2 \otimes \ldots [|g\rangle_k]_{N_0} \right\},
\end{aligned}
$$

are accessible, where $\mathcal{S}$ represents the symmetric superposition operator. $|P\rangle_k$ is the product state in which all the atoms on site k are on the ground state. On the other hand, $|R\rangle_k$ is an extension of the two-atom case we considered in Section 5.4, a symmetric superposition of the N_0 possible states in which one atom is excited. Thus, it describes a delocalized collective excitation all over the site, known in the literature as 'superatom' [89, 90]. The effective Rabi frequency for the laser coupling between these two collective states (see Fig. 6.1) is given by ${}_k\langle R| H_\mathrm{L} |P\rangle_k = {}_k\langle P| H_\mathrm{L} |R\rangle_k = \Omega_0\sqrt{N_0} \equiv \Omega$. Taking all this into account, in Eq. (6.1) we can replace $\Omega_0 r_k^\dagger b_k \to \Omega \sigma_+^{(k)} = (\Omega/2)[\sigma_x^{(k)} + i\sigma_y^{(k)}]$, where $\sigma_i^{(k)}$ are the Pauli spin matrices:

$$
\sigma_x = \begin{pmatrix} 0 & 1 \\ 1 & 0 \end{pmatrix} \qquad \sigma_y = \begin{pmatrix} 0 & -i \\ i & 0 \end{pmatrix} \qquad \sigma_z = \begin{pmatrix} 1 & 0 \\ 0 & -1 \end{pmatrix},
$$

so the laser Hamiltonian can be rewritten as

$$
H_\mathrm{L} = \Omega \sum_{k=1}^{L} \sigma_x^{(k)} + \Delta \sum_{k=1}^{L} n_k. \tag{6.2}
$$

Since we consider the extension of the external wavefunctions to be much smaller than the lattice spacing, we can assume $\phi_k(\mathbf{x}) \approx \delta(\mathbf{x} - \mathbf{P}_k)$ (with $\mathbf{P}_k$ representing the coordinates of the center of the

site k) and rewrite the van-der-Waals potential between two (super)atoms in the state $|R\rangle$ located at the sites i and j, as

$$V_{|i-j|} = \int d\mathbf{x}_1 d\mathbf{x}_2 \, |\phi_i(\mathbf{x}_1)|^2 \, |\phi_j(\mathbf{x}_2)|^2 \, V(|\mathbf{x}_1 - \mathbf{x}_2|) \approx V(|\mathbf{P}_i - \mathbf{P}_j|).$$

Hence, the interaction yields $V_d = -C_6/x_d^6$, where x_d is the separation between the (super)atoms located d sites apart, and the interaction Hamiltonian reads

$$H_{\text{int}} = \sum_{k=1}^{L} \sum_{l=1}^{d} V_l n_k n_{k+l},$$

with the Rydberg number operator $n_k = [1+\sigma_z^{(k)}]/2$ and the boundary condition $\sigma_j^{(1)} = \sigma_j^{(L+1)}$ (ring lattice). When the range of the interactions is much smaller than the ring size, one can approximate the van-der-Waals potential as $V_d = -C_6/(ad)^6$. Thus, the interaction Hamiltonian can be rewritten in terms of the nearest neighbor interaction $\beta \equiv V_1 = -C_6/a^6$ as

$$H_{\text{int}} = \beta \sum_{k=1}^{L} \sum_{l=1}^{d} \frac{n_k n_{k+l}}{l^6}.$$

Summarizing, the complete Hamiltonian that drives the dynamics of a frozen laser-driven Rydberg gas confined to a monodimensional ring lattice can be written as

$$H = \sum_{k=1}^{L} \left[\Omega \sigma_x^{(k)} + \Delta n_k + \beta \sum_{l=1}^{d} \frac{n_k n_{k+l}}{l^6} \right]. \tag{6.3}$$

Hence, the relevant parameters in our system will be: (i) the ones related to the laser, i.e., the single-atom Rabi frequency Ω_0 and detuning Δ, which can be time-dependent and (ii) the interaction strength between Rydberg atoms represented by β and its maximal range, da. Throughout this work, we consider the regime where the detuning is much smaller than both the collective Rabi frequency and the interaction strength, i.e., $|\Delta| \ll \Omega, \beta$. As a consequence, the behavior of the system will be determined by the strength ratio of the laser and the interaction. In particular, we study here the two limiting cases. In Chapters 7 and 8, we consider that the interaction is much stronger than the laser field, so that the double excitation is forbidden in neighboring sites (perfect blockade). In Chapter 9, the regime where the laser field is much stronger than the nearest neighbor interaction, $\Omega \gg \beta$, is studied.

6.2. Analysis of the symmetries

Our goal is to study the dynamics of the system under the action of Hamiltonian (6.3) from a given initial state. To this end, first we take into account the symmetries of the system and its Hamiltonian, since they lead to a significant simplification of the problem when solving the time-dependent Schrödinger equation.

There are two basic symmetries on a ring lattice which are of interest in our system: cyclic shifts by l sites and the reversal of the order of the lattice sites. The former is represented by the unitary operators $\mathcal{X}_l$ with $l = 1, 2, \ldots, L$ where $\mathcal{X}_l = \mathcal{X}_1^l$, while the latter operation is the parity and is denoted by $\mathcal{R}$. The action of these operations on the spin ladder operators $\sigma_{\pm}^{(k)}$ is defined through

$$\mathcal{R}^{\dagger} \sigma_+^{(k)} \mathcal{R} = \sigma_+^{(L-k+1)} \qquad \qquad \mathcal{R}^{\dagger} \sigma_-^{(k)} \mathcal{R} = \sigma_-^{(L-k+1)}$$
$$\mathcal{X}_l^{\dagger} \sigma_+^{(k)} \mathcal{X}_l = \sigma_+^{(k+l)} \qquad \qquad \mathcal{X}_l^{\dagger} \sigma_-^{(k)} \mathcal{X}_l = \sigma_-^{(k+l)},$$

from where follows that the Hamiltonian (6.3) is invariant under these operations ($[H, \mathcal{X}_l]$ = $[H, \mathcal{R}]$ = 0). In other words, both shift and reversal operations correspond to conserved quantities. Our complete Hilbert space is in principle spanned by all the possible configurations in the ring, taking into account that each site can be only in two states, $|P\rangle$ or $|R\rangle$. Thus, for an increasing site number L, the exact solution of this problem becomes quickly intractable as the dimension of the total Hilbert grows as 2^L. However, if the system is initialized in an eigenstate with respect to $\mathcal{X}_l$ and $\mathcal{R}$, the time evolution will not take place in the entire Hilbert space, but merely in the subspace spanned by the states with the same quantum number with respect to $\mathcal{X}_l$ and $\mathcal{R}$.

In practise, the natural initial situation will be that in which all atoms are in the ground state, i.e., all sites in the product state $|P\rangle$,

$$|0\rangle = \prod_{k=1}^{L} |P\rangle_k \,.$$

Studying the symmetry properties of this initial state where no Rydberg atom is excited tells us that it is an eigenstate of *all* cyclic shifts and the reversal operator with eigenvalue 1:

$$\mathcal{X}_l |0\rangle = |0\rangle \qquad \mathcal{R} |0\rangle = |0\rangle \,.$$

We will refer to such a state that has eigenvalue 1 with respect to $\mathcal{X}_l$ and $\mathcal{R}$ as being *fully-symmetric*. Only a small subset of the 2^L states spanning the whole Hilbert space actually has these properties. In particular, each of these fully-symmetric states can be understood as a superposition of all states that are equivalent under rotation and reversal of the sites. For example, when one only (super)atom is excited on the ring, the corresponding fully-symmetric state (denoted by the subscript S) reads

$$|1\rangle_S = \frac{1}{\sqrt{L}} \mathcal{S} \left\{ |R\rangle_1 \otimes |P\rangle_2 \otimes \ldots |P\rangle_L \right\} \,.$$

In summary, only the states from this fully-symmetric subspace can be actually accessed in the course of the system's time evolution under Hamiltonian (6.3).

The dimension of the problem is like this dramatically reduced. To pick an example, for $L = 10$ the dimension of the Hilbert space decreases from $2^{10} = 1024$ down to 78. For our computations we need an algorithm to quickly generate the maximally symmetric states among which the evolution takes place. Such an algorithm is discussed in Appendix D.1. There, these states are called bracelets, and are recursively generated in an optimal way. The amount of CPU time grows only proportional to the number of bracelets produced [113].

7. Strong interaction: Perfect blockade

A great simplification of the Hamiltonian (6.3) is achieved in the so-called perfect blockade regime which we are going to introduce and analyze here. Within this regime, we study numerically the time evolution of the system through different local properties as the Rydberg density, the correlation functions and the entanglement. In the last section of the chapter we relax the perfect blockade condition and test like this the validity of our approximations.

7.1. Perfect blockade regime

As already pointed out, the interaction between Rydberg atoms is quickly decaying with the distance. In particular, the next-nearest neighbor interaction is a factor of $64\cos^6\left(\pi/L\right)$ smaller than the nearest neighbor one ($V_2 \ll \beta$). At the same time, here we are going work in a regime where the laser field strength given by the collective Rabi frequency is much stronger than the next nearest neighbor interaction, i.e., $\Omega \gg V_2$. As a consequence, we will thus consider that only nearest neighbor interaction takes place. The Hamiltonian for the entire atomic ensemble then reads

$$H = \sum_{k=1}^{L}\left[\Omega\sigma_x^{(k)} + \Delta n_k + \beta n_k n_{k+1}\right]. \tag{7.1}$$

Thus, the system can be described as a periodic arrangement of spin-1/2 particles, where the two spin states, corresponding to the two internal states of the (super)atoms, $|P\rangle_k$ and $|R\rangle_k$, interact via an Ising-type potential. In this picture, the Rabi frequency Ω and the combination of $\Delta + \beta$ can be effectively interpreted as perpendicular magnetic fields.

Initially, the laser is turned off $\Omega(0) = 0$. Thus, the spectrum of the Hamiltonian H is that of the interaction Hamiltonian $H_{\text{int}} = \beta\sum_{k=1}^{L} n_k n_{k+1}$. It is composed by L degenerate subspaces spanned by states that have the same number of pairs of neighboring excitations $\nu = 0, 1, ..., L-2, L$, with corresponding energy $E_\nu = \nu\beta$, (note that the subspace $\nu = L-1$ is not included because of the impossibility of having $L-1$ pairs of neighboring excitations in a ring).
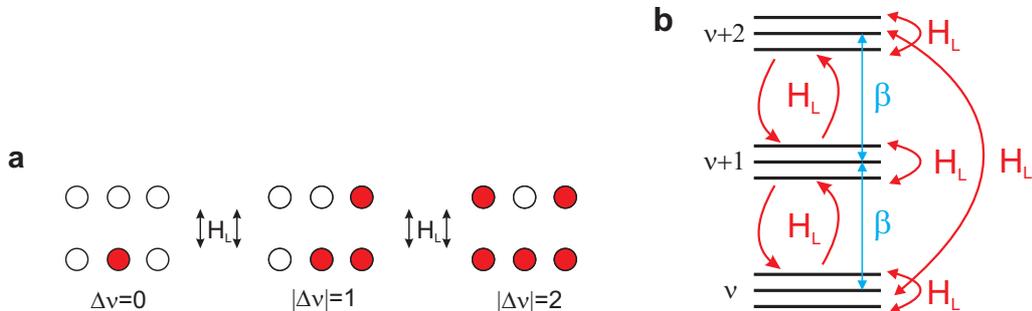
Figure 7.1.: a: The action of the laser creates or annihilates an excitation $|R\rangle$ (red circles), that gives rise to a difference of pair of excitations $\Delta\nu = 0, \pm1, \pm2$ depending on the neighboring sites. **b**: Energy level structure of the Hamiltonian (6.3) with $\beta \gg \Omega$. The spectrum consists of highly degenerate subspaces which are labeled by ν energetically separated by β, except the levels with $\nu = L-2$ and $\nu = L$, which are separated by 2β (see text for explanation). The laser (H_L) causes an energy splitting of the degenerate levels. In addition, it couples states belonging to a given ν-subspace and connects subspaces with $|\nu - \nu'| = 1, 2$.

Let us discuss the action of the laser Hamiltonian H_L, that is switched on instantaneously at a given time $t_0 = 0$. Its operation creates or destroys a (super)atom state $|R\rangle_k$ on the k-th site of the ring. This leads to three different situations depending on the state of the neighboring sites: i) both in the state $|P\rangle$, ii) one in $|P\rangle$ and one in $|R\rangle$, or iii) both in state $|R\rangle$ (see Fig. 7.1a). The difference of number or pairs of neighboring excitations is $\Delta\nu = 0, \pm 1, \pm 2$, respectively. Thus, H_L drives the dynamics within a given ν-subspace and couples subspaces with $|\nu - \nu'| = 1, 2$.

We consider now that $\beta \gg \Omega$ (see Fig. 7.1b), i.e., the interaction energy of two neighboring Rydberg atoms is larger than the collective Rabi frequency. Let us point out that in this limit we are effectively replacing the van-der-Waals interaction by an interaction potential whose value is $\beta \gg \Omega$ for nearest neighbors and 0 for atoms which are further apart (remember that $\Omega \gg V_2$). This model is then valid provided that

$$1 \gg \Omega/\beta = a^6 \Omega/C_6 \gg 1/64,$$

i.e., Ω has to be much smaller than the nearest neighbor interaction but at the same time much larger than the next nearest neighbor interaction, e.g., $\beta = 10\Omega$.

We can use perturbation theory to estimate the probability of transition between states coupled by H_L, which we consider here to be a time-independent perturbation to the interaction Hamiltonian. Hence, the probability of transition between states that are nearly degenerate, i.e., belonging to the same ν-subspace, is proportional to Ω, while the transitions between subspaces with $|\nu - \nu'| = 1, 2$, energetically separated by β and 2β, respectively, occur with a probability Ω^2/β. As a consequence, for sufficiently strong interaction, one can neglect the inter-subspace transitions.

The physical initial state is $|0\rangle = \prod_{k=1}^{L} |P\rangle_k$, where no Rydberg excitation is present. This state belongs to the subspace with $\nu = 0$ which, as we have pointed out, we consider uncoupled to any other state including higher number of excitation pairs. We call this the *perfect blockade* approach since the time evolution takes place now only in a space spanned by states where no neighboring Rydberg excitation takes place, i.e., the set of states $\{|\Phi\rangle\}$ such that

$$H_{\text{int}} |\Phi\rangle = 0. \tag{7.2}$$

It is valid for timescales larger than the time the system takes to perform a transition between adjacent ν-subspaces, i.e., such that $t \ll \beta/\Omega^2$.

The restriction to the $\nu = 0$ subspace leads to a further reduction of the dimension of Hilbert space in which the temporal evolution takes place. For example, for $L = 10$ the number of states to be considered in the basis set expansion decreases from 78 to 14. This is to be compared to the 1024 states which span the entire Hilbert space of the system.

7.2. Graph: general behavior of expectation values of observables

The laser Hamiltonian H_L couples states in the Hilbert space whose number of excitations differ by one. Moreover, due to the differences in the spatial distribution of the excitations only certain states are connected by the laser. A convenient way to illustrate the coupling is a graph as shown in Fig. 7.2. Here vertices in the same column correspond to states that contain the same number of Rydberg atoms, and they are denoted by that number. A subscript is added when more than one configuration with the same excitation number is possible. Note that, for an even (odd) number of sites the maximal number of Rydberg atoms in one of these states is $\frac{L}{2}$ ($\frac{L-1}{2}$). The way these states are coupled is qualitatively similar for different lattice sizes L so, for simplicity reasons, we discuss here the lattice with $L = 10$. Starting from the initial state $|0\rangle$, there are several excitations paths with different probabilities that connect the states. The larger the amount of Rydberg atoms, the more constraints are found to allocate the next excitation. As a consequence, we encounter several excitation paths that do not reach the state with the maximal number of Rydberg excitations, but
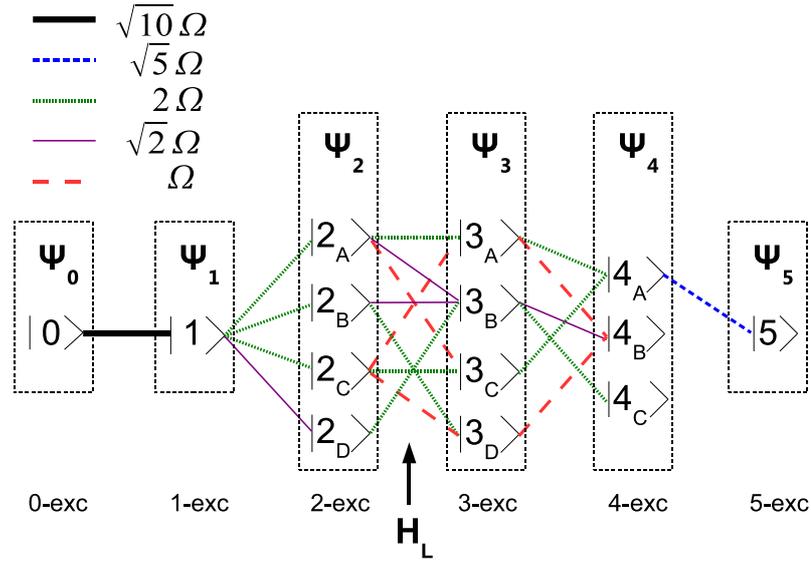
Figure 7.2.: Graph with the basis of fully-symmetric states for $L = 10$ in which the time evolution takes place. In each column a subspace of a given number of Rydberg excitations is shown, see text for further information. The laser (Hamiltonian H_L) couples only states belonging to adjacent subspaces. The coupling strength (transition probability) between the individual states is encoded in the colors and line style.

end in others, e.g., the $|4_B\rangle$ and $|4_C\rangle$ states for $L = 10$. The features of these frustrated states strongly depend on the lattice size, and their amount increases as L is increased. In particular, their existence provokes small quantitative differences in the dynamics of two lattices with different L for large times.

The previous features are reflected in the time evolution of all expectation values of the observables we are going to study throughout this work. As an example, in Fig. 7.3, we show the typical appearance of the temporal evolution of the Rydberg number n_r obtained from theoretical studies [81, 114, 82, 115]. In this case and in general every time evolution, the dynamics can be always divided into two different domains. At small times ($t \leq t_{trans}$) n_r rises first quadratically in t showing subsequently a number of oscillations with high contrast. After this transient period the oscillations diminish and n_r approaches a constant value around which it performs small amplitude fluctuations which decrease with increasing system size. This general appearance is independent of the exact details of the system, e.g., the actual arrangement of the atoms and the boundary conditions. In experiments which are carried out in disordered gases the individual oscillations might not be observable since averaging over many experimental realizations also means averaging over many different spatial distributions of the atoms [83]. Each of these distributions gives rise to a different shape of the oscillating features in Fig. 7.3 and eventually the oscillations are washed out.

7.3. Numerical results: time evolution of expectation values of observables

7.3.1. Two-sites density matrix

Let us start by introducing the reduced density matrix of two neighboring sites, since it is needed to investigate the temporal evolution of local properties such as the mean density of Rydberg atoms
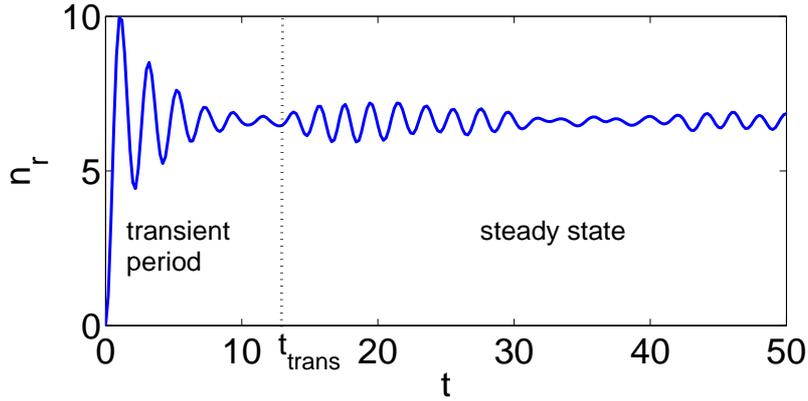
Figure 7.3.: Number of Rydberg atoms as a function of time when initially no Rydberg atom is excited. One observes an initial (transient) phase with large contrast oscillations followed by a steady state. These features do not depend on the actual details of the system, i.e., the exact atomic interaction, the atomic arrangement and the boundary conditions. The data here is shown for a ring lattice with 25 sites. The time is given in units of the inverse collective Rabi frequency Ω^{-1}.

or the entanglement between two adjacent sites. The density matrix of the full system is given by

$$\rho(t) = |\Psi(t)\rangle\langle\Psi(t)|. \tag{7.3}$$

On can verify that the expectation value of an observable $\hat{A}$ can be obtained using the density matrix by

$$\langle\Psi(t)|\hat{A}|\Psi(t)\rangle \equiv \hat{A}(t) = \text{Tr}\left(\rho(t)\hat{A}\right),$$

where the trace of an operator is defined as the sum of the diagonal elements of the matrix representing the operator, or the integral if the operator is continuous. Since we are interested in two-body properties, as the entanglement or the correlations, we are interested in the two-sites reduced density matrix. It is obtained from the total density matrix (7.3) by performing the partial trace over all the sites but two,

$$\rho^{(12)}(t) = \text{Tr}_{3,4...L}\left(\rho(t)\right).$$

Since the wavefunction $|\Psi(t)\rangle$ is spanned in the subspace of fully-symmetric states, all sites are indistinguishable and we can take 1 and 2 as representative adjacent lattice sites. The basis for the two-sites states is given by $\{|PP\rangle, |PR\rangle, |RP\rangle, |RR\rangle\}$. The restriction to the fully symmetric subspace (indistinguishability of the two sites) imposes

$$\begin{aligned} \langle PR|\rho^{(12)}|PR\rangle &= \langle RP|\rho^{(12)}|RP\rangle \equiv \chi \\ \langle PP|\rho^{(12)}|PR\rangle &= \langle PP|\rho^{(12)}|RP\rangle \equiv \zeta, \end{aligned}$$

while the perfect blockade prevents the excitation of atoms in two neighboring sites and hence the entries

$$\langle\psi|\rho^{(12)}|RR\rangle = \langle RR|\rho^{(12)}|\psi\rangle = 0$$

for $|\psi\rangle = \{|PP\rangle, |PR\rangle, |RP\rangle, |RR\rangle\}$. As a consequence, the reduced density matrix has the particularly simple form:

$$\rho^{(12)}(t) = \begin{pmatrix} \eta & \zeta & \zeta & 0 \\ \zeta^* & \chi & \xi & 0 \\ \zeta^* & \xi^* & \chi & 0 \\ 0 & 0 & 0 & 0 \end{pmatrix}, \tag{7.4}$$
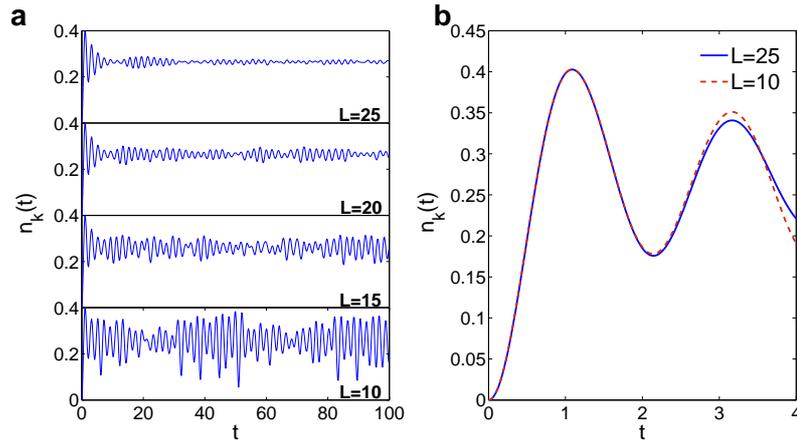
Figure 7.4.: Expectation value of the Rydberg density (7.6) versus time for **a**: four different ring sizes and $t \leq 100$ (units of Ω^{-1}), and **b**: detail of the short time evolution for $L = 10$ and 25. The computations have been performed assuming perfect blockade of the adjacent neighbor.

where η, χ, ζ and ξ are four time-dependent (complex) parameters. In particular, η and χ are real, and due to the normalization of the wavefunction, $\text{Tr}_{1,2}\,\rho^{(12)}(t) = \eta + 2\chi = 1$. Hence, only three of these parameters are independent.

Since we are also interested in single-particle properties such as the density of Rydberg states, we calculate as well the single particle density matrix performing the trace over the states of site number 2, yielding

$$\rho^{(1)}(t) = \text{Tr}_2\left(\rho^{(12)}(t)\right) = \begin{pmatrix} 1 - \chi & \zeta \\ \zeta^* & \chi \end{pmatrix}. \tag{7.5}$$

7.3.2. Rydberg density

The first local property under consideration is the time evolution of the expectation value of the Rydberg density given by the Rydberg number operator in one site $n_k = (1/2)\left[1 + \sigma_z^{(k)}\right]$. By using Eq. (7.5) one obtains this quantity in terms of one of the time-dependent entries of the density matrix

$$n_k(t) = \text{Tr}\left(\rho^{(1)}(t)n_k\right) = \chi, \tag{7.6}$$

so the total number of Rydberg atoms evaluates to

$$n_\text{r}(t) = L\,n_k(t) = L\chi.$$

In Fig. 7.4a we show $n_k(t)$ as a function of time for different lattice sizes. In the right panel (Fig. 7.4b) a magnified view of the short time dynamics is provided for $L = 10$ and 25.

We observe at first a steep increase, which is proportional to t^2 (time in units of Ω^{-1}), that culminates in a pronounced peak located at $t = 1.09$. This peak is independent of the lattice size, as we are still witnessing the short time behavior. For much larger times, $n_k(t)$ becomes dependent of L and oscillates with a frequency $f \approx 0.48$ about a mean value of $\overline{n_k(t)} \approx 0.26$. This mean value and also f turn out to be independent of the ring size, however, the exact shape of $n_k(t)$ strongly depends on L. A similar result and a possible explanation of the nature of this value is given in Ref. [81]. The time averages are performed by means of numerical integration over time in a large enough interval $t \in [5, 200]$. The lower limit of this interval is chosen large enough to avoid the initial effects of turning on the laser. The higher one is kept shorter than the corresponding revival time. The amplitude of the oscillations decreases considerably with increasing lattice size. This amplitude can be measured by means of the standard deviation. For $L = 10$, a quasi-steady
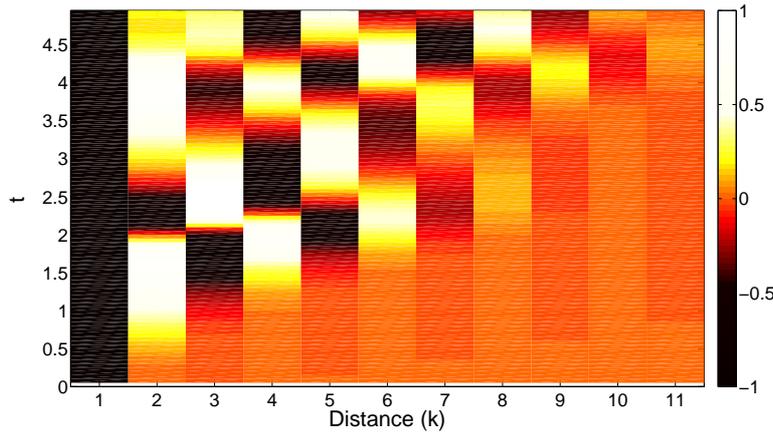
Figure 7.5.: Short time behavior of the density-density correlations $g_2(k,t)$ for $L = 25$. Correlations emerge successively during the time evolution (time in units of Ω^{-1}). Due to the perfect blockade condition strong oscillations of $g_2(k,t)$ with a period $k = 2$ are observed.

state with large fluctuations characterized by a standard deviation $\sigma(n_k(t)) = 0.062$ about $\overline{n_k(t)}$ is established, while in the case of $L = 25$ these fluctuations become smaller $\sigma(n_k(t)) = 0.0065$. The steady state encountered here is studied in depth in Chapter 8, where its approximate analytical form is found.

7.3.3. Density-density correlation function

In this subsection we are going to study the time evolution of the equal-time density-density correlation function. This quantity measures the conditional probability of finding two simultaneously excited atoms at a distance of k sites from each other normalized to the probability of uncorrelated excitation. It is defined as

$$g_2(k,t) = \frac{n_1 n_{1+k}(t)}{n_1(t) n_{1+k}(t)} - 1.$$

This correlation function will give as a result $g_2(k,t) = 0$ when the two sites separated by a distance ka are completely uncorrelated, and $g_2(k,t) > 0 \, (< 0)$ for correlation (anticorrelation) between the sites.

Figure 7.5 illustrates the initial evolution of $g_2(k,t)$ in the time interval $t \in [0,5]$ for a $L = 25$ lattice, i.e., the short-time behavior. The temporal and spatial structure can be understood by observing the properties of the laser Hamiltonian H_L which drives the excitation dynamics. At the beginning only a single particle at site 1 is excited. As a consequence, we observe that, due to the perfect blockade condition, the neighboring site cannot be excited, so $g_2(1,0) = -1$ (in general, $g_2(1,t) = -1$ for all times). With the exception of the neighbor site, the probability of excitation of a second atom is uniform, it can occur at arbitrary position. As a consequence, there are no correlations for very short times (g_2 has uniform zero value). The correlations emerge successively as time increases, starting with an augment at $k = 2$, the density-density correlation function for that distance reaches a maximum at $t \approx 1.5$. The high probability of finding two excitations at the distance $k = 2$, i.e., a large value of $g_2(2,t)$, automatically gives rise to a decrease of $g_2(3,t)$ due to Rydberg blockade. For larger times, a regular pattern of enhanced and suppressed density-density correlations characterizes the dynamics. The regular pattern of the density-density correlation functions at short times is lost as time increases. As in the case of the Rydberg density, for longer times $g_2(k,t)$ exhibits pronounced fluctuations that decrease with L and rapid oscillations around a mean value.
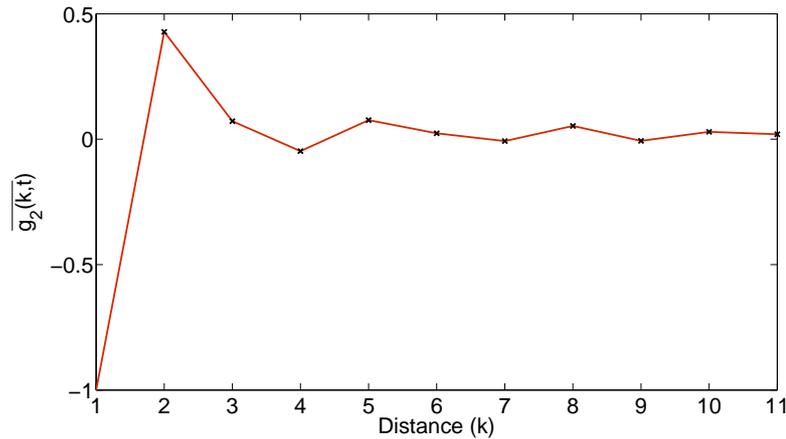
Figure 7.6.: Time-averaged density-density correlations $\overline{g_2(k,t)}$ for $L = 25$. For distance $k = 1$, the value is -1 due to the perfect blockade. $\overline{g_2(k,t)}$ assumes a maximum for $k = 2$ (next-nearest neighbor). For larger distances, only weak correlations are visible.

In Fig. 7.6 we show the time-averaged density-density correlation function, $\overline{g_2(k,t)}$, in the stationary long time regime as a function of k, for a lattice of 25 sites. This function shows a maximum for $k = 2$, while for larger intersite distances it approaches the constant value 1, i.e., no correlations. As a consequence, we conclude that the density-density correlations are only short ranged after the initial period in which also long ranged correlations are of importance.

7.3.4. Entanglement

We study the quantum and classical correlations and the entanglement of two neighboring sites in this system by means of the *two-party correlation measure* [116] and the *entanglement of formation* [117]. These quantities can be directly related to the entries of the reduced density matrix discussed previously.

Two-party correlation. The two-party correlation measure [116] is based on the trace distance [118] and it is defined as

$$M_C\left(\rho^{(12)}\right) = \frac{2}{3}\mathrm{Tr}|\rho^{(12)} - \rho^{(1)} \otimes \rho^{(2)}|, \tag{7.7}$$

where $|A| \equiv \sqrt{A^\dagger A}$ is the positive square root of $A^\dagger A$. Its physical meaning is the distance between the state $\rho^{(12)}$ and its reduced product state $\rho^{(1)} \otimes \rho^{(2)}$. It takes into account both the classical correlation between two sites and the quantum coherence. It generalizes the classical distance in the sense that if the two operators commute then it is equal to the classical trace or Kolmogorov distance between the eigenvalues of $\rho^{(12)}$ and $\rho^{(1)} \otimes \rho^{(2)}$. We show the time evolution of this correlation measure in Fig. 7.7a for different sizes of the ring. Initially, for the product state $|0\rangle = \prod_{k=1}^{L} |P\rangle_k$, there are no correlations. Analogously to the previously analyzed quantities, M_C exhibits an L-independent short time behavior which here is characterized by large amplitude oscillations. It is followed by an L-dependent regime, where M_C presents smooth oscillations around the mean value $\overline{M_C} = 0.19$. As expected, the amplitude of these oscillations decreases with increasing lattice size.

We are now interested in finding a classical counterpart to this correlation measure. To this end, we make use of the density matrix properties. The diagonal elements of a density matrix represent the probability of finding the corresponding configuration of the sites. For example, in $\rho^{(12)}$, (see equation (7.4)), η and χ represent the probability of the two sites to be in the states $|PP\rangle$ and $|PR\rangle$ or $|RP\rangle$, respectively; note that the sites are indistinguishable. In the same way, the diagonal
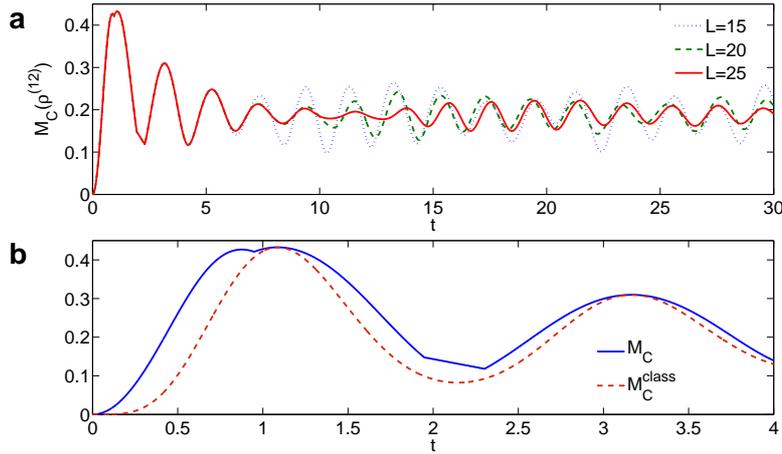
Figure 7.7.: a: time evolution (time in units of Ω^{-1}) of the two-party correlation measure $M_C\left(\rho^{(12)}\right)$ for long times and various lattice sizes. **b**: Short time behavior of $M_C\left(\rho^{(12)}\right)$ and its classical counterpart for $L = 25$.

components of the reduced product density matrix $\rho^{(1)} \otimes \rho^{(2)}$ provides the probability of the two sites being in the corresponding product state, e.g., $(1-\chi)^2$ for the state $|P\rangle_1 \otimes |P\rangle_2$.

We take these diagonal elements $d_i^{(12)}$ and $d_i^{(1\otimes2)}$ of the matrices $\rho^{(12)}$ and $\rho^{(1)}\otimes\rho^{(2)}$, respectively, as classical probability distributions. The Kolmogorov distance between these distributions, is defined here as:

$$M_C^{\text{class}}\left(\rho^{(12)}\right) \equiv \frac{2}{3}\sum_{i=1}^{4}|d_i^{(12)} - d_i^{(1\otimes2)}|, \tag{7.8}$$

and it provides a classical measure of the two-party correlation. In terms of the parameters of the density matrix this quantity is reduced to

$$M_C^{\text{class}}\left(\rho^{(12)}\right) = \frac{8}{3}\chi^2. \tag{7.9}$$

The classical and the total two-party correlation functions are presented in Fig. 7.7b for $t \leq 4$ and 25 sites. One of the main features due to the quantum behavior of the system is the appearance of the two consecutive peaks of M_C at $t = 0.88$ and $t = 1.09$. Note that the classical counterpart M_C^{class} reproduces only the second maximum. Hence, the existence of the first one can be only justified by quantum arguments. Due to the absolute values in expression (7.7), two discontinuities appear in the derivative of M_C around $t \approx 1.9$ and $t \approx 2.3$. They are, however, not observed in M_C^{class} since it only depends on the single, smoothly varying, parameter of the density matrix, χ.

To get a deeper insight into the quantum effects on the correlations, the difference between the total two-party correlation and the classical measure is shown in Fig. 7.8 as a function of time. We have performed a fit to the local maxima of this numerical difference using an exponential decreasing function. The contribution of the quantum correlations loses importance as time is increased and, at the same time, the classical dynamics starts to dominate the correlations between two neighboring sites.

Concurrence and entanglement of formation. For a general state of two qubits represented by means of its two-particles density matrix ρ, the concurrence is given by [117]

$$C(\rho) = \max\{0, \lambda_1 - \lambda_2 - \lambda_3 - \lambda_4\}, \tag{7.10}$$
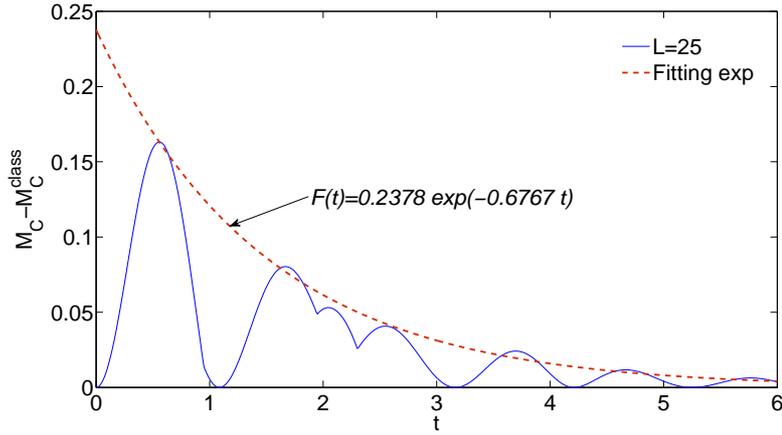
Figure 7.8.: Difference between the two-party correlation measure and its classical counterpart for $L = 25$. The dashed line corresponds to an exponential fit to the envelope of this difference.

where the λ_i are the square roots of the eigenvalues, in decreasing order, of the matrix $\rho\tilde{\rho}$, where $\tilde{\rho}$ is the flipped matrix of the two-qubit general state ρ, i.e.,

$$\tilde{\rho}^{(12)} = (\sigma_y \otimes \sigma_y)\left(\rho^{(12)}\right)^* (\sigma_y \otimes \sigma_y).$$

The entanglement of formation of a state of two qubits is defined in terms of this concurrence as

$$E(\rho) = h\left(\frac{1 + \sqrt{1 - C(\rho)^2}}{2}\right),$$

with $h(x) = -x\log_2 x - (1-x)\log_2(1-x)$. This quantity provides a measure of the resources needed to create a certain entangled state, and its range goes from 0 to 1.

Using the two-sites density matrix describing our system (7.4), and its corresponding flipped matrix, we obtain the following λ_i:

$$\lambda_1 = (\chi + |\xi|); \qquad \lambda_2 = |\chi - |\xi||; \qquad \lambda_3 = \lambda_4 = 0.$$

These values give rise to two different regimes for the concurrence:

$$C\left(\rho^{(12)}\right) = \left\{ \begin{array}{ll} 2|\xi| & \chi > |\xi| \\ 2\chi & \chi < |\xi| \end{array} \right. .$$

The first condition $\chi > |\xi|$ always holds for any size L of the lattice, so the concurrence yields

$$C\left(\rho^{(12)}\right) = 2|\xi|. \tag{7.11}$$

The time evolution of the entanglement for the lattices with sites $L = 15, 20$ and 25 is presented in Fig. 7.9a, and an enhancement of the behavior at short times for $L = 25$ is shown in Fig. 7.9b. Again, two different time domains can be distinguished. For short times, the entanglement of formation is independent of the ring size. Its maximal value, $E(\rho) = 0.23$, is reached at $t = 0.73$; for a further increase of time, $E(\rho)$ drastically decreases, e.g., the second peak at $t = 2.05$ is reduced roughly by 80%. In the long time regime, the entanglement becomes weaker with $E(\rho)$ eventually approaching zero with characteristic fluctuations for each L. The amplitudes of these fluctuations become smaller as L is increased.
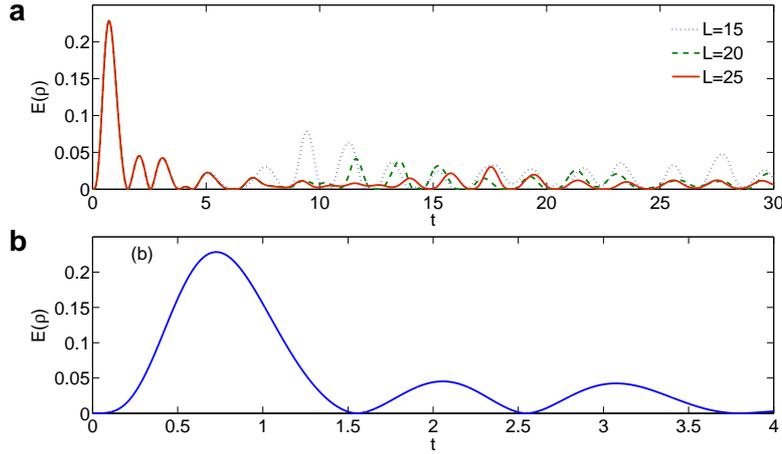
Figure 7.9.: time evolution of the entanglement of formation for **a**: long time and several sizes of the system and **b**: short time for $L = 25$.

7.4. Non-perfect Blockade

The above discussed phenomena have been investigated in the perfect blockade regime, which assumes that the energy scale associated to the van-der-Waals interaction is infinitely large compared to the one related to the laser interaction, i.e., $\beta \gg \Omega$. Since the initial state has no Rydberg excitations, the dynamics of the system is restricted to a small subspace including those eigenstates of H_{int} with eigenvalue zero. However, for large but finite values of β/Ω, the states with $\nu = 0$ are coupled to those with $\nu > 0$ and, as a consequence, these higher excitations might influence the dynamics.

In this section, we go beyond the perfect blockade approach and explore these couplings including their effect of up to order Ω/β. We thereby derive an effective Hamiltonian by dividing the eigenstates of H_{int} into two sets, characterized by their respective quantum number ν. The first set of states is formed by the subspace $\nu = 0$, whereas the second one contains the rest of energetically high-lying excitations. In this framework, the Hamiltonian can be written as (with $\Delta = 0$)

$$H \equiv \begin{pmatrix} PHP & PHQ \\ QHP & QHQ \end{pmatrix},$$

where P and Q are the projectors on the subspaces with energy $\nu = 0$ and $\nu > 0$, respectively. A general wavefunction can be decomposed as

$$\Psi \equiv \begin{pmatrix} P\Psi \\ Q\Psi \end{pmatrix},$$

and, hence, the time-dependent Schrödinger equation reads:

$$i\partial_t \begin{pmatrix} P\Psi \\ Q\Psi \end{pmatrix} = \begin{pmatrix} PHP & PHQ \\ QHP & QHQ \end{pmatrix} \begin{pmatrix} P\Psi \\ Q\Psi \end{pmatrix}. \tag{7.12}$$

Due to the large energetic gap between the different subspaces and since the initial state is $|0\rangle$ that belongs to the subspace with $\nu = 0$, the transition probability to states with $E_\nu \neq E_0$ is very small. Thus, we can introduce an approximation assuming that the time variation of $Q\Psi$ is very small and can therefore be neglected, i.e., $\partial_t(Q\Psi) = 0$ (adiabatic elimination of the high-lying energy levels). Hence, the equation of motion (7.12) is reduced to

$$i\partial_t(P\Psi) = \left(PHP - PHQ(QHQ)^{-1}QHP \right)(P\Psi). \tag{7.13}$$

Note that, in this expression, $PHP \equiv H_P$ is the Hamiltonian within the perfect blockade regime. Whereas, the second term provides the first correction to this Hamiltonian and represents the contribution of the couplings between the $\nu = 0$ and $\nu > 0$ subspaces. In practice, the subspace with $\nu = 0$ is only coupled to those with $\nu = 1$ and 2 (see Fig. 7.1) by the Hamiltonian (6.3). As a consequence, the Hamiltonian can be rewritten as

$$H \equiv \begin{pmatrix} H_P & \Omega_{01} & \Omega_{02} & 0 \\ \Omega_{10} & \beta + \Omega_1 & \Omega_{12} & \Omega_{1R} \\ \Omega_{20} & \Omega_{21} & 2\beta + \Omega_2 & \Omega_{2R} \\ 0 & \Omega_{R1} & \Omega_{R2} & \beta_R + \Omega_R \end{pmatrix}, \tag{7.14}$$

where the subscript R denotes the energetic levels with $\nu > 2$, and the Ω_{ab} represents the part of the laser Hamiltonian that couples the states of the subspaces with $\nu = a$ and $\nu' = b$, e.g., Ω_{01} represents the block that couples the $\nu = 0$ and $\nu' = 1$ subspaces. In expression (7.14), QHQ can be decomposed into the sum of a diagonal matrix, $\bar{\beta}$, including the interaction between the subspaces, and a full matrix containing the couplings $\bar{\Omega}$,

$$QHQ = \begin{pmatrix} \beta & 0 & 0 \\ 0 & 2\beta & 0 \\ 0 & 0 & \beta_R \end{pmatrix} + \begin{pmatrix} \Omega_1 & \Omega_{12} & \Omega_{1R} \\ \Omega_{21} & \Omega_2 & \Omega_{2R} \\ \Omega_{R1} & \Omega_{R2} & \Omega_R \end{pmatrix} \equiv \bar{\beta} + \bar{\Omega}.$$

The inverse of this matrix can be approximated by

$$(QHQ)^{-1} = \frac{1}{\bar{\beta} + \bar{\Omega}} \approx \bar{\beta}^{-1} - \bar{\beta}^{-1}\bar{\Omega}\bar{\beta}^{-1} + \dots,$$

where we have used the Neumann series $(\mathbb{I} - T)^{-1} = \sum_{n=0}^{\infty} T^n$ for a square matrix T whose norm satisfies that $\|T\| < 1$. Since $\beta \gg \Omega_{ab}$ for any a and b, this condition is accomplished for $T = \bar{\beta}^{-1}\bar{\Omega}$. Finally, we obtain the following expression for the effective Hamiltonian

$$H_{\text{eff}} = H_P - \frac{\Omega_{01}\Omega_{10}}{\beta} - \frac{\Omega_{02}\Omega_{20}}{2\beta} + O(1/\beta^2), \tag{7.15}$$

where we only consider the first three terms and neglect higher order corrections.

Let us now discuss the regime of validity of the approximate Hamiltonian (7.15). To this end it is instructive to study a case in which the full Hamiltonian (6.3) is numerically tractable. This however, can only be done for a small number of sites. In the absence of the laser the eigenstates of Hamiltonian (6.3) are those of H_{int}, i.e., the highly degenerate ν-manifolds. As soon as the laser is turned on this degeneracy is lifted and all the ν manifolds split up. However, if β is sufficiently large the manifolds are still well separated. This regime is presented in Fig. 7.10 where we show a histogram of the eigenenergies (density of states) for a lattice with $L = 15$ and $\beta = 20$ in units of Ω. Since in this case the system can contain at most 15 pairs of consecutive Rydberg atoms, we observe 15 manifolds, i.e., $0 \leq \nu \leq 15$ (remember that the value $\nu = 14$ does not exist, as we explained at the beginning of Section 7.1). The energetic separation between the central states of two neighboring subspaces is given by β. A magnified view of the spectral structure for the low-lying excitations is shown in the inset of Fig. 7.10. Within the framework of the adiabatic elimination the contribution of the $\nu = 1$ and 2 manifolds is included up to order $\frac{\Omega}{\beta}$ in the effective Hamiltonian (7.15). The validity of this approximation is restricted to parameter regimes in which states belonging to different manifolds are energetically well-separated, e.g., two adjacent manifolds must not overlap. For $L = 15$, $\beta = 20$ is the minimal value needed to ensure this separation. For larger lattices sizes, the value of β has to be increased since with growing L the ν-manifolds contain more and more states and thus become successively broader. For example, the width of the $\nu = 0$ manifold scales proportional to L.
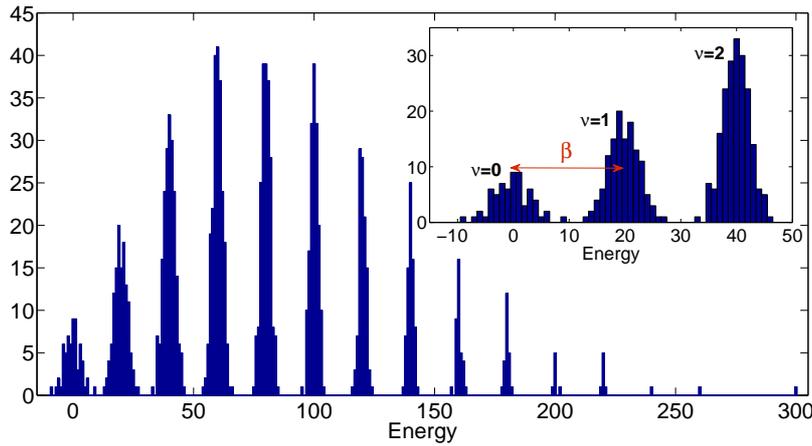
Figure 7.10.: Histogram of all the eigenvalues (density of states) of the full Hamiltonian for a system with $L = 15$ and $\beta = 20$ (units of Ω). The parameters are chosen such that the individual ν-manifolds are still recognizable. The inset shows a magnified view of the manifolds with $\nu = 0, 1, 2$, which are broadened by the interaction with the laser.
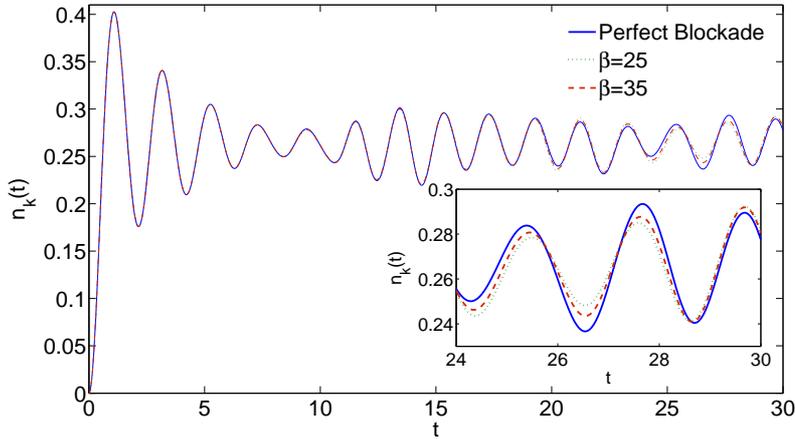
Figure 7.11.: The Rydberg density as a function of time for $L = 20$ computed with the perfect blockade treatment, and with the adiabatic elimination scheme using $\beta = 25$ and 35.

We have investigated the dynamics of a ring with $L = 20$ sites in the framework of the adiabatic elimination using $\beta = 25$ and 35. In Figs. 7.11 and 7.12 we show the Rydberg density and a density-density correlation function (for $k = 2$) and compare them with the results obtained within the perfect blockade approximation. The occurring deviations are small. Only minor differences are observed at large times, and we encounter relative errors below 6.5% and 4% for $\beta = 25$ and 35, respectively. The results show that the approximated inclusion of higher ν-subspaces in the dynamics does only lead to small quantitative changes in the behavior of the investigated properties. As anticipated, the deviations reduce significantly as β is increased. More qualitative differences are expected to occur if the r^{-6}-tail of the Rydberg-Rydberg interaction is properly accounted for.

7.5. Summary and conclusions

In this chapter we have performed a numerical analysis of the laser-driven Rydberg excitation dynamics of atoms confined to a ring lattice. By exploiting the symmetry properties of the system and employing the assumption of a perfect Rydberg blockade we were able to perform numerically
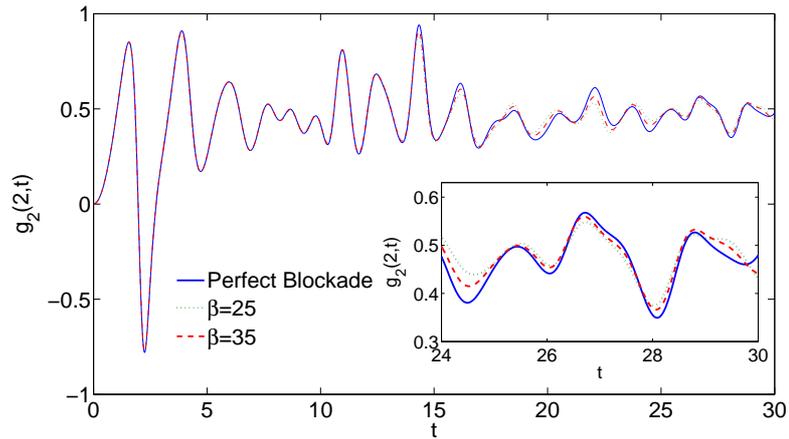
Figure 7.12.: Correlation function for $k = 2$ as a function of time for $L = 20$ computed with the perfect blockade treatment, and with the adiabatic elimination scheme using $\beta = 25$ and 35.

exact calculations in lattices with up to $L = 25$ sites. Our findings show that the temporal evolutions of the physical quantities, e.g., the Rydberg density and the density-density correlations, can be divided into two domains. For short times, one observes an L-independent universal behavior with large amplitude oscillations. For longer times, the dynamics is crucially determined by the lattice size and the analyzed properties appear to assume a quasi steady state with only small temporal fluctuations. Moreover, we studied the evolution of the entanglement as well as the quantum and classical correlations of two neighboring sites. By separating the quantum and classical part of the two-party correlation we showed that quantum correlations between neighboring sites decay rapidly as time passes. In addition, the entanglement between neighboring sites turned out to be weak in the long time limit after a quick initial increase. We eventually relaxed the perfect blockade condition by taking into account higher excitation subspaces via adiabatic elimination. Propagating the initial vacuum state with the corresponding effective Hamiltonian has only small effect on the time evolution of the investigated observables.

In the present work we have been focusing on the dynamical properties of this system. A next step would be to focus on the corresponding static properties, such as eigenstates and eigenvalues. We address this topic in Chapter 9, where we characterize the many-particle eigenstates and explain how to address them experimentally.

Most of the results presented in this chapter are published in Ref. [114].

8. Thermalization of a strongly interacting 1D Rydberg lattice gas

The steady state shown in Fig. 7.3 is the result of a purely *coherent dynamics of a closed system* and does not come about due to dissipation stemming from the coupling to an external bath. In this chapter we perform a closer investigation of this steady state. In particular, we study the evolution of the atomic gas in excitation number space, i.e., between subspaces of the system's Hilbert space which contain the same number of Rydberg atoms. Throughout, we employ the *perfect blockade* model of a Rydberg gas introduced in Section 7.1. When studying the evolution in excitation number space under the action of the laser, we find that the strong interaction causes quasi-random couplings between regions of the Hilbert space which contain a different (and well-defined) number of Rydberg atoms. This randomness allows us to derive an effective equation for the time evolution of the probability of being in a subspace with certain fixed excitation number. The resulting equation possesses a steady state which solely depends on the dimension of the excitation number subspaces. A comparison to the results obtained from the numerically exact propagation of the Schrödinger equation performed in the previous chapter shows good agreement.

8.1. Hamiltonian in excitation number space

Due to the strong interaction a formulation of the problem in terms of the physical degrees of freedom (localized atoms) seems disadvantageous. Instead, it appears more natural to base the discussion on the graph depicted in Fig. 7.2. Initially the system is localized on the leftmost vertex of the graph, i.e., it resides in the vacuum state $|0\rangle = \prod_{k=1}^{L} |P\rangle_k$. Once the laser is turned on, coupling to neighboring vertices is established and the propagation of population through the graph sets in. Eventually, the mean Rydberg number is determined by the probability $\rho_m(t)$ of the system to be in the subspace containing m excitations:

$$n_{\mathrm{r}}(t) = \sum_{m=0}^{n_{\max}} m \, \rho_m(t), \tag{8.1}$$

where $n_{\max}$ is the next integer smaller than or equal to $L/2$. $\rho_m(t)$ is hereby the probability density derived from $|\Psi(t)\rangle = \exp(-iH_L t)\,|0\rangle$ and integrated over each column of the graph. Note that the expressions

$$n_{\mathrm{r}}(t) = \langle \Psi(t)| \sum_{k=1}^{L} \frac{1 + \sigma_z^{(k)}}{2} |\Psi(t)\rangle$$

and (8.1) are equivalent.

In order to make the excitation number spaces explicitly appear in the equations, we use the following matrix representation of the wave function:

$$\boldsymbol{\Psi} = \begin{pmatrix} \vdots \\ \boldsymbol{\Psi}_{m-1} \\ \boldsymbol{\Psi}_m \\ \boldsymbol{\Psi}_{m+1} \\ \vdots \end{pmatrix} = \boldsymbol{\Psi}_0 \oplus ... \oplus \boldsymbol{\Psi}_m \oplus ... \oplus \boldsymbol{\Psi}_{n_{\max}}.$$

The vectors Ψ_m are the projections of the wave function onto the space with m excitations and contain $\dim_m$ components which are labeled by the indices $\alpha_m = 1, ..., \dim_m$, i.e., $\dim_m$ is the number of possibilities of placing m Rydberg atoms on the ring that are compatible with the constraint (7.2). The probabilities ρ_m are defined by

$$\rho_m = \mathbf{\Psi}_m^\dagger \mathbf{\Psi}_m. \tag{8.2}$$

In this representation the Hamiltonian becomes

$$H = \begin{pmatrix} 0 & \ddots & 0 & 0 & 0 \\ \ddots & 0 & \mathcal{C}_{n-1,n} & 0 & 0 \\ 0 & \mathcal{C}_{n-1,n}^\dagger & 0 & \mathcal{C}_{n,n+1} & 0 \\ 0 & 0 & \mathcal{C}_{n,n+1}^\dagger & 0 & \ddots \\ 0 & 0 & 0 & \ddots & 0 \end{pmatrix} \tag{8.3}$$

where the operators $\mathcal{C}_{n-1,n}$ and $\mathcal{C}_{n-1,n}^\dagger$ connect the subspaces which contain $n-1$ and n Rydberg atoms. Each of the subspaces contains $\dim_n$ states. Hence, $\mathcal{C}_{n,n+1}$ is a $\dim_n \times \dim_{n+1}$-matrix. The block structure of the Hamiltonian (8.3) is a direct consequence of the property of the laser Hamiltonian to couple only subspaces whose excitation number differs by one.

The projection operator onto the space containing n Rydberg atoms is given by $|n\rangle\langle n|$, and we can define $\Psi_n = \langle n \,|\, \Psi \rangle$. This allows us to rewrite Hamiltonian (8.3) more compactly as

$$H = \sum_{n,m=0}^{n_{\max}} |m\rangle\langle m| H |n\rangle\langle n| = \sum_{n=0}^{n_{\max}-1} \left[\mathcal{C}_{n,n+1} |n\rangle\langle n+1| + \mathcal{C}_{n,n+1}^\dagger |n+1\rangle\langle n| \right].$$

8.2. Time evolution in the excitation number subspace

8.2.1. Time evolution of the projection operators

Our goal is to obtain the time evolution of the projection operators $|m\rangle\langle m|$. This will eventually enable us to calculate the quantities $\rho_m(t)$. To this end, we consider the Heisenberg equation of motion

$$\partial_t |m\rangle\langle m| = i \left[H, |m\rangle\langle m| \right]$$

which can be formally integrated to yield

$$|m\rangle\langle m|_t - |m\rangle\langle m|_0 = i \int_0^t dt' \left[H, |m\rangle\langle m|_{t'} \right].$$

For small times τ, we obtain up to second order

$$|m\rangle\langle m|_\tau - |m\rangle\langle m|_0 = i\tau \left[H, |m\rangle\langle m|_0 \right] - \frac{\tau^2}{2} \left[H, \left[H, |m\rangle\langle m|_0 \right] \right]. \tag{8.4}$$

With $|m\rangle\langle m|_0 \equiv |m\rangle\langle m|$ the first commutator evaluates to

$$\begin{aligned} \left[H, |m\rangle\langle m| \right] &= \mathcal{C}_{m-1,m} |m-1\rangle\langle m| + \mathcal{C}_{m,m+1}^\dagger |m+1\rangle\langle m| \\ &\quad - \mathcal{C}_{m,m+1} |m\rangle\langle m+1| - \mathcal{C}_{m-1,m}^\dagger |m\rangle\langle m-1| \\ &= \mathcal{C}_{m,m-1}^\dagger |m-1\rangle\langle m| - \mathcal{C}_{m,m-1} |m\rangle\langle m-1| \\ &\quad + \mathcal{C}_{m,m+1}^\dagger |m+1\rangle\langle m| - \mathcal{C}_{m,m+1} |m\rangle\langle m+1|. \end{aligned}$$

a

b
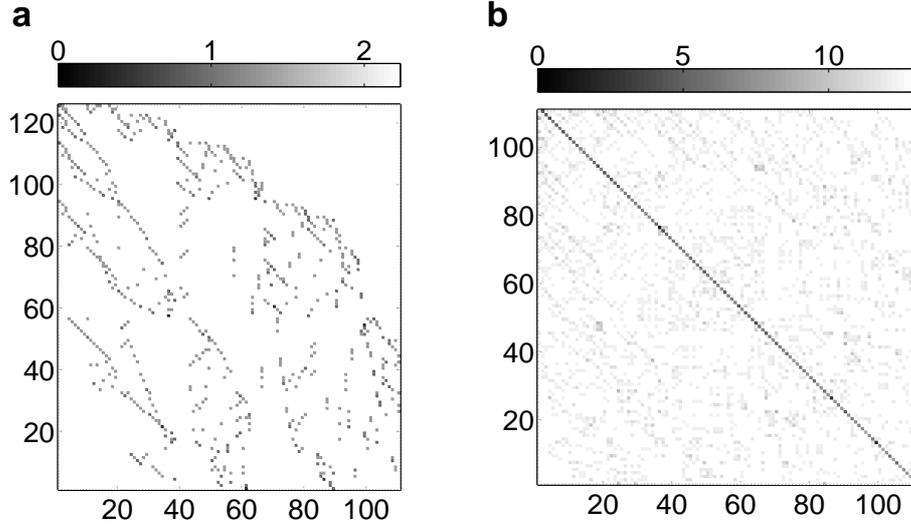
Figure 8.1.: **a**: Representation of the matrix $\mathcal{C}_{5,6}$ for $L = 20$ and **b**: The product $\mathcal{C}_{5,6}\mathcal{C}_{6,5}$, that is a quasi-diagonal matrix, which supports the assumption of the entries of the matrices $\mathcal{C}^{\dagger}_{m-1,m}$ being uncorrelated.

where we have used $\mathcal{C}_{m-1,m} = \mathcal{C}^{\dagger}_{m,m-1}$. The second double-commutator becomes

$$
\begin{aligned}
\frac{1}{2}\left[H,[H,|m\rangle\langle m|]\right] &= \left[\mathcal{C}_{m,m+1}\mathcal{C}^{\dagger}_{m,m+1} + \mathcal{C}_{m,m-1}\mathcal{C}^{\dagger}_{m,m-1}\right]|m\rangle\langle m| \\
&\quad -\mathcal{C}^{\dagger}_{m,m-1}\mathcal{C}_{m,m-1}|m-1\rangle\langle m-1| - \mathcal{C}^{\dagger}_{m,m+1}\mathcal{C}_{m,m+1}|m+1\rangle\langle m+1| \\
&\quad -\mathcal{C}^{\dagger}_{m-1,m}\mathcal{C}_{m,m+1}|m-1\rangle\langle m+1| - \mathcal{C}^{\dagger}_{m,m+1}\mathcal{C}_{m,m-1}|m+1\rangle\langle m-1| \\
&\quad +\frac{1}{2}\left[\mathcal{C}^{\dagger}_{m-1,m-2}\mathcal{C}^{\dagger}_{m,m-1}|m-2\rangle\langle m| + \mathcal{C}_{m,m-1}\mathcal{C}_{m-1,m-2}|m\rangle\langle m-2|\right. \\
&\quad +\left.\mathcal{C}^{\dagger}_{m+1,m+2}\mathcal{C}^{\dagger}_{m,m+1}|m+2\rangle\langle m| + \mathcal{C}_{m,m+1}\mathcal{C}_{m+1,m+2}|m\rangle\langle m+2|\right].
\end{aligned}
$$

8.2.2. Effective equation of motion for ρ_m

Using Eq. (8.4) and the definition $\rho_m = \boldsymbol{\Psi}^{\dagger}_m \boldsymbol{\Psi}_m = \langle \Psi \mid m\rangle\langle m \mid \Psi\rangle$ we find

$$
\rho_m(\tau) - \rho_m(0) = i\tau\,\langle\Psi|\,[H,|m\rangle\langle m|]\,|\Psi\rangle - \frac{\tau^2}{2}\,\langle\Psi|\,[H,[H,|m\rangle\langle m|]]\,|\Psi\rangle. \tag{8.5}
$$

The first commutator contains terms of the form

$$
\begin{aligned}
\langle\Psi\mid m-1\rangle\,\mathcal{C}^{\dagger}_{m,m-1}\,\langle m\mid\Psi\rangle &= \boldsymbol{\Psi}^{\dagger}_{m-1}\mathcal{C}^{\dagger}_{m,m-1}\boldsymbol{\Psi}_m \\
&= \sum_{\alpha_{m-1}=1}^{\dim_{m-1}}\sum_{\beta_m=1}^{\dim_m}\left[\boldsymbol{\Psi}^{\dagger}_{m-1}\right]_{\alpha_{m-1}}\left[\mathcal{C}^{\dagger}_{m,m-1}\right]_{\alpha_{m-1},\beta_m}\left[\boldsymbol{\Psi}_m\right]_{\beta_m} \\
&= \sum_{\alpha_{m-1}\beta_m}\left[\boldsymbol{\Psi}^{\dagger}_{m-1}\right]_{\alpha_{m-1}}\left[\mathcal{C}_{m,m-1}\right]_{\beta_m,\alpha_{m-1}}\left[\boldsymbol{\Psi}_m\right]_{\beta_m}, \tag{8.6}
\end{aligned}
$$

where we have exploited that $\mathcal{C}^{\dagger}_{m-1,m}$ is a real matrix.

The interaction between the Rydberg atoms manifests itself in the structure of the matrices $\mathcal{C}^{\dagger}_{m-1,m}$, which were initially constructed in a product basis in which the single atoms constitute the fundamental degrees of freedom. The strong interaction, however, favors collective excitations

which are complex superpositions of the single atom excitations. It is thus reasonable to assume that the single atom degrees of freedom are so strongly mixed that the entries of $\mathcal{C}^{\dagger}_{m-1,m}$ can be regarded as uncorrelated. Saying that the elements of a real matrix M of dimension $\dim_f \times \dim_c$ are uncorrelated means that they accomplish

$$\langle M_{ij} M_{kl} \rangle - \langle M_{ij} \rangle \langle M_{kl} \rangle = \kappa \delta_{ik} \delta_{jl},$$

or, in other words,

$$\langle (MM^{\dagger})_{il} \rangle = \sum_{j=1}^{\dim_c} \langle M_{ij} M_{jl} \rangle = \kappa \delta_{il} + \overline{m}^2,$$

where we have denoted the average value of the entries by $\overline{m}$. If, as it is the case with the $\mathcal{C}_{m-1,m}$ matrices, the average value $\overline{m}$ is much smaller than the autocorrelation coefficient κ, one sees that the corresponding product matrix is diagonal. In Fig. 8.1a we represent the matrix $\mathcal{C}_{5,6}$ for $L = 20$ and the corresponding product $\mathcal{C}_{5,6}\mathcal{C}_{6,5}$ in Fig. 8.1b, and one can observe that in effect the entries of these matrices can be considered uncorrelated. In this case the expression

$$\Sigma = \sum_{\alpha_{m-1}\beta_m} \left[\Psi^{\dagger}_{m-1}\right]_{\alpha_{m-1}} \left[\mathcal{C}_{m,m-1}\right]_{\beta_m,\alpha_{m-1}} \left[\Psi_m\right]_{\beta_m}$$

just becomes a sum of random complex numbers. Its magnitude $|\Sigma|$ can be estimated as follows: The components of the wave vector can be approximated by $[\Psi_m]_{\beta_m} \approx (\dim)^{-1/2} e^{i\phi_{\beta_m}}$, with $\dim = \sum_{n=0}^{n_{\max}} \dim_n$ and ϕ_{β_m} being some phase. With this we can obtain

$$|\Sigma| \sim \frac{c_{m,m-1}}{\dim} \left| \sum_{\alpha_{m-1}\beta_m} e^{i(\phi_{\beta_m} - \phi_{\alpha_{m-1}})} \right| \approx \frac{c_{m,m-1}}{\dim} \sqrt{\dim_m \dim_{m-1}},$$

where we have assumed that the complex numbers $e^{i(\phi_{\beta_m} - \phi_{\alpha_{m-1}})}$ are randomly (uniformly) distributed. This allows us to employ the relation $|\sum_{k=1}^{L} e^{i\alpha_k}| \approx \sqrt{L}$ since in case of randomly distributed α_k we are just dealing with a random walk in two dimensions. The constant $c_{m,m-1}$ relates to the mean value of the entries of the matrix $\mathcal{C}_{m,m-1}$.

The same line of argument holds true for terms stemming from the double commutator which are of the form

$$\langle \Psi \mid m \rangle \mathcal{C}_{m,m+1} \mathcal{C}_{m+1,m+2} \langle m+2 \mid \Psi \rangle. \tag{8.7}$$

Since the entries of the matrices $\mathcal{C}_{m,m+1}$ and $\mathcal{C}_{m+1,m+2}$ are not correlated, their product is again a matrix with randomly distributed elements. The magnitude of these terms can be estimated by employing again the picture of the random walk in two dimensions. The modulus of (8.7) then approximately evaluates to $c_{m,m+1,m+2}\sqrt{\dim_m \dim_{m+2}}/\dim$, where $c_{n,m+1,m+2}$ is a constant related to the mean value of the entries of $\mathcal{C}_{m,m+1}\mathcal{C}_{m+1,m+2}$.

Qualitatively different, however, are the terms of the form

$$\langle \Psi \mid m \rangle \mathcal{C}_{m,m+1} \mathcal{C}^{\dagger}_{m,m+1} \langle m \mid \Psi \rangle = \sum_{\alpha_m \beta_m} \left[\Psi^{\dagger}_m\right]_{\alpha_m} \left[\Psi_m\right]_{\beta_m} \sum_{\gamma_{m+1}} \left[\mathcal{C}_{m,m+1}\right]_{\alpha_m,\gamma_{m+1}} \left[\mathcal{C}_{m,m+1}\right]_{\beta_m,\gamma_{m+1}},$$

where the matrix $\mathcal{C}_{m,m+1}$ appears twice. Since the matrix elements of $\mathcal{C}_{m,m+1}$ are uncorrelated only the diagonal elements of the matrix product yield on average a non-zero value, hence

$$\sum_{\gamma_{m+1}} \left[\mathcal{C}_{m,m+1}\right]_{\alpha_m,\gamma_{m+1}} \left[\mathcal{C}_{m,m+1}\right]_{\beta_m,\gamma_{m+1}} \approx \left[\kappa_{m,m+1}\right]_{\alpha_m} \delta_{\alpha_m,\beta_m}.$$

Moreover, since the results cannot depend on the choice of the basis functions spanning a given m-excitation subspace, we can say that $[\kappa_{m,m+1}]_{\alpha_m} = \kappa_{m,m+1}$ and, thus,

$$\begin{aligned}
\langle \Psi \mid m \rangle \mathcal{C}_{m,m+1} \mathcal{C}^{\dagger}_{m,m+1} \langle m \mid \Psi \rangle &\approx \kappa_{m,m+1} \sum_{\alpha_m} \left[\Psi^{\dagger}_m\right]_{\alpha_m} \left[\Psi_m\right]_{\alpha_m} \\
&= \kappa_{m,m+1} \Psi^{\dagger}_m \Psi_m = \kappa_{m,m+1} \rho_m(0). \tag{8.8}
\end{aligned}$$

Hence, estimating $\kappa_{m,m+1} \propto \dim_{m+1}$ the modulus of these (diagonal) terms is proportional to $\dim_m \dim_{m+1}/\dim$.

We now return to Eq. (8.5). We neglect all terms of the form (8.6) and (8.7) and keep only the dominant ones, e.g., those which contain products of the form $\mathcal{C}_{m,m+1} \mathcal{C}^\dagger_{m,m+1}$. By this we obtain

$$
\begin{aligned}
\rho_m(\tau) - \rho_m(0) \quad &\approx \quad -\tau^2 \left[\kappa_{m,m+1} + \kappa_{m,m-1}\right] \rho_m(0) \\
&\quad + \tau^2 \left[\kappa_{m-1,m}\rho_{m-1}(0) + \kappa_{m+1,m}\rho_{m+1}(0)\right].
\end{aligned}
$$

Here we have used

$$
\sum_{\alpha_m} \left[\mathcal{C}_{m,m+1}\right]_{\alpha_m,\beta_{m+1}} \left[\mathcal{C}_{m,m+1}\right]_{\alpha_m,\gamma_{m+1}} \approx \kappa_{m+1,m}\delta_{\beta_{m+1},\gamma_{m+1}},
$$

from which follows that

$$
\frac{\kappa_{m+1,m}}{\kappa_{m,m+1}} = \frac{\dim_m}{\dim_{m+1}}.
$$

We can thus make the ansatz $\kappa_{m,m+1} = u_m\dim_{m+1}$ and $\kappa_{m+1,m} = u_m\dim_m$ and find, omitting the $t = 0$ argument of $\rho_m(0)$,

$$
\begin{aligned}
\rho_m(\tau) - \rho_m \quad &\approx \quad -\tau^2 \left[u_m\dim_{m+1} + u_{m-1}\dim_{m-1}\right] \rho_m \\
&\quad + \tau^2 \left[u_{m-1}\dim_m\rho_{m-1} + u_m\dim_m\rho_{m+1}\right].
\end{aligned} \tag{8.9}
$$

This equation does not take into account coherent processes which have effectively been eliminated by the neglect of terms of the form (8.6) and (8.7). Thus Eq. (8.9) cannot be valid for arbitrary small values of τ as here certainly coherent effects dominate the evolution. Instead, the interval τ has to be chosen sufficiently large such that terms of the form (8.8) dominate all other contributions whose importance diminishes due to the summation of complex numbers with random phases. Eq. (8.9) is thus a map that propagates the vector $\rho(t_0)$ by a 'coarse-grained' timestep τ, i.e., $\rho(t_0) \rightarrow \rho(t_0 + \tau)$. τ is thereby chosen much smaller than the typical timescale which governs the evolution of $\rho_m(t)$.

8.3. The steady state

The steady state is defined through

$$
\rho_n^{\text{steady}}(\tau) - \rho_n^{\text{steady}} = 0, \tag{8.10}
$$

i.e., it is a fix point of the mapping (8.9). The mapping contains the unknown coefficients u_m which include information about how adjacent excitation subspaces are connected. Fortunately, in order to determine the steady state their knowledge is not necessary. It is only required that $u_m \neq 0$, which is always the case. The solution of Eq. (8.10) is given by

$$
\rho_n^{\text{steady}} = \frac{\dim_n}{\dim}. \tag{8.11}
$$

Thus it is only the number of states contained in a given excitation number subspace that determines the steady state. It is actually possible to calculate the dimension of the subspaces with fixed number of excitations, analytically. This is done by counting all states of the single atom product basis that contain m excited atoms and obey condition (7.2). The result is

$$
\rho_m^{\text{steady}} = \frac{1}{\dim} \frac{L}{L-m} \binom{L-m}{m} \qquad \text{with} \qquad \dim = \sum_{m=0}^{n_{\max}} \frac{L}{L-m} \binom{L-m}{m}. \tag{8.12}
$$

Note, that this result encompasses all possible basis states and not only the fully symmetric ones which constitute the graph (7.2). It is interesting to see how ρ_m^{steady} behaves in the limit of large L, where we have $n_{\text{max}} = L/2$. It is convenient to introduce the variable $\alpha = m/L$ which is the number of Rydberg atoms divided by the number of sites. Using Stirling's formula we can approximate Eq. (8.12) by

$$\rho_m^{\text{steady}} \propto \frac{1}{\sqrt{2\pi L}} \sqrt{\frac{1-\alpha}{\alpha(1-2\alpha)}} \left(\frac{(1-\alpha)^{1-\alpha}}{\alpha^\alpha (1-2\alpha)^{1-2\alpha}} \right)^L . \tag{8.13}$$

This function has a very pronounced peak and, for large L, we can approximate $\rho_m^{\text{steady}}(\alpha)$ by a Gaussian. The position of the maximum of the function is the solution of the equation

$$\ln \alpha + \ln (1-\alpha) - 2\ln (1-2\alpha) - \frac{1}{L(1-2\alpha)} + \frac{1}{2L\alpha(1-\alpha)} = 0,$$

where $\ln(x)$ is the natural logarithm. Since the number of sites L is taken to be very large, we can neglect the last two terms, and then obtain that the function (8.13) assumes its maximum at

$$\alpha_{\text{max}} = \frac{1}{2} \left[1 - \frac{1}{\sqrt{5}} \right] \approx 0.276.$$

Around this peak value the squared width of $\rho_m^{\text{steady}}(\alpha)$ is given by

$$\sigma_\alpha^2 = \frac{1}{5\sqrt{5}L}$$

Hence, for large L the probability distribution in particle number space is strongly peaked with an overwhelming weight on α_{max}. The mean number of Rydberg atoms in the steady state is thus expected to be $\bar{n}_r = \alpha_{\text{max}} \times L$ and the fluctuation should vanish. The value of $\bar{n}_r$ is slightly bigger than the values reported in Ref. [81] and in the previous chapter of this work. As we will see in the next section this is due to the particular choice of the initial state. In Appendix B, a more thorough derivation of the form of the steady state in performed for a blockade radius that goes beyond the nearest neighbor site. There, the results are also compared to the ones obtained from a numerical time evolution of the system.

The distribution $\rho_m^{\text{steady}}(\alpha)$ contains the full statistics of the Rydberg atom number count. Strong interactions are known to have an effect on the counting statistics leading to a sub-Poissonian distribution [119, 120] of the Rydberg number. A measure for this is given by the Mandel Q-parameter

$$Q = \frac{\bar{n_r^2} - \bar{n}_r^2}{\bar{n}_r} - 1, \tag{8.14}$$

which is negative/positive for a sub-/super-Poissonian distribution of the Rydberg atom number count. In the steady state we find

$$Q_{\text{steady}} = \frac{L\sigma_\alpha^2}{\alpha_{\text{max}}} - 1 = \frac{\sqrt{5} - 9}{10} \approx -0.676 \tag{8.15}$$

which shows the expected sub-Poissonian behavior.

For the sake of completeness let us consider the case of non-interacting atoms. Here one obtains for the probability density

$$\rho_m(t) = \binom{L}{m} \sin^{2L} t \cos^{2L-2m} t \tag{8.16}$$

and hence the probability density in excitation number space performs an oscillatory motion at all times.
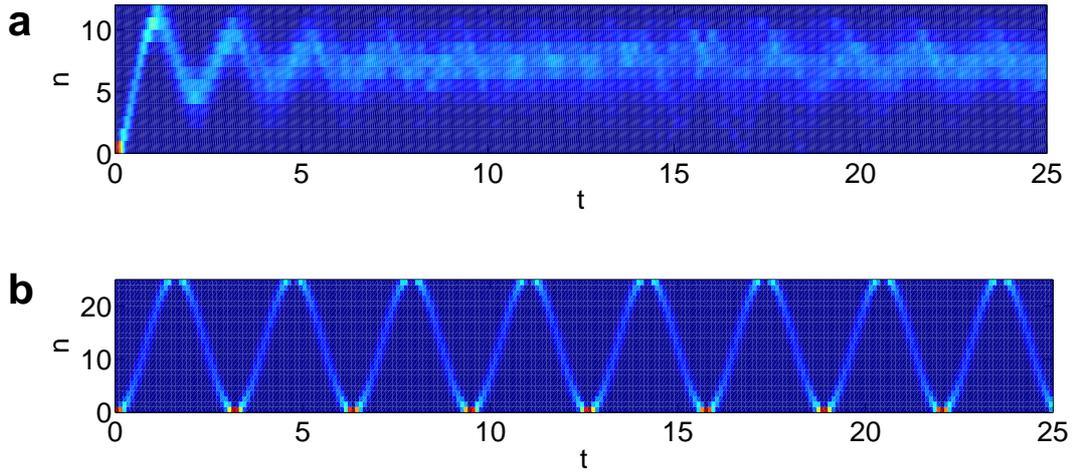
Figure 8.2.: Temporal evolution of the system consisting of 25 atoms in particle number space. Initially all atoms are in the ground state, i.e., $\rho_0 = 1$. **a:** In the interacting case (perfect blockade) the system reaches eventually a state in which the probability density localizes in excitation number space. **b:** This is not the case in the absence of interactions. Here, the wave packet performs coherent oscillations with maximal amplitude. Note the different scale of the n-axis.
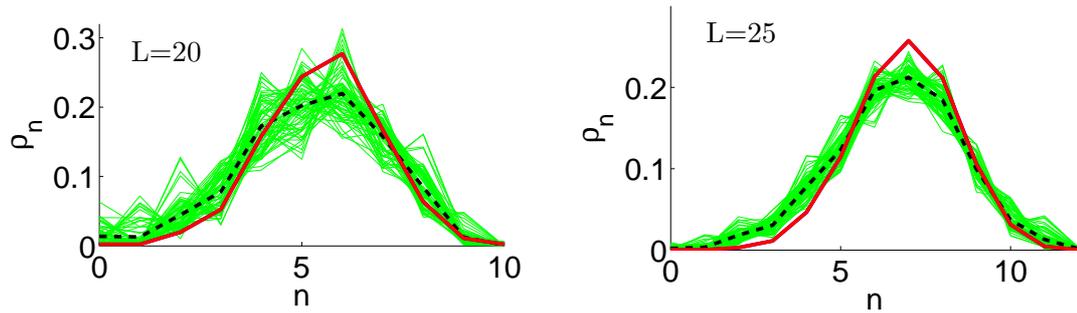
Figure 8.3.: Probability density ρ_n in excitation number space for $L = 20$ and $L = 25$. The green (thin) curves are snapshots taken during the interval $100 \le t \le 104$. For these times the calculated Rydberg number shows the steady state shown in Fig. 7.3. The dashed curve is obtained by taking the average over the set of snapshots. The red curve shows ρ_n^{steady} as given by Eq. (8.10).

8.4. Numerical results

We are now going to compare the results that we obtained in the previous section to the actual data extracted from a numerical propagation of the Schrödinger equation. In order to make the numerical solution feasible we massively exploit the symmetry properties of the system. In all numerical calculations we refer to the set of basis states which are invariant under cyclic shifts and reversal of the lattice sites as has been outlined in Section 6.2. Also, we operate only in a subspace of the space which is spanned by all states being compatible with the perfect blockade condition (7.2).

8.4.1. Evolution into the steady state

Let us start by inspecting the evolution of ρ_n when choosing the vacuum as initial state, i.e., $\rho_0 = 1$, and $L = 25$. The result is shown in Fig. 8.2a. For $t \le 5$ we observe a well-defined wave packet which propagates through the excitation number space performing an oscillatory motion. For longer times
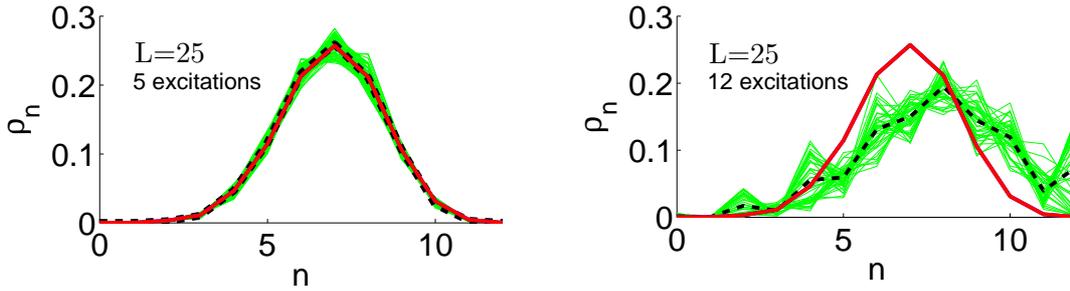
Figure 8.4.: The same plot as in Fig. 8.3 using a state containing 5 and 12 excitations as initial state. In the former case the fluctuations around the average value are small and the agreement with ρ_n^{steady} is remarkable. The latter shows substantial deviations from the steady state (8.11).

the amplitude of the oscillations decreases, however, the wave packet remains localized. There are still significant fluctuations visible. In particular in the interval $15 \leq t \leq 25$ remnants of the initial oscillations can be observed. In comparison to the non-interacting case which is shown in Fig. 8.2b the localization in excitation number space is apparent. As expected from Eq. (8.16) here the wave packet exhibits coherent oscillations with large amplitude.

8.4.2. The steady state and its dependence on the initial condition

We now proceed by monitoring $\rho_n(t)$ over a time-interval in which the number of Rydberg atoms shows the steady state behavior - here we choose $100 \leq t \leq 104$. The result is depicted in Fig. 8.3 for two values of L, 20 and 25. The thin green curves show individual snapshots of $\rho_n(t)$ taken at different times. In addition, we present also the average of $\rho_n(t)$ taken over the considered time-interval. The fluctuations around this average decrease significantly with increasing L. This is in accordance with the behavior of the Rydberg number n_r whose fluctuations around the mean value also diminish as L increases (see Chapter 7 and Ref. [114]). This supports the assumptions that in the limit of very large L indeed a steady state with extremely little fluctuations is established. For both values of L shown in Fig. 8.3 a comparison to the steady state result (8.11) (thick red curve) reveals a shift of the probability distribution to smaller n. These deviations appear to stem from the particular choice of the initial state: The state $|\Psi(0)\rangle = |0\rangle$ is localized at the leftmost vertex of the network. In this region of the graph the matrices $\mathcal{C}_{n,n+1}$ are, however, not actually random since the 'randomness' is caused by the interaction which has little or no effect when the number of Rydberg atoms is only very small, i.e., $n = 0, 1, 2$.

   That this 'edge effect' appears to be indeed the cause of the deviation of the probability distribution from ρ_n^{steady} is corroborated by the data shown in Fig. 8.4. Here we present the same plot as in Fig. 8.3 but the initial state has to be chosen from the subspace containing 5 excitations, e.g., it is located in the central region of the graph. The effect is not only a much better agreement of the data with ρ_n^{steady} but also a significant decrease of the fluctuations about the average of $\rho_n(t)$. This behavior is generic for initial states chosen from excitation number subspaces with large dimensions.

   Large deviations of the steady state from Eq. (8.11) are again encountered when the initial state is located close to the right hand edge of the graph, i.e., when its number of Rydberg atoms is close to n_{max} (see Fig. 8.4). Hence, it becomes evident that Eq. (8.9) is not unconditionally valid. It constitutes a reliable approximation only if the initial state belongs to a particle number subspace of sufficiently large dimension, i.e., far from the beginning and end of the graph 7.2. That it also works well, when as initial state the vacuum is chosen, is not evident.
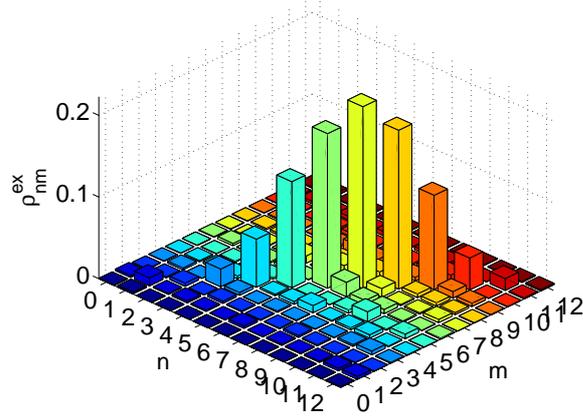
Figure 8.5.: Reduced density matrix in excitation number space ρ^{ex} at $t = 140$. ($L = 25$, initial state $|0\rangle$). Shown is the absolute value of the entries. ρ^{ex} is well-approximated by a completely mixed state.

8.4.3. Reduced density matrix in excitation number space

So far we have only studied the probability density distribution in excitation number space. Further insights can be gained by examining the reduced density matrix in excitation number space ρ^{ex} as this quantity eventually determines the outcome of a measurement of the number of Rydberg atoms. Its elements are defined by

$$\rho^{\text{ex}}_{nm} = \sum_{\alpha=1}^{\min(\dim_m, \dim_n)} \left[\boldsymbol{\Psi}_n \otimes \boldsymbol{\Psi}_m^\dagger \right]_{\alpha\alpha}. \tag{8.17}$$

In Fig. 8.5 we present a snapshot of $|\rho^{\text{ex}}|$ for a system of 25 sites at the time $t = 140$. The initial state was $|0\rangle$. We clearly observe that the entries of the main diagonal dominate the off-diagonal entries. Hence, there is negligible coherence between excitation number subspaces which have a large dimension. Consequently, the reduced density matrix is well approximated by a classical mixture $\rho^{\text{ex}} \approx \sum_{n=0}^{n_{\max}} \rho_n |n\rangle \langle n|$. The strong interaction between the atoms in conjunction with the laser driving erases the phase relation between excitation number subspaces. So tracing out all degrees of freedom but those being relevant for the measurement of the Rydberg number, leaves us with a density matrix of a completely mixed state. This gives actually the impression that the steady state we observe is a state with maximal entropy, since only the dimension of the excitation number subspaces determines the outcome of the measurement (see Eq. (8.11)). In fact we are dealing with a pure state at all times and only the particular measurement we are performing gives us the impression of observing a completely mixed state.

8.4.4. Connection with the microcanonical ensemble

Note that all the information about the steady state could as well have been obtained by considering a microcanonical ensemble. Here, the microstates are just given by the zero energy eigenstates $\{|\phi\rangle\}$ of the interaction Hamiltonian H_{int} defined through condition (7.2) and the steady state given in Eq. (8.12) can be obtained directly by counting the number of these microstates. The fundamental assumption underlying the microcanonical ensemble is that each of the microstates has equal weight. This assumption can clearly not be justified in the absence of the laser, even though all states have the same energy. Only when the laser is present, the microstates $\{|\phi\rangle\}$ defined by (7.2) become strongly mixed and are, thus, no longer eigenstates of the system. However, they no longer possess strictly zero energy but are rather distributed over an energy interval which is centered at zero

and whose width is proportional to $L\Omega$. In other words, although the laser produces a widening of the energy window occupied by the states, it also provides the necessary ingredient that eventually allows the system to thermalize, the equiprobability of the microstates.

At this point we want to remark that the microcanonical prediction to the steady state (8.12) involves all zero energy eigenstates of H_{int}. On the other hand, the numerical results of Section 8.4 involve only a subset of all accessible states, i.e., the fully symmetric set of eigenstates. The observed agreement between the two approaches suggests that the number of fully symmetric eigenstates with a given excitation number m is proportional to $\dim_m$.

8.5. Summary and conclusions

We have investigated the origin of the steady state value of the Rydberg number which is exhibited in a laser driven Rydberg gas after an initial transient period. Starting from Heisenberg's equation we have derived an effective equation of motion for the probability density in excitation number space. This effective equation of motion which is coarse-grained in time exhibits a steady state. When comparing this steady state to actual numerical simulations excellent agreement is found provided that the initial state was chosen from an excitation subspace with sufficiently large dimension. In case of an initial state containing a very small/large number of excitations still a steady state is established, however, deviations from the analytical result are obtained.

We have visualized the system by a graph whose vertices are represented by eigenstates of the interatomic interaction. Coupling between the vertices is established by the laser-atom interaction. A similar mapping was applied in Refs. [121, 122] where interacting fermions were studied by means of a graph. Here, a transition between localized and delocalized eigenstates has been found to take place as a function of the interaction strength. In our system we are in the regime of strong interaction and the eigenstates are delocalized throughout the entire graph. The observed localization in excitation number space and hence also the observation of a steady state value of n_{r} is a purely statistical effect, owed to the strongly peaked function $\dim_m$.

It would be interesting to see whether a distribution of the Rydberg number count similar to Eq. (8.11) and - more specifically - the calculated values for the mean Rydberg number and the Mandel Q-parameter can be observed in actual experiments. Studying the shape and the temporal evolution of the distribution should yield insights into how this steady state is established as the interaction strength increases. Since our simple model is not expected to be valid in higher dimension experiments with Rydberg atoms in lattices could also help here to clarify whether and, if so, how a steady state is established.

Most of the results presented here can be found in the reference [97].

9. Strong laser driving: fermionic collective excitations

So far, we have studied our system's time evolution in the perfect blockade regime and found that it eventually thermalizes to a steady state. This state turns out to be a strongly mixed state product of the action of the laser field. It the following chapter, we pursue a different aim: to create many-particle pure states. To do so, we make use of the same system, described by the Hamiltonian (6.3), in a different parameter regime. In particular, we choose the strong laser driving regime ($\Omega \gg \beta$), and find that in this situation the Hamiltonian is exactly solvable. We characterize the arising many-particle states and show how to eventually excite them by just tuning the parameters of the laser. Finally, we introduce a fluctuating Rabi frequency in our Hamiltonian and make evident that it allows us to study fermions exposed to a disorder potential.

9.1. Constrained dynamics

Here we focus on the limit $\Omega \gg \beta$, i.e., the laser coupling is much stronger than the interaction between atoms. In this regime we can also assume that only nearest neighbor interaction occurs, which is justified since here $\Omega \gg \beta \gg V_2$. Thus, the Hamiltonian that describes the dynamics of the system reads as (7.1), i.e.,

$$H = \sum_{k=1}^{L} \left[\Omega \sigma_x^{(k)} + \Delta n_k + \beta n_k n_{k+1} \right]. \tag{9.1}$$

In this regime, the first term of the Hamiltonian (9.1) is the dominant one and it is convenient to make it diagonal by means of a rotation of the basis. This is achieved by the unitary transformation $U = \prod_{k=1}^{L} \exp\left(-i\frac{\pi}{4}\sigma_y^{(k)}\right)$ which brings $\sigma_x \to \sigma_z$ and $\sigma_z \to -\sigma_x$. When applied to Hamiltonian (9.1), it yields

$$H = U^\dagger H_{\text{spin}} U = \frac{\beta L}{4} + H_{\text{xy}} + H_1 + H_2, \tag{9.2}$$

with

$$H_{\text{xy}} = \sum_{k=1}^{L} \left[\Omega \sigma_z^{(k)} + \frac{\beta}{4} \left(\sigma_+^{(k)} \sigma_-^{(k+1)} + \sigma_-^{(k)} \sigma_+^{(k+1)} \right) \right] \tag{9.3}$$

$$H_1 = \frac{\Delta}{2} \sum_{k=1}^{L} \left(1 - \sigma_x^{(k)} \right) \tag{9.4}$$

$$H_2 = \frac{\beta}{4} \sum_{k=1}^{L} \left[\left(\sigma_+^{(k)} \sigma_+^{(k+1)} + \sigma_-^{(k)} \sigma_-^{(k+1)} \right) - 2\sigma_x^{(k)} \right], \tag{9.5}$$

where H_{xy} is the famous xy-model of a spin chain with a transverse magnetic field.

Let us now analyze the importance of the individual contributions of H. As we can see in Fig. 9.1, the spectrum of H decays into manifolds of states which are separated by gaps whose width is approximately 2Ω. This is caused by the dominant first term of H_{xy}. The eigenstates of $\sigma_z^{(k)}$ are - in terms of the (super)atom states - given by

$$|\pm\rangle_k = \frac{1}{\sqrt{2}} U^\dagger \left[|P\rangle_k \pm |R\rangle_k \right]$$
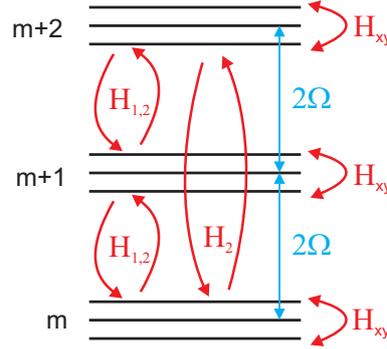
Figure 9.1.: Level structure in the regime $\Omega \gg \beta$ and $|\Delta| \ll \Omega$. The spectrum splits into manifolds which can be labeled by the quantum number m of the operator $\sum_k \sigma_z^{(k)}$. For sufficiently large Ω, the coupling between manifolds that is established only by H_1 and H_2 can be neglected. The (constrained) dynamics inside the m-subspaces is then determined by H_{xy}.

with $\sigma_z^{(k)} |\pm\rangle_k = \pm |\pm\rangle_k$. Thus, each of the manifolds that determine the coarse structure of the spectrum is spanned by a set of product states that have the same number of (super)atoms in the state $|+\rangle$. In Fig. 9.1, these manifolds are denoted by m, which is the eigenvalue of the states with respect to the operator $\sum_{k=1}^{L} \sigma_z^{(k)}$.

The second term of H_{xy} conserves the total number of $|+\rangle$ (super)atoms. In other words, it couples only states that belong to the same m-manifold and that are nearly degenerate. As a consequence, the strength of these intra-manifold couplings due to H_{xy} is proportional to β. Conversely, H_1 and H_2 couple states that belong to manifolds with different number of (super)atoms in the state $|+\rangle$. In particular, H_1 and the last term of H_2 flip one of the (super)atoms from $|+\rangle$ to $|-\rangle$ or viceversa. Thus, the coupled states belong to different manifolds with $\Delta m = \pm 1$, energetically separated by 2Ω. The two first terms of H_2 drive a similar process, flipping always two contiguous (super)atoms in the same state simultaneously, i.e., $|++\rangle \to |--\rangle$ or $|--\rangle \to |++\rangle$. As a result, these terms connect states with eigenvalue m to those with $m \pm 2$, which are separated roughly by 4Ω. These features are reflected in Fig. 9.1. The transition rates between m-manifolds corresponding to H_1 and H_2 can be estimated by second order perturbation theory to be of the order Δ^2/Ω and β^2/Ω, respectively. Hence, for sufficiently strong driving $\Omega \gg \beta$, their contribution can be neglected and the system's dynamics is constrained inside the m-manifolds. As a consequence, the Hamiltonian that drives the intra-manifold dynamics, H_{xy}, *effectively drives the dynamics of the entire system in this parameter regime*. This Hamiltonian is analytically solvable, and we thus have access to the actual spectrum and eigenstates of the system. The diagonalization of this Hamiltonian relies on the so-called Jordan-Wigner transformation and a Fourier transform that we explain thoroughly in the following paragraph [123].

9.2. Jordan-Wigner transformation on a ring

The Pauli matrices in the Hamiltonian (9.3) obey anti-commutation and commutation relations when they belong to the same and different sites, respectively. Thus, the algebra is neither bosonic nor fermionic. This difficulty can be overcome by the Jordan-Wigner transformation,

$$c_k^\dagger = \sigma_+^{(k)} \prod_{j=1}^{k-1} \left(-\sigma_z^{(j)} \right) \quad c_k = \prod_{j=1}^{k-1} \left(-\sigma_z^{(j)} \right) \sigma_-^{(k)}, \tag{9.6}$$

which introduces the operators $c_k^\dagger$ and c_k that obey the canonical fermionic algebra

$$\{c_i^\dagger, c_j\} = \delta_{i,j} \qquad \{c_i^\dagger, c_j^\dagger\} = \{c_i, c_j\} = 0.$$

After this transformation, (9.3) takes on the form

$$
H_{\mathrm{xy}} = \sum_{k=1}^{L} \left[2\Omega \left(c_k^\dagger c_k - \frac{1}{2} \right) + \frac{\beta}{4} \left(c_k^\dagger c_{k+1} + c_{k+1}^\dagger c_k \right) \right]
$$
$$
- \frac{\beta}{4} \left(c_L^\dagger c_1 + c_1^\dagger c_L \right) \left(e^{i\pi n_+} + 1 \right). \tag{9.7}
$$

Thus, the Hamiltonian has been transformed into one which describes a chain of spinless fermions with nearest neighbor hopping. The last term of (9.7) appears due to the periodic boundary conditions. It depends on the operator $n_+ = \sum_{j=1}^{L} c_j^\dagger c_j$, which counts the total number of fermions, which is also equivalent to the number of (super)atoms in the state $|+\rangle$. Thus, depending on the parity of the number of fermions of the state, H_{xy} reads

$$
H_{\mathrm{xy}}^{(\mathrm{e/o})} = \sum_{k=1}^{L} 2\Omega \left(c_k^\dagger c_k - \frac{1}{2} \right) + \frac{\beta}{4} \sum_{k=1}^{L-1} \left(c_k^\dagger c_{k+1} + c_{k+1}^\dagger c_k \right)
$$
$$
\mp \frac{\beta}{4} \left(c_L^\dagger c_1 + c_1^\dagger c_L \right),
$$

for even (e) or odd (o) parity, respectively.

These two cases can be accounted for simultaneously in a convenient way by introducing a matrix representation for the fermionic operators. They are projected onto the subspaces with even and odd eigenvalue of n_+ by means of the projectors $P_{\mathrm{e/o}} = \left[1 \pm e^{i\pi n_+} \right]/2$, with $P_{\mathrm{e}} + P_{\mathrm{o}} = \mathbf{1}$. Since the Hamiltonian H_{xy} conserves the number of fermions, i.e., $\left[H_{\mathrm{xy}}, e^{i\pi n_+} \right] = 0$, it is diagonal in this representation and can be decomposed as

$$
H_{\mathrm{xy}} = \begin{pmatrix} P_{\mathrm{e}} H_{\mathrm{xy}} P_{\mathrm{e}} & P_{\mathrm{e}} H_{\mathrm{xy}} P_{\mathrm{o}} \\ P_{\mathrm{o}} H_{\mathrm{xy}} P_{\mathrm{e}} & P_{\mathrm{o}} H_{\mathrm{xy}} P_{\mathrm{o}} \end{pmatrix} \equiv \begin{pmatrix} H_{\mathrm{xy}}^{(\mathrm{e})} & 0 \\ 0 & H_{\mathrm{xy}}^{(\mathrm{o})} \end{pmatrix}.
$$

We now introduce new matrix-valued creation and annihilation operators of the form

$$
\gamma_k^\dagger = \begin{pmatrix} 0 & c_k^\dagger \\ c_k^\dagger & 0 \end{pmatrix} \qquad \gamma_k = \begin{pmatrix} 0 & c_k \\ c_k & 0 \end{pmatrix},
$$

which obey the fermionic algebra provided c_k and $c_k^\dagger$ are fermionic operators. The Hamiltonian can be conveniently rewritten as

$$
H_{\mathrm{xy}} = 2\Omega \sum_{k=1}^{L} \left(\gamma_k^\dagger \gamma_k - \frac{1}{2} \right) + \frac{\beta}{4} \sum_{k=1}^{L-1} \left(\gamma_k^\dagger \gamma_{k+1} + \gamma_{k+1}^\dagger \gamma_k \right)
$$
$$
- \frac{\beta}{4} \left(\gamma_L^\dagger \gamma_1 + \gamma_1^\dagger \gamma_L \right) e^{i\pi n_+}, \tag{9.8}
$$

with

$$
e^{i\pi n_+} = \begin{pmatrix} 1 & 0 \\ 0 & -1 \end{pmatrix}.
$$

The diagonalization of the Hamiltonian (9.8) is achieved by performing the following Fourier transform

$$
\gamma_k^\dagger = \frac{1}{\sqrt{L}} \sum_{n=1}^{L} V_{nk} \Lambda_n^\dagger \quad \gamma_k = \frac{1}{\sqrt{L}} \sum_{n=1}^{L} V_{nk}^\dagger \Lambda_n,
$$

with the Fourier coefficients being

$$V_{nk} = \begin{pmatrix} e^{-i\frac{2\pi}{L}(n-1/2)k} & 0 \\ 0 & e^{-i\frac{2\pi}{L}nk} \end{pmatrix}.$$

The operators $\Lambda_n^\dagger$ and Λ_n are matrix-valued

$$\Lambda_n^\dagger = \begin{pmatrix} 0 & P_e\eta_n^\dagger \\ P_o\eta_n^\dagger & 0 \end{pmatrix} \qquad \Lambda_n = \begin{pmatrix} 0 & \eta_n P_o \\ \eta_n P_e & 0 \end{pmatrix},$$

with $\eta_n^\dagger$ and η_n being fermionic creation and annihilation operators, respectively. Defining the eigenvalue matrix ϵ_n as

$$\epsilon_n = 2 \begin{pmatrix} \cos\left[\frac{2\pi}{L}(n-1/2)\right] & 0 \\ 0 & \cos\left[\frac{2\pi}{L}n\right] \end{pmatrix},$$

the diagonalized Hamiltonian (9.8) reads

$$H_{\mathrm{xy}} = -L\Omega + \sum_{n=1}^{L}\left(2\Omega + \frac{\beta}{4}\epsilon_n\right)\Lambda_n^\dagger\Lambda_n. \tag{9.9}$$

As we will see in the next section, the introduction of the matrix-valued fermionic operators has the advantage that excited states can be constructed by applying products of $\Lambda_n^\dagger$ to the ground state. As a consequence, this matrix notation allows us to automatically distinguish between the odd and even fermion cases, which otherwise has to be done manually.

9.3. Many-body states

9.3.1. Fully-symmetric states

The ground state of Hamiltonian (9.9) is given by

$$|G\rangle = \prod_{k=1}^{L}|-\rangle_k$$

and it is fully-symmetric. Excited states that contain N fermions are in general formed by successive application of the creation operator, i.e., $|N_{pq\ldots}\rangle = \Lambda_p^\dagger\Lambda_q^\dagger\ldots|G\rangle$. However, not all combinations will give rise to states that belong to the fully-symmetric subset of states accessible by a time-evolution defined in Section 6.2.

Let us start considering the possible cases of a single-fermion excitation. For a fully-symmetric state we require $O^\dagger|1_p\rangle = O^\dagger\Lambda_p^\dagger|G\rangle = O^\dagger\Lambda_p^\dagger O|G\rangle = \Lambda_p^\dagger|G\rangle = |1_p\rangle$, i.e.,

$$O^\dagger\Lambda_p^\dagger O|G\rangle = \Lambda_p^\dagger|G\rangle,$$

with O being a placeholder for $\mathcal{X}$ and $\mathcal{R}$. After some algebra one finds that

$$\begin{aligned} \mathcal{R}^\dagger\eta_p^\dagger\mathcal{R} &= e^{i\frac{2\pi}{L}p}\eta_{L-p}^\dagger e^{i\pi n_+} \\ \mathcal{X}^\dagger\eta_p^\dagger\mathcal{X} &= e^{-i\frac{2\pi}{L}p}\eta_p^\dagger e^{i\pi c_1^\dagger c_1} + \frac{1}{\sqrt{L}}c_1^\dagger\left(e^{i\pi n_+} - 1\right). \end{aligned}$$

Since $e^{i\pi n_+}|G\rangle = |G\rangle$ and $e^{i\pi c_1^\dagger c_1}|G\rangle = |G\rangle$, only the single excitation with $p = L$ is symmetric under cyclic shifts and reversal. Hence, the only one-fermion state that can be reached by the time evolution reads

$$|1\rangle = \Lambda_L^\dagger|G\rangle.$$

To have a better physical understanding of this state, it is convenient to write it in terms of the atomic operators,

$$|1\rangle = \frac{1}{\sqrt{L}} \sum_{k=1}^{L} \sigma_+^{(k)} |G\rangle .$$

Thus, $|1\rangle$ is a spin wave or, in other words, a superatom that extends over the entire lattice. These states are of interest since they can be used as a resource for single photon generation.

For the two-fermion states, we follow the same procedure and demand

$$O^\dagger \Lambda_p^\dagger \Lambda_q^\dagger O |G\rangle = \Lambda_p^\dagger \Lambda_q^\dagger |G\rangle .$$

One finds that

$$\begin{aligned}
\mathcal{R}^\dagger \eta_p^\dagger \eta_q^\dagger \mathcal{R} &= e^{i\frac{2\pi}{L}(p+q-1)} \eta_{L-q+1}^\dagger \eta_{L-p+1}^\dagger \\
\mathcal{X}^\dagger \eta_p^\dagger \eta_q^\dagger \mathcal{X} &= e^{-i\frac{2\pi}{L}(p+q-1)} \eta_p^\dagger \eta_q^\dagger + \frac{e^{i\frac{\pi}{L}}}{\sqrt{L}} \left[e^{-i\frac{2\pi}{L}p} \eta_p^\dagger - e^{-i\frac{2\pi}{L}q} \eta_q^\dagger \right] c_1^\dagger \left(e^{i\pi n_+} - 1 \right) ,
\end{aligned}$$

from where one sees that the condition $p + q - 1 = L$ has to be accomplished. As a result, the fully-symmetric states are

$$|2_p\rangle = \Lambda_p^\dagger \Lambda_{L-p+1}^\dagger |G\rangle ,$$

with $p = 1 \ldots \lfloor L/2 \rfloor$. These are entangled states formed by superpositions of two-atom excitations in the ring with opposite momentum. This is more clearly seen by writing everything in terms of the Pauli matrices

$$|2_p\rangle = \frac{2}{iL} \sum_{k>k'} \sin\left(\frac{2\pi}{L}(p - 1/2)(k - k') \right) \sigma_+^{(k)} \sigma_+^{(k')} |G\rangle .$$

These states are potentially interesting for the production of photon pairs. How they can be actually accessed will be discussed in Sec. 9.4.

Finally, let us illustrate how the three-fermion excitations are formed. We have

$$R^\dagger \eta_p^\dagger \eta_q^\dagger \eta_r^\dagger R = e^{i\frac{2\pi}{L}(p+q+r)} \eta_{L-p}^\dagger e^{i\pi n_+} \eta_{L-q}^\dagger e^{i\pi n_+} \eta_{L-r}^\dagger e^{i\pi n_+} = -e^{i\frac{2\pi}{L}(p+q+r)} \eta_{L-p}^\dagger \eta_{L-q}^\dagger \eta_{L-r}^\dagger e^{i\pi n_+} .$$

and thus fully symmetric three-fermion states are of the form

$$|3_{pqr}\rangle = \frac{1}{\sqrt{2}} \left(\Lambda_p^\dagger \Lambda_q^\dagger \Lambda_r^\dagger - \Lambda_{L-p}^\dagger \Lambda_{L-q}^\dagger \Lambda_{L-r}^\dagger \right) |G\rangle , \tag{9.10}$$

with $p + q + r = L, 2L$. Writing these eigenexcitations back in terms of the spin operators yields

$$|3_{pqr}\rangle = -\frac{\sqrt{2}i}{L^{3/2}} \sum_{k>k'>k''} \sum_{\substack{\text{perm} \\ (pqr)}} \varepsilon_{pqr} \sin\left[\frac{2\pi}{L}(kp + k'q + k''r) \right] \sigma_+^{(k)} \sigma_+^{(k')} \sigma_+^{(k'')} |G\rangle ,$$

where ε_{pqr} is the Levi-Civita symbol. In a similar way, states with higher number of fermions are obtained.
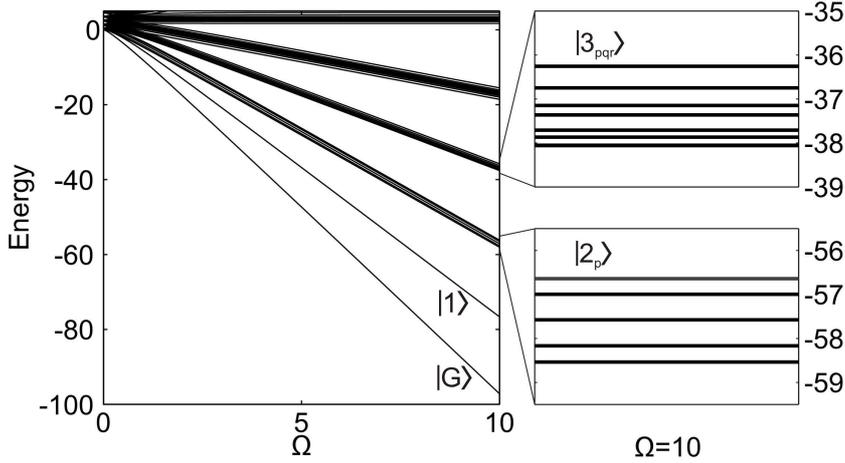
Figure 9.2.: Spectrum of Hamiltonian H (9.2) for a lattice of $L = 10$ sites versus the laser driving Ω in units of β. In the right insets, the energies of the two- and three-fermion states are shown for $\Omega = 10$. Five two-fermion and eight three-fermion eigenenergies arise as it is analytically predicted for this lattice size.

9.3.2. Energy spectrum

Now that we have analyzed the eigenstates of the system we will focus on the corresponding eigenenergies. In the course of this investigation we will also perform a comparison of the analytic results to the ones obtained from a numerical diagonalization of the Hamiltonian (6.3). This will allow us to assess the accuracy of our analytical approach.

Let us begin with the ground state energy. From Eq. (9.9) we can read off the value

$$E_G = -L\left(\Omega - \frac{\beta}{4}\right), \tag{9.11}$$

where we have included the general energy-offset $\beta L/4$ (see Eq. (9.2)). For $\Delta = 0$, $\Omega = 10$, $\beta = 1$ and $L = 10$, the result is $E_G = -97.5$. This is to be compared with the numerical value of -97.63 which is obtained by diagonalizing the Hamiltonian (6.3). We find both results to be in good agreement. For the first excited state we obtain

$$E_1 = E_G + 2\Omega + \frac{\beta}{2}.$$

Using the same set of parameters, the energy of the single-fermion state is $E_1 = -77.0$, which is very close to the numerically exact value -77.11. The energies of higher eigenexcitations are given by

$$E_{2p} = E_G + 4\Omega + \beta \cos\left[\frac{2\pi}{L}(p - 1/2)\right],$$

with $p = 1 \ldots \lfloor L/2 \rfloor$, for the two-fermion case and

$$E_{3pqr} = E_G + 6\Omega + \frac{\beta}{2}\left[\cos\left(\frac{2\pi}{L}p\right) + \cos\left(\frac{2\pi}{L}q\right) + \cos\left(\frac{2\pi}{L}r\right)\right],$$

with $p + q + r = L, 2L$, for the three-fermion one. For $L = 10$, we obtain five and eight different eigenenergies for the two- and three-fermion states, respectively (see insets in Fig. 9.2). In the Tables 9.1 and 9.2 we perform a comparison between the analytical and the numerical results. A difference of less than a 0.2% is observed in all cases.

The discrepancies between analytical and numerical values are mainly caused by second order energy shifts due to H_1 and H_2 (Eqs. (9.4) and (9.5)). These contributions vanish only in the

p	E_{2p}	Numerical
1	-56.55	-56.64
2	-56.91	-56.99
3	-57.50	-57.58
4	-58.09	-58.17
5	-58.45	-58.54

Table 9.1.: Energies (in units of β) of the five two-fermion states $|2_p\rangle$ for $L = 10$, $\Delta = 0$ and $\Omega = 10$ and comparison with the numerically exact values.

p	q	r	E_{3pqr}	Numerical
1	9	10	-36.19	-36.26
2	8	10	-36.69	-36.75
1	2	7	-37.10	-37.15
3	7	10	-37.31	-37.36
1	3	6	-37.65	-37.71
4	6	10	-37.81	-37.87
1	4	5	-38.00	-38.05
2	3	5	-38.00	-38.06

Table 9.2.: Energies (in units of β) of the eight three-fermion states $|3_{pqr}\rangle$ for $L = 10$, $\Delta = 0$ and $\Omega = 10$ and comparison with the numerically exact values.

limits $\beta/\Omega \to 0$ and $\Delta/\Omega \to 0$. Here, we will calculate them for a finite ratio. There is a constant term in H_1 which is proportional to Δ that gives rise to a global energy shift $E^{(1)} = L\Delta/2$. Being aware of this shift facilitates the comparison between the numerically exact and the approximate analytical eigenvalues for $\Delta \neq 0$.

Let us focus first on the ground state. H_1 and H_2 only couple states whose number of fermions differ by one or two (Fig. 9.1). As a consequence, only $|1\rangle$ and $|2_p\rangle$ contribute to the second order correction of the energy of the ground state. It yields

$$E_G^{(2)} = -\frac{L|\Delta + \beta|^2}{8\Omega + 2\beta} - \frac{\beta^2}{4}\left(1 + \frac{2}{L}\right)^2 \sum_{p=1}^{\lfloor L/2 \rfloor} \frac{\sin^2\left[\frac{2\pi}{L}(p - 1/2)\right]}{4\Omega + \beta\cos\left[\frac{2\pi}{L}(p - 1/2)\right]}. \tag{9.12}$$

Analogously, we calculate the energy shift of the first excited state, $|1\rangle$, due to H_1 and H_2. In this case, we have to compute the effect of $|G\rangle$, $|2_p\rangle$ and $|3_{pqr}\rangle$. The resulting energy correction is given by

$$E_1^{(2)} = \frac{L|\Delta + \beta|^2}{8\Omega + 2\beta} - \frac{|\Delta + \beta|^2}{L} \sum_{p=1}^{\lfloor L/2 \rfloor} \frac{\cot^2\left[\frac{\pi}{L}(p - 1/2)\right]}{2\Omega + \frac{\beta}{2}\left(2\cos\left[\frac{2\pi}{L}(p - 1/2)\right] - 1\right)}. \tag{9.13}$$

Taking the parameters $\Delta = 0$, $\Omega = 10$, $\beta = 1$ and $L = 10$, these shifts yield $E_G^{(2)} = -0.14$ and $E_1^{(2)} = -0.10$. The corrected energies of the ground and the single-fermion state are now $E_G = E_G^{(0)} + E_G^{(1)} + E_G^{(2)} = -97.64$ and $E_1 = E_1^{(0)} + E_1^{(1)} + E_1^{(2)} = -77.10$, much closer to the numerically exact ones of -97.63 and -77.11, respectively. We will later see that these energy corrections can be also useful for the selective excitation of many-particle states in the lattice.

9.3.3. Correlation functions

In this subsection we are going to study the density-density correlation function of the many-particle states. This quantity measures the conditional probability of finding two simultaneously excited

atoms at a distance x from each other normalized to the probability of uncorrelated excitation. It is defined - for a fully-symmetric state $|\Psi\rangle$ - as

$$g_2(x, \Psi) = \frac{\langle n_1 n_{1+x} \rangle_\Psi}{\langle n_1 \rangle_\Psi^2} - 1,$$

where we have used $\langle n_a \rangle_\Psi = \langle n_b \rangle_\Psi$ for all sites. The correlation function will give $g_2(x, \Psi) = 0$ when two sites separated by a distance x are completely uncorrelated, and $g_2(x, \Psi) > 0\,(< 0)$ for correlation (anticorrelation) between the sites.

In particular, for the case $|\Psi\rangle = |2_p\rangle$, the correlation function can be analytically calculated. In terms of the expectation values of the spin operators, it reads $g_2(x, 2_p) = \left\langle \sigma_+^{(1)} \sigma_-^{(1+x)} + \sigma_-^{(1)} \sigma_+^{(1+x)} \right\rangle_{2_p}$. For $x = 0$ we have $g_2(0, 2_p) = 1$ and for $x > 0$ the calculation yields

$$g_2(x, 2_p) = \frac{4}{L^2} \left[(L - 2x) \cos\left[\frac{2\pi}{L}(p - 1/2)x \right] + 2 \sin\left[\frac{2\pi}{L}(p - 1/2)x \right] \cot\left[\frac{2\pi}{L}(p - 1/2) \right] \right].$$

By inspecting this expression for the allowed values $p = 1, \ldots \lfloor L/2 \rfloor$, some general statements can be made:

i) Independently of the total number of sites L, there are always two 'extremal' cases (see Fig. 9.3a) which correspond to $p = 1$ and $p = \lfloor L/2 \rfloor$: For $p = 1$, the correlation function shows a positive maximum at $x = 1$, i.e., nearest neighbor, and then decreases monotonically and smoothly with the distance, staying always positive; for $p = \lfloor L/2 \rfloor$, the nearest neighbor is pronouncedly anticorrelated, the next-nearest neighbor is correlated and this pattern of correlation-anticorrelation persists with increasing distance.

ii) For $p = \lfloor L/2 \rfloor$, the oscillations of $g_2(x, 2_p)$ are more pronounced for even L than for odd L, see Fig. 9.3a. Indeed, the ratio of the amplitudes of the correlations for $x = 1$ and $x = \lfloor L/2 \rfloor$ is,

$$\frac{g_2(1, 2_{\frac{L}{2}})}{g_2(\frac{L}{2}, 2_{\frac{L}{2}})} \sim 1 \qquad \frac{g_2(1, 2_{\frac{L-1}{2}})}{g_2(\frac{L-1}{2}, 2_{\frac{L-1}{2}})} \sim L^3,$$

in the even and odd cases, respectively. Also, for an even number of sites, the correlation functions of the two extreme cases accomplish $g_2(x, 2_{\frac{L}{2}}) = (-1)^x g_2(x, 2_1)$, i.e., the envelope of the oscillating function $g_2(x, 2_{\frac{L}{2}})$ is given by the smoothly decreasing $g_2(x, 2_1)$.

iii) For a fixed value of p, the amplitude of the correlations decreases with increasing number of sites as $1/L$, as can be seen in Fig. 9.3b.

Numerically, we have observed agreement to the analytical results shown in Fig. 9.3. As expected, this agreement improves with a decreasing ratio β/Ω. The correlations could be directly monitored experimentally provided that a site-resolved detection of atoms in the $|+\rangle$-state is possible. The next section will deal with the open question of how these correlated states can be experimentally accessed.

9.4. Excitation of many particle states

Our aim is to selectively excite correlated many-body states by a temporal variation of the laser parameters. Initially the atoms shall be in the product state $|0\rangle = \prod_{k=1}^{L} |P\rangle_k$ and the laser shall be turned off, i.e., $\Omega_0(0) = 0$ and $\Delta(0) = \Delta_0$. Starting from these initial conditions, the goal is to vary $\Omega_0(t)$ and $\Delta(t)$ such that at the end of the sequence, i.e., at $t = t_{\text{final}}$, the detuning is zero and the laser driving is much larger than the interaction ($\Delta(t_{\text{final}}) = 0$ and $\Omega(t_{\text{final}})/\beta \gg 1$). This final situation corresponds to the right-hand side of the spectrum presented in Fig. 9.2.

Once a desired many-particle state has been populated, and due to the limited lifetime of the highly excited levels, which is in the order of several μs (e.g., 66 μs for Rb in the 60s state), we
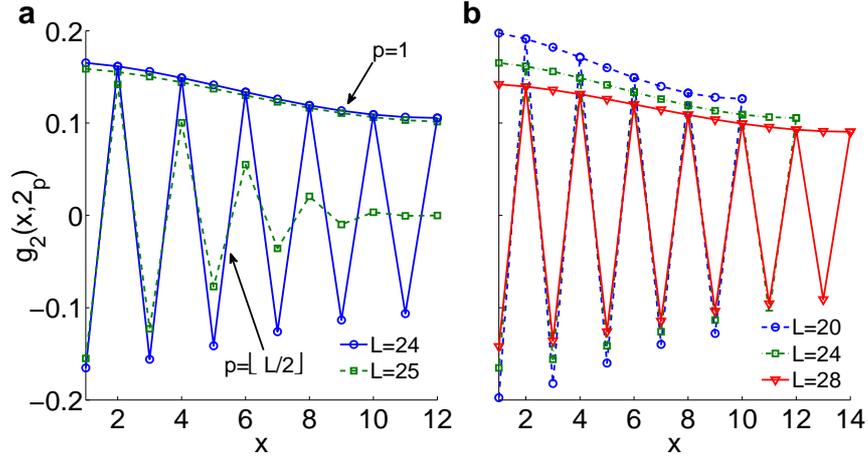
Figure 9.3.: Density-density correlation functions of the $|2_p\rangle$ states. **a:** For $p = 1$ and $p = \lfloor L/2 \rfloor$, the correlations show completely different behavior, i.e., smoothly decreasing and strongly oscillating, respectively. These oscillations are much more pronounced for the even value of $L = 24$ than for the odd, $L = 25$. **b:** The magnitude of the correlations decreases as the number of sites L is enhanced, as can be seen for $L = 20, 24, 28$.

want to map it to an stable configuration. To do so, we first turn off the laser ($\Omega = 0$) and then switch on a second one whose action can be described by the Hamiltonian

$$H_{\mathrm{map}} = \Omega_s \sum_{k=1}^{L} \left(s_k^\dagger r_k + r_k^\dagger s_k \right) + \beta \sum_{k=1}^{L} n_k n_{k+1}. \tag{9.14}$$

In this expression, $s_k^\dagger$ and s_k stand for the creation and annihilation operators of an single-atom stable storage state $|s\rangle$ on site k, respectively. In the limit where the interaction is much smaller than the Rabi frequency of this transition, i.e., $\Omega_s \gg \beta$, we can neglect the second term of this Hamiltonian. Thus, performing a global π-pulse to the considered many-particle state means to perform the mapping $|r\rangle \to |s\rangle$, such that a stable configuration is achieved.

Hence, the difficulty lies in finding a 'trajectory' or sequence $(\Omega_0(t), \Delta(t))$ for which at $t = t_{\mathrm{final}}$ only a single many-particle state is occupied. We propose two different methods to achieve this goal in the following paragraphs.

9.4.1. Direct trajectory

In certain cases, one can guess a trajectory $(\Delta(t), \Omega_0(t))$ like the ones shown in Fig. 9.4 that eventually connects $|0\rangle$ with a desired eigenstate of H_{xy} [115, 124], but this is not always possible. The general appearance of the laser sequence strongly depends on the sign of the initial detuning Δ_0. In Fig. 9.4 the two possible scenarios (taking $\Delta_0 \neq 0$) are depicted. For $\Delta_0 < 0$, the initial state is not the ground state of the system when the laser is turned off ($\Omega = 0$). As a consequence, this initial state suffers several avoided crossings with other levels when Ω is increased. Thus, it is not easy to find a path through the spectrum that connects it to a single desired eigenstate of H_{xy}, as the one shown in Fig. 9.4a. A more general framework for finding a proper trajectory is provided by Optimal Control theory [125]. Here, the desired fidelity with which the final state is achieved can be set and certain constraints on the trajectory can be imposed. This method is successfully applied to quantum information processing [126], molecular state preparation [127] and optimization of number squeezing of an atomic gas confined to a double well potential [128]. The case of $\Delta_0 > 0$ will be treated thoroughly in the next subsection.
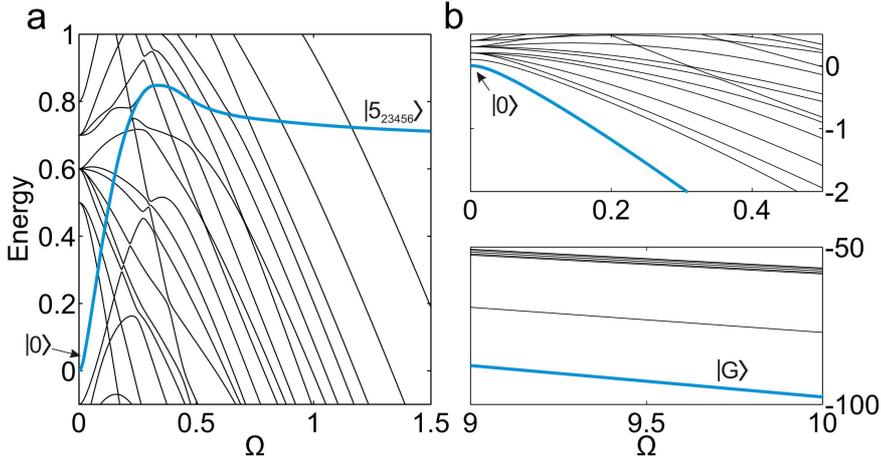
Figure 9.4.: Possible trajectories $(\Delta(t), \Omega_0(t))$ through the spectrum of H with $\Delta_0 \neq 0$ (units of β). **a**: When $\Delta_0 < 0$, the ground state at $\Omega = 0$ does not coincide with the initial state, $|0\rangle$, and the energy of the initial state goes through a number of avoided crossings. A possible path through them to reach the state $|5_{23456}\rangle$ is shown. **b**: If $\Delta_0 > 0$, the initial state $|0\rangle$ is adiabatically connected to the ground state $|G\rangle$.
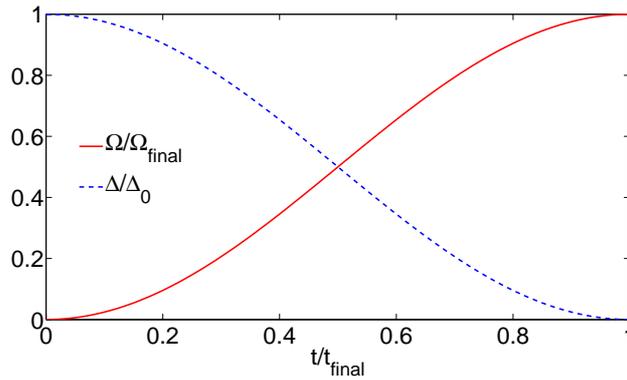
Figure 9.5.: Shapes of the variation of the parameters of the laser $\Omega(t)$ and $\Delta(t)$ in the from given by (9.15) and (9.16), respectively.

9.4.2. Excitation from the ground state

We present here a different route to populate single many-particle states. This is accomplished in two steps: First, one has to prepare the ground state $|G\rangle$ of Hamiltonian (9.3) in the limit $\Omega \gg \beta$; once the ground state is populated, the single-fermion and two-fermion many-particle states can be accessed by means of an oscillating detuning, that gives rise to a time-dependent H_1.

Step 1: Let us start by explaining how to vary the laser parameters to prepare the ground state $|G\rangle$. In particular, when setting $\Delta_0 > 0$, the ground state of the system at $\Omega = 0$ coincides with the initial state $|0\rangle$. With increasing Ω, it is adiabatically connected to the ground state $|G\rangle$ of H_{xy} (see Fig. 9.4b). The problem that we can encounter here is that non-adiabatic transitions to other energy levels occur when increasing Ω, so that we do not populate only $|G\rangle$ but also other states. To avoid this, we choose a large enough value of Δ_0 when the laser is still turned off ($\Omega = 0$). This increases the energy gap between $|0\rangle$ and other energy levels, and, as a consequence, suppresses non-adiabatic transitions. This initial detuning can be decreased as Ω increases so that in the desired regime, i.e., $\Omega_{\text{final}} \equiv \Omega(t_{\text{final}}) \gg \beta$, it is set to zero. As an example, we propose the following
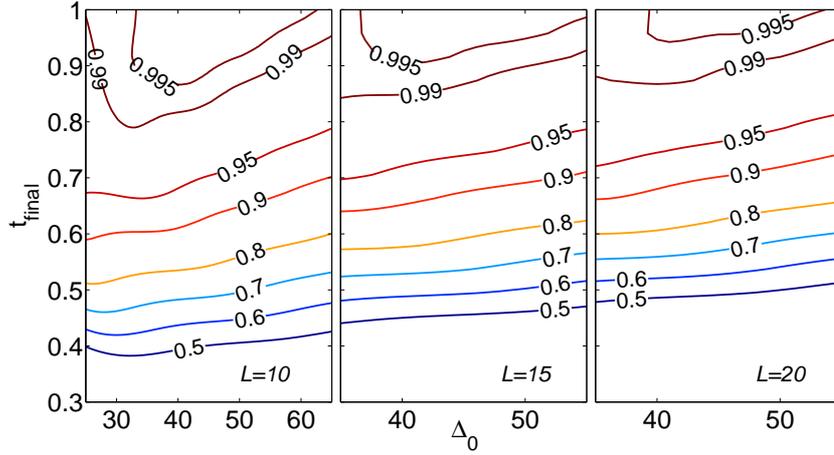
Figure 9.6.: Fidelity $|\langle\Phi(t_{\text{final}})|G\rangle|^2$ when populating the ground state of H_{xy} from the initial state via variation of the parameters of the laser $\Omega(t)$ and $\Delta(t)$ in the form given by (9.15) and (9.16), respectively ($\Omega_{\text{final}} = 10$ in units of β). Several initial values of the detuning and time intervals, as well as different lattice sizes, are considered. For a fixed value of Δ_0 (units of β), better fidelities are obtained for larger time intervals (units of $1/\beta$). For a fixed time interval, there is an optimal value of Δ_0 for every lattice size, around $\Delta_0 \approx 45$.

shapes of $\Omega(t)$ and $\Delta(t)$

$$\Omega(t) = \Omega_{\text{final}} \sin^2\left(\frac{\pi t}{2t_{\text{final}}}\right) \tag{9.15}$$

$$\Delta(t) = \Delta_0\left[1 - \sin^2\left(\frac{\pi t}{2t_{\text{final}}}\right)\right], \tag{9.16}$$

that are shown in Fig. 9.5. The obtained fidelity $|\langle\Phi(t_{\text{final}})|G\rangle|^2$ for different values of the initial detuning Δ_0 and time intervals t_{final} is given in Fig. 9.6, where $\Phi(t_{\text{final}})$ stands for the wavefunction of the final state (where $\Omega_{\text{final}} = 10\beta$). One can see that it is actually possible to populate the desired state with high fidelity, e.g., over 99% is achieved for all considered lattice sizes with $\Delta_0 = 45\beta$ and $t_{\text{final}} = 0.9\beta^{-1}$. We find that: i) the fidelity depends only weakly on the lattice size although the dimension of the Hilbert space grows exponentially with L, and ii) as expected, for a fixed value of the initial detuning, the fidelity increases with the increasing length of the time interval. Note that the timescale and the fidelity of this whole process is also limited by the lifetime of the Rydberg state. To illustrate this, let us take the 43s state of Rb and a lattice constant of $a = 3\,\mu m$. We find then that a fidelity of above 99% is achieved for $t_{\text{final}} = 0.27\,\mu s$ and a (collective) Rabi frequency of $\Omega = 33.5\,\text{MHz}$. Accounting for the limited lifetime of the 43s state ($T_0 \approx 100\,\mu s$), the fidelity decreases by a factor of $f_L = \left[\exp\left(-t_{\text{final}}/T_0\right)\right]^L$. For example, for a lattice size of $L = 20$ and the previous choice of parameters, the achieved fidelity is eventually $99\% \times f_L = 94\%$. This effect can be diminished by a different choice of parameters: A change of the principal quantum number to $n = 50$ and a lattice constant of $a = 3.5\,\mu m$ increase the fidelity to 97%. This is at the expense of an increased Rabi frequency which now has to be $\Omega = 84.2\,\text{MHz}$.

If there is only one atom per site, and based on the fact that $|G\rangle = \prod_{k=1}^{L}|-\rangle_k$ is a product state, an alternative procedure to this adiabatic passage can be envisaged. Starting from the vacuum $|0\rangle$ (also a product state with every atom in $|g\rangle$), we perform a global $\pi/2$-pulse to the single-atom transition $|g\rangle \to |s\rangle$. As a result, we obtain a product state where every atom is in a superposition $[|g\rangle + i|s\rangle]/\sqrt{2}$. In a second step, a π-pulse with the mapping laser described by the Hamiltonian (9.14) and with $\Omega_s \gg \beta$, transfers every atom to the state $[|g\rangle - |r\rangle]/\sqrt{2}$, i.e., we have prepared the ground state $|G\rangle$. It is worth remarking that this method eliminates the lifetime limitation in this first stage.
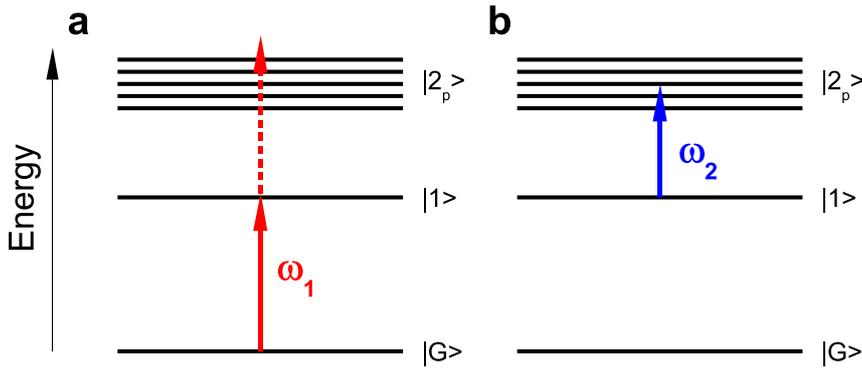
Figure 9.7.: Sketch of the excitation of the single-fermion and two-fermion states by means of an oscillating (radiofrequency) detuning using a not too large value of Ω. **a:** In a first step, the population is transferred by a π-pulse to the single-fermion state by tuning the frequency of the detuning on resonance with the gap $\omega = \omega_1$. **b:** A second π-pulse with ω tuned to match ω_2 addresses the corresponding $|2_p\rangle$ state, bearing in mind that $\beta \gg \Delta_{\text{osc}}$ in this step.

Step 2: Let us show now how to address the single-fermion and two-fermion states from this ground state $|G\rangle$. As we explained in Section 9.1, the Hamiltonian H_1, associated with the detuning, drives transitions between neighboring manifolds, i.e., $\Delta m = \pm 1$, (see Fig. 9.1). We exploit this fact and introduce an oscillating detuning of the form $\Delta(t) = \Delta_{\text{osc}} \cos(\omega t)$. If we tune ω to coincide with the gap between two given states, this detuning acts effectively as a laser that couples them resonantly with a Rabi frequency that is proportional to Δ_{osc}.

Using this oscillating detuning, we want to transfer the population from the ground to the first excited state (Fig. 9.7a). To do so, ω is tuned to be on resonance with the corresponding energy gap, i.e., $\omega = \omega_1 = E_1 - E_G$, and by a π-pulse we populate $|1\rangle$. One has to take into account that in the limit of $\Omega \gg \beta$ the energy gap between any two neighboring manifolds is equal, i.e., also higher lying excitations are populated. To avoid this effect and address only the $|1\rangle$ state, we can choose a not too large value of Ω. In this regime, the second order level shifts caused by H_1 and H_2, that are roughly given by Δ^2/Ω and β^2/Ω, respectively (see Section 9.3.2), become increasingly important. In particular, as it is sketched in Fig. 9.7a, the gap between $|1\rangle$ and any of the $|2_p\rangle$ levels becomes more and more different from ω_1 and, as a consequence, the unwanted transitions fall out of resonance. Analogously, the same procedure could be used to address the two-fermion many-particle states (see Fig. 9.7b). The first π-pulse resonant with the $|G\rangle \to |1\rangle$ transition, is followed by another π-pulse with ω tuned to coincide with the energy gap of the specific $|1\rangle \to |2_p\rangle$ transition, $\omega = \omega_2 = E_{2p} - E_1$. The separation between neighboring $|2_p\rangle$ states is of the order of β and the Rabi frequency of the transition is proportional to Δ_{osc}. As a consequence, to populate only a single level of the two-fermion manifold, the parameters have to accomplish that $\beta \gg \Delta_{\text{osc}}$ and, at the same time, Δ_{osc} has to be large enough in order to perform the transfer at a time interval that is much shorter than the lifetime of the Rydberg state.

9.5. Disorder

So far we have assumed a constant Rabi frequency Ω. We will now consider a situation in which it is not constant but fluctuates from site to site randomly around the mean value Ω, i.e., $\Omega \to \Omega_k$, with $\Omega_k = \Omega + \delta\Omega_k$ being a distribution such that the average of $\delta\Omega_k$ is equal to 0. In Eq. (9.9) the fluctuating part $\delta\Omega_k$ introduces a random single particle potential for the fermions, and gives rise to the Hamiltonian of Anderson localization [129]. Hence, a lattice gas of Rydberg atoms offers the possibility to study fermions in a disorder potential although no external atomic motion takes place.
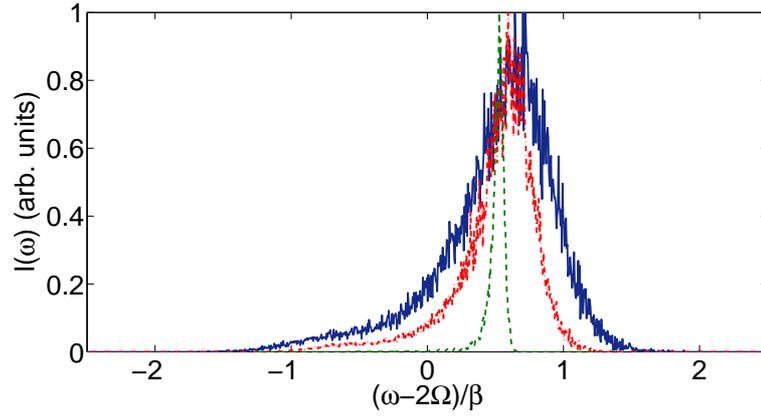
Figure 9.8.: Absorption profile (excitation probability of a single fermion state) for the $|G\rangle \to |1\rangle$ transition for three strengths of disorder, $\Omega/\beta = 10$ and $L = 50$. The disorder strength is controlled by the fluctuations of the Rabi frequency around the mean value, $\delta\Omega_k$. The results are averages over 1000 realizations.

The Hamiltonian (9.3) in this situation yields

$$H_{\text{xy}}^{(\text{d})} = \sum_{k=1}^{L} \left[\Omega_k \sigma_z^{(k)} + \frac{\beta}{4} \left(\sigma_+^{(k)} \sigma_-^{(k+1)} + \sigma_-^{(k)} \sigma_+^{(k+1)} \right) \right],$$

so that, after the Jordan-Wigner transformation, it reads

$$H_{\text{xy}}^{(\text{d})} = H_{\text{xy}} + \sum_{k=1}^{L} 2\delta\Omega_k c_k^\dagger c_k,$$

except for an energy offset given by $\sum_{k=1}^{L} \delta\Omega_k$. To diagonalize this Hamiltonian, we use a transformation of the type

$$c_k^\dagger = \sum_{n=1}^{L} V_{nk} \eta'^\dagger_n \qquad c_k = \sum_{n=1}^{L} V_{nk}^* \eta'_n,$$

such that the Hamiltonian yields

$$H_{\text{xy}}^{(\text{d})} = -L\Omega + \sum_{n=1}^{L} \Sigma_n \eta'^\dagger_n \eta'_n,$$

with Σ_n being the corresponding eigenvalues.

The disorder destroys the symmetry properties of the system and hence also the selection rules for transitions between many-particle states. As a consequence, there are now in general L single-fermion states (instead of 1, $|1\rangle = \eta_L |G\rangle$) accessible from the state $|G\rangle$ when an oscillating detuning is applied. These new single-fermion states are given by the application of the new creation operators, that diagonalize the Hamiltonian, to the ground state, i.e.,

$$\left| 1'_n \right\rangle = \eta'^\dagger_n |G\rangle = \sum_{k=1}^{L} V_{nk}^* c_k^\dagger |G\rangle \qquad n = 1, \ldots, L.$$

Instead of a single sharp line at $\omega_1 = E_1 - E_G$ the (averaged) absorption profile of the $|G\rangle \to |1\rangle$-transition broadens and becomes asymmetric, see Fig. 9.8. This disorder-induced line broadening can be detected by counting the number of $|+\rangle$-atoms as a function of the excitation frequency ω.

For small values of the disorder, one can obtain an approximation to the red wing using perturbation theory. To do so, we have to obtain the squared of the matrix element $\langle 1'_n | H_1 | G \rangle$, with

$$H_1 = \frac{1}{2} \sum_{k=1}^{L} \left(1 - \sigma_x^{(k)} \right),$$

so that

$$\frac{1}{2} \langle 1'_n | \sum_{k=1}^{L} \left(1 - \sigma_x^{(k)} \right) | G \rangle = -\frac{1}{2} \langle 1'_n | \sum_{k=1}^{L} \sigma_+^{(k)} | G \rangle = -\sqrt{\frac{L}{2}} \langle 1'_n | 1 \rangle,$$

with $|1\rangle$ being the spin wave eigenfunction of the xy-Hamiltonian without disorder. Thus, the calculation of the intensity of absorption is reduced to obtain the overlap

$$\langle 1'_n | 1 \rangle = \frac{1}{\sqrt{L}} \sum_{k,l} V_{nl}^* \langle G | c_l c_k^\dagger | G \rangle = \frac{1}{\sqrt{L}} \sum_{k=1}^{L} V_{nk}^* = \mathbf{V}_n^\dagger \mathbf{V}_L^{(0)},$$

where $\mathbf{V}_n$ and $\mathbf{V}_n^{(0)}$ represent two sets of eigenvectors:

- When there is no disorder, the Hamiltonian reads $H_{xy} = -L\Omega + \sum_{ij} c_i^\dagger A_{ij} c_j$, with

$$A_{ij} = \begin{cases} 2\Omega & i = j \\ \beta/4 & i = j+1, j = i+1 \\ 0 & \text{otherwise} \end{cases},$$

whose diagonal form is given by $D^{(0)} = \mathbf{V}^{(0)\dagger} A \mathbf{V}^{(0)}$. Its eigenfunctions and eigenvalues are given by

$$V_{nk}^{(0)} = \frac{e^{-i\frac{2\pi}{L}nk}}{\sqrt{L}} \qquad D_n^{(0)} = 2\Omega + \frac{\beta}{2} \cos \frac{2\pi}{L} n,$$

so that, in particular,

$$V_{Lk}^{(0)} = \frac{1}{\sqrt{L}}.$$

- When there is disorder, $H_{xy}^{(d)} = -L\Omega + \frac{\beta}{4} \sum_{ij} c_i^\dagger A'_{ij} c_j$, where $A' = A + B$ such that $B_{ij} = (2\delta\Omega_i)\delta_{ij} \equiv d_i \delta_{ij}$. Here, the eigenvectors that diagonalize the matrix A' are the set $\mathbf{V}_n$. We can treat B as a small perturbation and, thus, write

$$\mathbf{V}_n^\dagger = \mathbf{V}_n^{(0)\dagger} + \sum_{m \neq n} \frac{\mathbf{V}_m^{(0)} B \mathbf{V}_n^{(0)\dagger}}{D_n^{(0)} - D_m^{(0)}} \mathbf{V}_m^{(0)\dagger}.$$

Taking these considerations into account, the overlap yields

$$\langle 1'_n | 1 \rangle = \mathbf{V}_n^{(0)\dagger} \mathbf{V}_L^{(0)} + \sum_{m \neq n} \frac{\mathbf{V}_m^{(0)} B \mathbf{V}_n^{(0)\dagger}}{D_n^{(0)} - D_m^{(0)}} \mathbf{V}_m^{(0)\dagger} \mathbf{V}_L^{(0)}.$$

Taking into account that

$$\mathbf{V}_n^{(0)\dagger} \mathbf{V}_L^{(0)} = \frac{1}{L} \sum_{k=1}^{L} e^{i\frac{2\pi}{L}nk} = \delta_{nL},$$

we can rewrite

$$
\begin{aligned}
\langle 1'_n | 1 \rangle &= \delta_{nL} + \frac{\mathbf{V}_L^{(0)} B \mathbf{V}_n^{(0)\dagger}}{D_n^{(0)} - D_L^{(0)}} (1 - \delta_{nL}) = \delta_{nL} + \frac{\sum_{j,k} V_{nj}^{(0)*} B_{jk} V_{Lk}^{(0)}}{D_n^{(0)} - D_L^{(0)}} (1 - \delta_{nL}) \\
&= \delta_{nL} + \frac{\sum_{j=1}^{L} d_j e^{i\frac{2\pi}{L}nj}}{L \left(D_n^{(0)} - D_L^{(0)} \right)} (1 - \delta_{nL}).
\end{aligned}
$$

The intensity of the absorption profile is given by the modulus squared of this overlap multiplied by $L/4$, and they yield $I(D_L^{(0)}) = L/4$ and

$$
\begin{aligned}
I(D_n^{(0)}) &= \frac{L}{4}\left|\langle 1'_n|1\rangle\right|^2 = \frac{\sum_{j,k} d_j d_k e^{i\frac{2\pi}{L}n(j-k)}}{4L\left|D_n^{(0)} - D_L^{(0)}\right|^2} = \frac{\sum_j d_j^2 + \sum_{j\neq k} d_j d_k e^{i\frac{2\pi}{L}n(j-k)}}{4L\left|D_n^{(0)} - D_L^{(0)}\right|^2} \\
&= \frac{\sum_j \delta\Omega_j^2 + \sum_{j\neq k} \delta\Omega_j \delta\Omega_k e^{i\frac{2\pi}{L}n(j-k)}}{L\left|D_n^{(0)} - D_L^{(0)}\right|^2} \qquad \text{for} \quad n \neq L,
\end{aligned}
\tag{9.17}
$$

where $d_j = 2\delta\Omega_j$ was used.

9.5.1. Quench of a superfluid

The spatial fluctuations of Ω_k can, for instance, be achieved by a speckle potential or standing waves with incommensurate frequencies [130, 131]. We present an alternative route in which the fluctuations of the Rabi frequency are caused by the fluctuating number of particles in each site around the mean value $N_0 = N_{\mathrm{g}}/L$ with N_{g} being the number of total atoms in the lattice with L sites, i.e., $N_k = N_0 + \delta N_k$. Thus,

$$
\Omega_k = \Omega_0 \sqrt{N_k} = \Omega_0 \sqrt{N_0 + \delta N_k} \approx \Omega\left(1 + \frac{\delta N_k}{2N_0}\right),
$$

where we have assumed that $\delta N_k \ll N_0$. In particular, we start in a situation in which N_{g} ground state atoms are prepared in a superfluid state of a weak lattice with L sites, i.e.,

$$
|\mathrm{SF}\rangle = \frac{1}{N_{\mathrm{g}}! L^{N_{\mathrm{g}}/2}}\left[\sum_{k=1}^{L} b_k^\dagger\right]^{N_{\mathrm{g}}} |\mathrm{vac}\rangle
$$

where $b_k^\dagger$ creates a ground state atom at site k. Disorder is introduced by a quench of this superfluid through a sudden increase of the depth of the lattice potential. We want to calculate the expected value of the operator $N_k = b_k^\dagger b_k$ for any site k, since the sites are indistinguishable. Thus, we have, for $k = L$,

$$
\langle\!\langle N_L \rangle\!\rangle \equiv \langle \mathrm{SF}| b_L^\dagger b_L |\mathrm{SF}\rangle = \frac{1}{N_{\mathrm{g}}! L^{N_{\mathrm{g}}}} \langle\mathrm{vac}|\left(\sum_{k=1}^{L} b_k\right)^{N_{\mathrm{g}}} b_L^\dagger b_L \left(\sum_{k=1}^{L} b_k^\dagger\right)^{N_{\mathrm{g}}} |\mathrm{vac}\rangle.
\tag{9.18}
$$

To write the previous expression in a simpler way, we separate the term $b_L^\dagger$ and b_L from the sums as follows

$$
\sum_{k=1}^{L} b_k^\dagger = \sum_{k=1}^{L-1} b_k^\dagger + b_L^\dagger = \sqrt{L-1}\, a^\dagger + b_L^\dagger,
$$

where $a^\dagger = \frac{1}{\sqrt{L-1}}\sum_{k=1}^{L-1} b_k^\dagger$ (and a) represents the creation (annihilation) operator of a boson delocalized in $L-1$ sites which obeys the usual bosonic commutation relations

$$
\left[a^\dagger, a\right] = 1, \qquad \left[a^\dagger, a^\dagger\right] = [a, a] = 0.
$$

With this, we can rewrite

$$
\left(\sum_{k=1}^{L} b_k^\dagger\right)^{N_{\mathrm{g}}} = \left(\sqrt{L-1}\, a^\dagger + b_L^\dagger\right)^{N_{\mathrm{g}}} = \sum_{l=0}^{N_{\mathrm{g}}} \binom{N_{\mathrm{g}}}{l} \sqrt{L-1}^{N_{\mathrm{g}}-l} b_L^{\dagger\, l} a^{\dagger\, N_{\mathrm{g}}-l},
$$

so that the quantity (9.18) can be now expressed as

$$
\begin{aligned}
\langle\!\langle N_L \rangle\!\rangle &= \frac{1}{N_{\mathrm{g}}! L^{N_{\mathrm{g}}}} \sum_{l,m=0}^{N_{\mathrm{g}}} \binom{N_{\mathrm{g}}}{l}\binom{N_{\mathrm{g}}}{m} \sqrt{L-1}^{\,2N_{\mathrm{g}}-l-m} \langle \mathrm{vac}| \, b_L^l b_L^\dagger b_L b_L^{\dagger\,m} a^{N_{\mathrm{g}}-l} a^{\dagger\,N_{\mathrm{g}}-m} |\mathrm{vac}\rangle \\
&= \frac{1}{N_{\mathrm{g}}! L^{N_{\mathrm{g}}}} \sum_{l=0}^{N_{\mathrm{g}}} \binom{N_{\mathrm{g}}}{l}^2 (L-1)^{N_{\mathrm{g}}-l} \langle \mathrm{vac}| \, b_L^l b_L^\dagger b_L b_L^{\dagger\,l} a^{N_{\mathrm{g}}-l} a^{\dagger\,N_{\mathrm{g}}-l} |\mathrm{vac}\rangle \\
&= \sum_{l=0}^{N_{\mathrm{g}}} \binom{N_{\mathrm{g}}}{l} \frac{(L-1)^{N_{\mathrm{g}}-l}}{L^{N_{\mathrm{g}}}} l = \sum_{l=0}^{N_{\mathrm{g}}} \binom{N_{\mathrm{g}}}{l} \left(\frac{1}{L}\right)^l \left(1-\frac{1}{L}\right)^{N_{\mathrm{g}}-l} l .
\end{aligned}
$$

In summary, we can see that the average occupation of the sites (for any site k) can be written then as

$$
\langle\!\langle N_k \rangle\!\rangle = \sum_{n=0}^{N_{\mathrm{g}}} P(n) n = N_0 ,
$$

where $P(n)$ is the probability distribution that determines the occupation N_k, and that is the binomial distribution with $p = 1/L$,

$$
P(n) = \binom{N_{\mathrm{g}}}{n} \left(\frac{1}{L}\right)^n \left(1-\frac{1}{L}\right)^{N_{\mathrm{g}}-n} . \tag{9.19}
$$

We can also obtain the second moment of this distribution, and we find it to be

$$
\langle\!\langle N_k^2 \rangle\!\rangle = N_0 \left(N_0 + 1 - \frac{1}{L} \right) .
$$

The same procedure can be followed to obtain the probability distribution related to the occupation of two different sites, and we find it to be given by

$$
P(n,m) = \binom{N_{\mathrm{g}}}{n}\binom{N_{\mathrm{g}}-n}{m} \left(\frac{1}{L}\right)^{n+m} \left(1-\frac{2}{L}\right)^{N_{\mathrm{g}}-n-m} , \tag{9.20}
$$

so the average occupation of two sites k and j with $k \neq j$ is

$$
\langle\!\langle N_k N_j \rangle\!\rangle = N_0 \left(N_0 - \frac{1}{L} \right) .
$$

With these results one can calculate that the fluctuation of the Rabi frequency $\delta\Omega_k = (\Omega/2N_0)\,\delta N_k$ is a random variable whose first two moments are given as

$$
\langle\!\langle \delta\Omega_k \rangle\!\rangle = \frac{\Omega}{2N_0} \langle\!\langle N_k - N_0 \rangle\!\rangle = 0
$$

and

$$
\langle\!\langle \delta\Omega_k\,\delta\Omega_j \rangle\!\rangle = \left(\frac{\Omega}{2N_0}\right)^2 \langle\!\langle (N_k - N_0)(N_j - N_0) \rangle\!\rangle = \left(\frac{\Omega}{2N_0}\right)^2 \left[\langle\!\langle N_k N_j \rangle\!\rangle - N_0^2 \right] = \frac{\Omega^2}{4N_0}\left[\delta_{kj} - \frac{1}{L}\right] . \tag{9.21}
$$

In this case, the perturbative approximation to the intensity profile of the transition $|G\rangle \to |1\rangle$ can be obtained analytically. We use the fact that $\delta\Omega_j$ is a random variable, and average the intensity (9.17) over many realizations. Hence, we can see that, since the values of $\langle\!\langle \delta\Omega_k^2 \rangle\!\rangle$ and $\langle\!\langle \delta\Omega_j \delta\Omega_k \rangle\!\rangle$ are independent of the site, one can write $\langle\!\langle \delta\Omega_k^2 \rangle\!\rangle \equiv \langle\!\langle \delta\Omega_1^2 \rangle\!\rangle$ and $\langle\!\langle \delta\Omega_j \delta\Omega_k \rangle\!\rangle \equiv \langle\!\langle \delta\Omega_1 \delta\Omega_{1+l} \rangle\!\rangle$ with $l \neq 0$, and hence

$$
\langle\!\langle \sum_{j=1}^{L} \delta\Omega_j^2 \rangle\!\rangle = \sum_{j=1}^{L} \langle\!\langle \delta\Omega_1^2 \rangle\!\rangle = L \langle\!\langle \delta\Omega_1^2 \rangle\!\rangle ,
$$

and

$$\left\langle\!\!\left\langle \sum_{j\neq k} \delta\Omega_j \delta\Omega_k e^{i\frac{2\pi}{L}n(j-k)} \right\rangle\!\!\right\rangle = \sum_{j\neq k} \langle\!\langle \delta\Omega_1 \delta\Omega_{1+l} \rangle\!\rangle e^{i\frac{2\pi}{L}n(j-k)} = \langle\!\langle \delta\Omega_1 \delta\Omega_{1+l} \rangle\!\rangle \sum_{j\neq k} e^{i\frac{2\pi}{L}n(j-k)} = -L\langle\!\langle \delta\Omega_1 \delta\Omega_{1+l} \rangle\!\rangle.$$

Thus, the averaged intensity yields (considering $\delta\Omega_k \ll 1$)

$$\langle\!\langle I(D_n^{(0)}) \rangle\!\rangle = \frac{L}{4} \langle\!\langle |\langle 1'_n|1\rangle|^2 \rangle\!\rangle = \frac{\langle\!\langle \delta\Omega_1^2 \rangle\!\rangle - \langle\!\langle \delta\Omega_1 \delta\Omega_{1+l} \rangle\!\rangle}{4\left|D_n^{(0)} - D_L^{(0)}\right|^2},$$

so, using the result (9.21), the perturbative approximation to the profile of absorption is, in this case, given by

$$\langle\!\langle I(D_n^{(0)}) \rangle\!\rangle = \frac{\Omega^2}{4N_0 \left|D_n^{(0)} - D_L^{(0)}\right|^2},$$

for $n \neq L$.

9.6. Summary and conclusions

In this chapter we have studied the collective excitation of a laser-driven Rydberg gas confined to a ring lattice. We have focused on the regime in which the interaction between the highly excited states is much weaker than the laser field. We found that the corresponding system can be described as a chain of spinless fermions whose dynamics is driven by the xy-model. This Hamiltonian can be analytically solved and, by exploiting the symmetries of the system, we were able to completely characterize the many-particle states arising. In particular, we have shown that the first excited state of the Hamiltonian corresponds to a spin wave or to an excitation which is completely delocalized all over the lattice. The two-fermion states could be expressed as a superposition of excitation pairs and an investigation of their density-density correlation function has been performed. We have demonstrated that the qualitative behavior of these correlations differs substantially from one state to another of the same two-fermion manifold, going from a smoothly decaying function to a pronounced correlation-anticorrelation pattern. The analytical eigenenergies of the xy-Hamiltonian were compared to the numerical exact ones of the complete Hamiltonian, and excellent agreement between both results has been found. Finally, we have investigated several paths for the selective excitation of the many-particle states. One of them relies on the variation of the laser parameters with time, finding trajectories from the initial to a given final many-body state. The other possibility we have presented makes use of an oscillating detuning which allows to access excitations starting from the ground state of the Hamiltonian. In each step, a π-pulse is performed with the frequency of the oscillation matching the energy gap between the involved states. Until that point we have considered an homogeneous occupation of the sites of the ring lattice. The situation of having a randomly fluctuating number of atoms per site would effectively lead to a disorder potential for the fermions. This implies as well a change in the symmetry properties of the system, so that more states become accessible by a time evolution.

Most of the results presented in this chapter can be found published in Refs. [132, 133].

10. Summary and outlook

To conclude this thesis, we would like to make a brief summary of its contents. Also, and more importantly, we mention possible directions of future work.

In the first part, the information-theoretic measure Fisher information is studied and its applications to fields that range from the statistics to quantum mechanics become apparent. First, we use the translationally invariant Fisher information as a local measure of the disorder of a quantum-mechanical system or the amount of gradient of its associated probability distribution. In particular, we focus here in the case of the D-dimensional hydrogenic atom in both position and momentum spaces. Let us point out that this information-theoretic quantity remains to be calculated for multidimensional hydrogenic Sturmians of non-spherical character (for example, parabolic or elliptic [134, 135, 136]) in the two complementary spaces.

Then, we use the Fisher information in its original form as a tool in the estimation theory, and apply it to the so-called Rakhmanov densities associated to the families of orthogonal polynomial that depend upon a parameter (Laguerre and Jacobi). Among the open problems in this direction let us first mention the computation of the parameter-based Fisher information of the generalized Hermite polynomials, the Bessel polynomials and the Pollaczek polynomials. A much more ambitious problem is the evaluation of the Fisher quantity for the general Wilson orthogonal polynomials among others. In addition, nothing is known for discrete orthogonal polynomials. In this case, however, the very notion of the parameter-based Fisher information is a subtle question [137, 138].

In the second part of this thesis, a gas of ultracold laser-driven Rydberg atoms trapped in a one-dimensional ring lattice has been studied. On one hand, the case of very strong interactions has been considered, where the numerical time evolution of the system showed the existence of a equilibrium state arising after a short period of time. The origin of this steady state product of a purely coherent dynamics was the topic of further investigation. On the other hand, the strong laser driving regime proved this system to open exciting perspectives for creating complex many-particle entangled states with interesting prospects for the study of disorder and the generation of non-classical light.

There are several natural extensions to this work that we list now here. In our considerations we have assumed that the atoms are strongly localized, i.e., $a \gg \sigma$. In practice there is a finite width of the wave-packet, caused by the uncertainty principle and finite temperature. This will lead to disorder also in the interaction energy β, which can be also treated in the present framework. Also, as we have pointed out, the main problem one has to face in this system is the limited lifetime of the Rydberg states, which is in the order of several microseconds. One could think of preparing a parallel system to the one described in this work but using polar molecules [139, 140], to overcome this lifetime limitation. Eventually, an interesting extension is also the investigation of the system in two-dimensional geometries, e.g., triangular or square lattices, as well as several rings disposed in concentric or cylindric configurations. In all these cases, the symmetries of the particular arrangement of the sites might give rise to new interesting many-particle states and/or significantly affect the time evolution of these systems.

Finally, we would like to highlight a further direction of work that unifies the two parts of this thesis. Recently, it has been investigated how Fisher information provides a sufficient condition to recognize multiparticle entanglement and, in addition, can be used as a measure of the usefulness of pure entangled states for sub-shot noise sensitivity of linear interferometer [141, 142]. The

usefulness in this respect of the many-particle entangled states arising in our Rydberg gas system in the strong laser driving regime is to be tested. A positive result would make the treated system even more interesting, overall given the feasibility of an experimental access to the states outlined in Section 9.4.

11. Conclusiones

En esta sección se describen brevemente los resultados más relevantes de este trabajo de tesis doctoral y se enumeran algunos problemas abiertos en este campo.

La primera parte de esta tesis está dedicada a la investigación de la información de Fisher y de varias de sus aplicaciones en estadística y mecánica cuántica. En primer lugar, se ha ilustrado la utilidad de la información de Fisher traslacionalmente invariante como medida local del desorden de un sistema mecanocuántico o de la cantidad de gradiente de la distribución de probabilidad asociada al mismo. En particular, se ha llevado a cabo este análisis en el átomo hidrogenoide D-dimensional tanto en el espacio de posiciones como en el de momentos. Una extensión natural de este trabajo sería el cálculo de esta magnitud teórico-informacional para sistemas cuánticos más complejos. De hecho, nuestro estudio se podría completar realizando un análisis similar para el caso de las funciones Sturmianas hidrogenoides de carácter no esférico (por ejemplo, parabólicos o elípticos [134, 135, 136]) en los dos espacios complementarios.

A continuación, se ha utilizado la forma original de la información de Fisher como herramienta en la teoría de estimación de parámetros. Se ha derivado esta magnitud para las llamadas densidades de Rakhmanov asociadas a las familias de polinomios ortogonales que dependen de un parámetro (los polinomios de Laguerre y de Jacobi). Entre los problemas abiertos en este campo merece la pena destacar el cálculo de la información de Fisher con respecto a un parámetro para los polinomios de Hermite generalizados, de Bessel, y de Pollaczek. Realizar un estudio similar para los polinomios ortogonales de Wilson sería un objetivo más ambicioso debido a la complejidad computacional que conlleva. Además, cabe mencionar que el estudio de los polinomios ortogonales de variable discreta es un campo aún poco explorado dado que, en este caso, la mera definición de la información de Fisher es una cuestión sutil [137, 138].

En la segunda parte de esta tesis, se ha estudiado un gas ultrafrío de átomos Rydberg confinado en una red circular monodimensional y excitado mediante un campo láser. Por un lado, se ha llevado a cabo un estudio numérico del régimen en el que la interacción entre átomos Rydberg es mucho más intensa que el acoplamiento con el campo externo. En este caso, la dinámica del sistema resulta estar caracterizada por un estado de equilibrio que se alcanza tras un corto periodo de tiempo. Se ha realizado una investigación en profundidad sobre el origen de este estado estacionario que es el producto de una dinámica puramente coherente y se ha encontrado una relación con el conjunto microcanónico. Por otro lado, en el régimen contrario, dominado por la interacción con el campo láser, se ha hallado la posibilidad de crear estados multiparticulares complejos y entrelazados, que son de gran interés para el estudio del desorden y la generación de estados fotónicos no clásicos.

En este trabajo, hemos supuesto que los átomos están altamente localizados en los pozos de la red. En realidad, existe una anchura asociada al paquete de ondas debida tanto al principio de incertidumbre como a la temperatura finita del sistema. Este factor trae como consecuencia un desorden asociado en este caso a la energía de interacción β, que aún ha de ser estudiado en profundidad. Por otro lado, el mayor problema al que nos enfrentamos en este sistema es la corta vida media de los estado Rydberg, del orden de los microsegundos. Una forma de evitar este problema es preparar un sistema similar usando moléculas diatómicas polares [139, 140]. Además, sería también interesante considerar redes ópticas bidimensionales con distintas simetrías como, por ejemplo, triangular, cuadrada, o anillos bien concéntricos o superpuestos en una configuración cilíndrica. En estos sistemas, las diferentes simetrías podrían afectar a la dinámica de los mismos, dando lugar a nuevos e interesantes fenómenos físicos, así como estados multiparticulares.

Para terminar, nos gustaría destacar una cuestión más, que unifica las dos partes de esta tesis. Recientemente se ha demostrado que la información de Fisher es capaz de proveer una condición suficiente para el reconocimiento de estados multiparticulares entrelazados. Además, esta medida se usa como indicador cuándo un estado puro entrelazado utilizado en interferometría lineal, ofrece como resultado una sensibilidad por debajo del límite del ruido inducido por el entorno debido a fluctuaciones del vacio (*shot-noise*) [141, 142]. Merece la pena comprobar si los estados multiparticulares que emergen del gas de átomos Rydberg aquí investigado son útiles en este contexto. Un resultado positivo en esta dirección dotaría al sistema tratado de aún mayor interés, sobre todo dado que estos estados pueden ser excitados experimentalmente, tal y como proponemos en la Sección 9.4.

A. Excitation to a Rydberg state by a two-photon transition

To excite a ground-state atom to a Rydberg state, a laser field is used, so the Hamiltonian that describes the process is given by the equation (5.3). In this framework, the population oscillates from the ground to the Rydberg state with a frequency given by the Rabi frequency of the laser.

In practise, this transition to the Rydberg state is usually achieved by means of a two-photon process, i.e., by means of an intermediate state. Let us consider as an example here the excitation of the 43s state of rubidium. In this case, the initial level is the 5s, ground state of the Rb, and the intermediate one used to achieve the Rydberg excitation is the 5p. Hence, there are two lasers involved in this process: one that drives the transition 5s-5p, and another one that couples 5p to 43s, with detunings Δ_1 and Δ_2, respectively (see Fig. A.1). Thus, the Hamiltonian describing this process in the basis $\{|5s\rangle, |5p\rangle, |43s\rangle\}$ can be written as

$$H = H_0 + H_{l1} + H_{l2} = \begin{pmatrix} \varepsilon_{5s} & 2\Omega_1 \cos\omega_1 t & 0 \\ 2\Omega_1 \cos\omega_1 t & \varepsilon_{5p} & 2\Omega_2 \cos\omega_2 t \\ 0 & 2\Omega_2 \cos\omega_2 t & \varepsilon_{43s} \end{pmatrix},$$

with $H_0 = \varepsilon_{5s}|5s\rangle\langle 5s| + \varepsilon_{5p}|5p\rangle\langle 5p| + \varepsilon_{43s}|43s\rangle\langle 43s|$ being the atomic Hamiltonian, and H_{l1} and H_{l2} representing the coupling of the two laser fields to the atom. The two Rabi frequencies are defined as $\Omega_1 \equiv \frac{E_1}{2}\langle 5s|z|5p\rangle$ and $\Omega_2 \equiv \frac{E_2}{2}\langle 5p|z|43s\rangle$ with E_1 and E_2 being the amplitudes of each of the laser fields, which are tuned to the energy gaps $\omega_1 = \varepsilon_{5p} - \varepsilon_{5s} - \Delta_1$ and $\omega_2 = \varepsilon_{43s} - \varepsilon_{5p} - \Delta_2$, respectively. We go to a rotating frame by means of two unitary transformations,

$$U_1 = \begin{pmatrix} 1 & 0 & 0 \\ 0 & e^{-i\omega_1 t} & 0 \\ 0 & 0 & e^{-i\omega_1 t} \end{pmatrix} \qquad U_2 = \begin{pmatrix} 1 & 0 & 0 \\ 0 & 1 & 0 \\ 0 & 0 & e^{-i\omega_2 t} \end{pmatrix},$$

such that

$$U = U_1 U_2 = \begin{pmatrix} 1 & 0 & 0 \\ 0 & e^{-i\omega_1 t} & 0 \\ 0 & 0 & e^{-i(\omega_1+\omega_2)t} \end{pmatrix}.$$
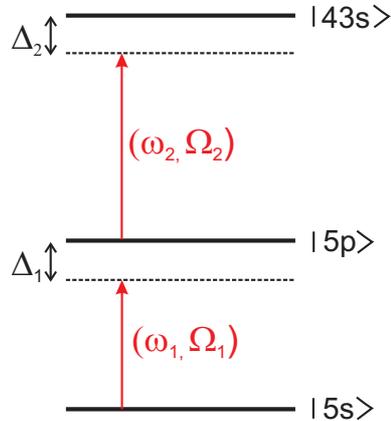
Figure A.1.: Scheme of the three levels and two lasers involved in the excitation of the Rydberg 43s state of Rb.

Applying this unitary transformation to the Schrödinger equation leads to an effective Hamiltonian

$$H_{\text{eff}} = U^\dagger H U - i U^\dagger \frac{\partial}{\partial t} U \approx \begin{pmatrix} 0 & \Omega_1 & 0 \\ \Omega_1 & \Delta_1 & \Omega_2 \\ 0 & \Omega_2 & \Delta_1 + \Delta_2 \end{pmatrix},$$

where we have eliminated the terms oscillating with a frequency $2\omega_1$ and $2\omega_2$ (RWA) and put the energy of the 5s state to zero. If we consider now that the first laser is far-detuned from the transition 5s to 5p, i.e., that $\Delta_1 \gg |\Delta_1 + \Delta_2|$, we can adiabatically eliminate the intermediate 5p level and obtain an approximate Hamiltonian for the new two-level system such that

$$H_{\text{eff}} \approx \frac{1}{\Delta_1} \begin{pmatrix} \Omega_1^2 & \Omega_1 \Omega_2 \\ \Omega_1 \Omega_2 & \Omega_2^2 + \Delta_1 (\Delta_1 + \Delta_2) \end{pmatrix}.$$

In summary, we have transformed the three-level initial system driven by two lasers into one two-level system where the two states involved are effectively coupled by a laser with effective Rabi frequency $\Omega_0 = \Omega_1 \Omega_2 / \Delta_1$ and detuning $\Delta = \Delta_1 + \Delta_2 + \left(\Omega_2^2 - \Omega_1^2 \right) / \Delta_1$.

B. Perfect blockade beyond the nearest neighbor

Throughout this work, we have been focused on the regime where only the nearest neighbors in the ring lattice interact. Some results are presented in this appendix for the case when more sites are considered, in particular in the perfect blockade regime. Originally, the interaction Hamiltonian derived in Section 6.1 reads

$$H_{\text{int}} = \sum_{k=1}^{L} \sum_{l=1}^{d} V_l n_k n_{k+d},$$

where d stands for the number of sites that separate the two Rydberg atoms, i.e., the maximal range of the interaction is given by approximately da, with a being the lattice constant. We have considered throughout this work only nearest neighbor, i.e., $d = 1$. When we made use of the perfect blockade approximation, we discussed that it implied that the potential is infinity inside the considered range and 0 outside, i.e., that Ω had to accomplish

$$1 \gg \frac{\Omega}{V_1} \gg \frac{1}{64}.$$

If instead of considering only nearest neighbor interaction we assume perfect blockade over a range given by d lattice sites, then the perfect blockade regime is accomplished if

$$1 \gg \frac{\Omega}{V_d} \gg \frac{d^6}{(d+1)^6},$$

condition that gets weaker the larger d becomes, e.g., for $d = 2$ and $d = 3$ it yields $1 \gg \Omega/V_2 \gg 0.088$ and $1 \gg \Omega/V_3 \gg 0.18$, respectively. Bearing this limitation in mind, we calculate numerically the mean number of Rydberg atoms excited following the procedure of Section 7.3.2 for $d \neq 1$, from where we get indication of a scaling $\overline{n_k(t)}_{\text{d}} \approx (2\,(d+1))^{-1}$. We obtain now an analytical approximation to these mean values from the steady state arising from the derivation in Section 8.3 in order to compare these results.

The steady state of the system, with a general maximal range of interactions determined by d in the perfect blockade regime, has been shown to be given by simply the number of states containing m excitations divided by the total dimension of the Hilbert space (8.11). This can be calculated analytically, and the result is

$$\rho_{md}^{\text{steady}} = \frac{1}{\dim} \frac{L}{L - md} \binom{L - md}{m} \qquad \text{with} \qquad \dim = \sum_{m=0}^{n_{\max}} \frac{L}{L - md} \binom{L - md}{m},$$

with $n_{\max} = \lfloor L/(d+1) \rfloor$. Now, we perform a change of variable to the density of excitations $\alpha = m/L$, such that

$$\binom{L - md}{m} = \binom{L - L\alpha d}{L\alpha} = \frac{(L - L\alpha d)!}{(L\alpha)!\,(L - L\alpha(d+1))!}.$$

If now we assume that the number of sites is very large, $L \gg 1$, and that the function is strongly peaked around the maximum of α, is located around $L/2(d+1)$, we can use Stirling's formula to approximate the steady state to

$$\rho_{md}^{\text{steady}} \propto \frac{1}{2\pi L} \sqrt{\frac{1 - \alpha d}{\alpha\,(1 - \alpha(d+1))}} \left(\frac{(1 - \alpha d)^{1-\alpha d}}{\alpha^\alpha (1 - \alpha(d+1))^{1-\alpha(d+1)}} \right)^L.$$

d	α_{max}	$\alpha_{\text{numerical}}$	$\sigma_\alpha^2 L$
1	0.276	0.26	0.089
2	0.194	0.17	0.050
3	0.151	0.12	0.033

Table B.1.: Analytical values form the derivation of the steady state and results from a numerical time evolution are compared. We observe that the results differ more from each other the larger the range of the interactions. In the last column, the analytical values of the squared standard deviation are presented.

This is a strongly peaked function that can be approximated by a Gaussian when L is large enough, $\rho_{md}^{\text{steady}} \propto \exp\left[g(L, \alpha, d)\right]$. The position of the maximum is obtained by the derivation of the function g with respect to α and equating to zero,

$$\frac{1}{2L\alpha} - \frac{1}{2L(1 - \alpha d)(1 - \alpha(d+1))} + \ln\alpha + d\ln\left[1 - \alpha d\right] - (d+1)\ln\left[1 - \alpha(d+1)\right] = 0.$$

Since we take L to be very large, in the previous expression the two first terms can be neglected, and thus the maximum can be obtained solving the following equation

$$\left(1 - \alpha_{\text{max}}(d+1)\right)^{d+1} = \alpha_{\text{max}}\left(1 - \alpha_{\text{max}}d\right)^d.$$

The inverse of the second derivative of $g(L, \alpha, d)$ with respect to α evaluated in the maximum α_{max} provides us also the squared of the standard deviation of the steady state. Again, the consideration of $L \gg 1$ is taken into account, and the corresponding terms are neglected, so that the result yields

$$\sigma_\alpha^2 = \frac{\alpha_{\text{max}}(1 - \alpha_{\text{max}}d)(1 - \alpha_{\text{max}}(d+1))}{L}.$$

The comparison of these values to the numerically obtained in Section 7.3.2 is reflected in Table B.1.

C. Perturbative corrections to the xy-model

In Section 9.3.2, we gave the expressions of the second order corrections to the energies obtained by means of the xy-model. These shifts appear due to the effect of the terms of the Hamiltonian H_1 and H_2, and in this Appendix a thorough calculation of the expressions (9.12) and (9.13) is presented.

In some cases it is convenient to use the expression of H_1 and H_2, i.e., (9.4) and (9.5), in terms of the fermionic operators $c_k^\dagger$ and c_k, so we perform the Jordan-Wigner transformation (9.6) and obtain

$$
H_1 = \frac{\Delta L}{2} - \frac{\Delta}{2} \sum_{k=1}^{L} \left(c_k^\dagger + c_k \right) e^{i\pi \sum_{j=1}^{k-1} c_j^\dagger c_j}
$$

$$
H_2 = \frac{\beta}{4} \sum_{k=1}^{L} \left(c_k^\dagger c_{k+1}^\dagger - c_k c_{k+1} \right) - \frac{\beta}{4} \left(c_L^\dagger c_1^\dagger - c_L c_1 \right) \left(e^{i\pi n_+} + 1 \right) - \frac{\beta}{2} \sum_{k=1}^{L} \left(c_k^\dagger + c_k \right) e^{i\pi \sum_{j=1}^{k-1} c_j^\dagger c_j}.
$$

The second order perturbative corrections to the energy of a general state $|\Psi\rangle$ are given by

$$
E_\Psi^{(2)} = \sum_{\Phi \neq \Psi} \frac{\left| \langle \Phi | H_1 + H_2 | \Psi \rangle \right|^2}{E_\Psi^{(0)} - E_\Phi^{(0)}},
$$

so that the problem is basically finding the expression of the corresponding matrix elements.

Let us consider first the ground state. To calculate the correction $E_G^{(2)}$ we need to obtain the matrix elements $\langle G | H_1 + H_2 | 1 \rangle$ and $\langle G | H_1 + H_2 | 2_n \rangle$ since H_1 and H_2 only couple states whose number of fermions differ by one or two. The matrix element between $|G\rangle$ and $|1\rangle$ reads

$$
\langle G | H_1 + H_2 | 1 \rangle = -\left(\frac{\beta}{2} + \frac{\Delta}{2} \right) \sum_{k=1}^{L} \langle G | c_k | 1 \rangle = -\frac{1}{\sqrt{L}} \left(\frac{\beta}{2} + \frac{\Delta}{2} \right) \sum_{k,j} \langle G | c_k c_j^\dagger | G \rangle = -\frac{\sqrt{L}}{2} \left(\beta + \Delta \right),
$$

and the matrix element between $|G\rangle$ and $|2_n\rangle$ is

$$
\begin{aligned}
\langle G | H_1 + H_2 | 2_n \rangle &= -\frac{\beta}{4} \langle G | \sum_{k=1}^{L} c_k c_{k+1} - 2 c_L c_1 | 2_n \rangle \\
&= -\frac{\beta}{4L} \sum_{p,q} e^{i\frac{2\pi}{L}(n-1/2)(p-q)} \left[\sum_k \langle G | c_k c_{k+1} c_p^\dagger c_q^\dagger | G \rangle - \langle G | 2 c_L c_1 c_p^\dagger c_q^\dagger | G \rangle \right] \\
&= -\frac{\beta(L+2)}{4L} \left[e^{i\frac{2\pi}{L}(n-1/2)} - e^{-i\frac{2\pi}{L}(n-1/2)} \right] \\
&= -\frac{i\beta(L+2)}{2L} \sin\left[\frac{2\pi}{L}(n-1/2) \right]
\end{aligned}
$$

where we have used that

$$
\begin{aligned}
\langle G | c_k c_{k+1} c_p^\dagger c_q^\dagger | G \rangle &= -\langle G | c_k c_p^\dagger c_{k+1} c_q^\dagger | G \rangle + \langle G | c_k c_q^\dagger | G \rangle \delta_{p,k+1} \\
&= -\langle G | c_k c_p^\dagger | G \rangle \delta_{q,k+1} + \delta_{p,k+1} \delta_{q,k} \\
&= \delta_{p,k+1} \delta_{q,k} - \delta_{q,k+1} \delta_{p,k}.
\end{aligned}
$$

Plugging in these results, the Eq. (9.12) is reproduced.

Analogously, we derive the energy shift (9.13) of the first excited state, the single-fermion $|1\rangle$, due to H_1 and H_2. In this case, we have to calculate the effect of the states $|G\rangle$, $|2_n\rangle$ and $|3_{lmn}\rangle$. The matrix element between $|1\rangle$ and $|2_n\rangle$ is given by

$$
\begin{aligned}
\langle 1| H_1 + H_2 |2_n\rangle &= -\left(\frac{\beta}{2} + \frac{\Delta}{2}\right) \sum_{k=1}^{L} \langle 1| \sigma_-^{(k)} |2_n\rangle \\
&= \frac{i\,(\beta + \Delta)}{L^{3/2}} \sum_{k,j} \sum_{p>q} \sin\left(\frac{2\pi}{L}(n-1/2)(p-q)\right) \langle G| \sigma_-^{(j)} \sigma_-^{(k)} \sigma_+^{(p)} \sigma_+^{(q)} |G\rangle \\
&= \frac{2i\,(\beta + \Delta)}{L^{3/2}} \sum_{k>j} \sin\left(\frac{2\pi}{L}(n-1/2)(k-j)\right) \\
&= \frac{i\,(\beta + \Delta)}{\sqrt{L}} \cot\left[\frac{\pi}{L}(n-1/2)\right],
\end{aligned}
$$

where we have used that

$$
\begin{aligned}
\langle G| \sigma_-^{(j)} \sigma_-^{(k)} \sigma_+^{(p)} \sigma_+^{(q)} |G\rangle &= \langle G| \sigma_-^{(j)} \sigma_+^{(p)} \sigma_-^{(k)} \sigma_+^{(q)} |G\rangle - \langle G| \sigma_-^{(j)} \sigma_z^{(k)} \sigma_+^{(q)} |G\rangle \delta_{kp} \\
&= -\langle G| \sigma_-^{(j)} \sigma_+^{(p)} \sigma_z^{(k)} |G\rangle \delta_{kq} - \langle G| \sigma_z^{(k)} \sigma_-^{(j)} \sigma_+^{(q)} |G\rangle \delta_{kp} - 2\langle G| \sigma_-^{(j)} \sigma_+^{(q)} |G\rangle \delta_{kp}\delta_{kj} \\
&= -\langle G| \sigma_+^{(p)} \sigma_-^{(j)} \sigma_z^{(k)} |G\rangle \delta_{kq} + \langle G| \sigma_z^{(j)} \sigma_z^{(k)} |G\rangle \delta_{kq}\delta_{jp} + \langle G| \sigma_z^{(k)} \sigma_z^{(j)} |G\rangle \delta_{kp}\delta_{jq} \\
&\quad + 2\langle G| \sigma_z^{(j)} |G\rangle \delta_{kp}\delta_{kj}\delta_{jq} = \delta_{kq}\delta_{jp} + \delta_{kp}\delta_{jq} - 2\delta_{kp}\delta_{kj}\delta_{jq}.
\end{aligned}
$$

On the other hand, the matrix element between $|1\rangle$ and $|3_{lmn}\rangle$ yields

$$
\begin{aligned}
\langle 1| H_1 + H_2 |3_{lmn}\rangle &= -\frac{\beta}{4} \sum_{k=1}^{L} \langle 1| c_k c_{k+1} |3_{lmn}\rangle = -\frac{i\sqrt{2}\beta}{4L^2} \sum_{k,j} \sum_{p,q,r} \sin\left[\frac{2\pi}{L}(pl + qm + rn)\right] \langle G| c_j c_k c_{k+1} c_p^\dagger c_q^\dagger c_r^\dagger |G\rangle \\
&= -\frac{i\sqrt{2}\beta}{4L^2} \sum_{k,j} \left\{ -\sin\left[\frac{2\pi}{L}(jl + km + (k+1)n)\right] + \sin\left[\frac{2\pi}{L}(kl + jm + (k+1)n)\right] \right. \\
&\quad + \sin\left[\frac{2\pi}{L}(jl + (k+1)m + kn)\right] - \sin\left[\frac{2\pi}{L}(kl + (k+1)m + jn)\right] \\
&\quad \left. - \sin\left[\frac{2\pi}{L}((k+1)l + jm + kn)\right] + \sin\left[\frac{2\pi}{L}((k+1)l + km + jn)\right] \right\} = 0,
\end{aligned}
$$

where we have used that

$$
\begin{aligned}
\langle G| c_j c_k c_{k+1} c_p^\dagger c_q^\dagger c_r^\dagger |G\rangle &= -\langle G| c_j c_k c_p^\dagger c_{k+1} c_q^\dagger c_r^\dagger |G\rangle + \langle G| c_j c_k c_q^\dagger c_r^\dagger |G\rangle \delta_{p,k+1} \\
&= \langle G| c_j c_k c_p^\dagger c_q^\dagger c_{k+1} c_r^\dagger |G\rangle - \langle G| c_j c_k c_p^\dagger c_r^\dagger |G\rangle \delta_{q,k+1} \\
&\quad - \langle G| c_j c_q^\dagger c_k c_r^\dagger |G\rangle \delta_{p,k+1} + \langle G| c_j c_r^\dagger |G\rangle \delta_{p,k+1}\delta_{q,k} \\
&= \langle G| c_j c_k c_p^\dagger c_q^\dagger |G\rangle \delta_{r,k+1} + \langle G| c_j c_p^\dagger c_k c_r^\dagger |G\rangle \delta_{q,k+1} \\
&\quad - \langle G| c_j c_r^\dagger |G\rangle \delta_{q,k+1}\delta_{p,k} - \langle G| c_j c_q^\dagger |G\rangle \delta_{p,k+1}\delta_{r,k} + \delta_{p,k+1}\delta_{q,k}\delta_{r,j} \\
&= -\langle G| c_j c_p^\dagger c_k c_q^\dagger |G\rangle \delta_{r,k+1} + \langle G| c_j c_q^\dagger |G\rangle \delta_{r,k+1}\delta_{p,k} \\
&\quad + \langle G| c_j c_p^\dagger |G\rangle \delta_{q,k+1}\delta_{r,k} - \delta_{q,k+1}\delta_{p,k}\delta_{r,j} - \delta_{p,k+1}\delta_{r,k}\delta_{q,j} + \delta_{p,k+1}\delta_{q,k}\delta_{r,j} \\
&= -\delta_{r,k+1}\delta_{q,k}\delta_{p,j} + \delta_{r,k+1}\delta_{p,k}\delta_{q,j} + \delta_{q,k+1}\delta_{r,k}\delta_{p,j} \\
&\quad - \delta_{q,k+1}\delta_{p,k}\delta_{r,j} - \delta_{p,k+1}\delta_{r,k}\delta_{q,j} + \delta_{p,k+1}\delta_{q,k}\delta_{r,j}.
\end{aligned}
$$

D. Numerical methods

D.1. Necklaces and bracelets

A *necklace* is defined to be representant (the lexicographically smallest element) of an equivalence class of k-ary strings under rotation. The set of all possible k-ary necklaces of length L is denoted $\mathbf{N}_k(L)$ and the cardinality of this set is denoted by $N_k(L)$. The enumeration formula for the necklaces is the following:

$$N_k(L) = \frac{1}{L} \sum_{d|L} \phi(d) k^{L/d}, \tag{D.1}$$

where $\phi(m)$ denotes the Euler's totient function, giving the number of numbers in the range $(1, m)$ that are relatively prime to m.

A *bracelet* is the corresponding representant of an equivalence class of k-ary strings under rotation and reversal (or a necklace that is also lexicographically minimal among the circular rotations of its reversal). The set of all k-ary bracelets is denoted $\mathbf{B}_k(L)$ and has cardinality $B_k(L)$. In each equivalence class associated with a given bracelet, there exists at most two necklaces: the bracelet itself and the necklace corresponding to the reversal of the bracelet (in some cases the two may be the same). For example, the equivalence class that contains the bracelet 0000100101 also contains the necklace 0010000101. The cardinality $B_k(L)$ is given by

$$B_k(L) = \begin{cases} \frac{1}{2}\left(N_k(L) + \frac{k+1}{2}k^{L/2}\right) & \text{L even} \\ \frac{1}{2}\left(N_k(L) + k^{(n+1)/2}\right) & \text{L odd.} \end{cases} \tag{D.2}$$

Here, we are interested in the creation of binary bracelets as they form a basis for the fully-symmetric many-particle states (with eigenvalue 1 with respect to the operations $\mathcal{X}$ and $\mathcal{R}$ introduced in Section 6.2). This is due to the two only possible internal states of the atoms and the special symmetry of our system. Numerically, all the possible necklaces of dimension L are created following the indications of the Ref. [143], where these are generated by means of a recursive algorithm

```
GenNecklaces(L, t, p, a);
if t > p then
   if mod(L, p) = 0 then
      print a;
   end if
else
   a(t) := a(t − p);
   GenNecklaces(L, t + 1, p, a);
   for j = a(t − p) to 1 do
      a(t) = j;
      GenNecklaces(L, t + 1, t, a);
   end for
end if
```

initialized to $t = 1$, $p = 1$ and $a(0) = 0$. Once the necklaces are created, the bracelets are obtained from the latter ones by taking each necklace, reversing the string, and comparing with the rest of

bracelets already stored. For example, for $L = 6$, there exist three possible necklaces with three 1's, i.e., $N_2(6;3) = \{(001011), (001101), (010101)\}$. In this part of the code the first necklace is stored as a bracelet, and the second and third are reversed and compared with the first one. As a result, only two bracelets arise, i.e., $B_2(6;3) = \{(001011), (010101)\}$.

D.2. Matrix representation of the Hamiltonian

To numerically create the Hamiltonian that represents the laser coupling between the two possible (super)atom states, i.e.,

$$H_{\mathrm{L}} = \Omega \sum_{k=1}^{L} \left(r_k + r_k^{\dagger} \right),$$

one has to take into account that we are working in a subspace of the Hilbert space spanned by the previously mentioned bracelets $\{|b_i\rangle\}$. The projection into the fully-symmetric subspace can be represented by the projector $P = \sum_{i=1}^{B_2(L)} |b_i\rangle \langle b_i|$ such that the creation and annihilation operators ($r_k^{\dagger}$ and r_k) in this basis accomplish

$$Pr_k^{\dagger}P = Pr_j^{\dagger}P \quad \text{and} \quad Pr_kP = Pr_jP \quad \forall\, k, j.$$

Taking this into account, the Hamiltonian in this fully-symmetric basis can be constructed as

$$\tilde{H}_{\mathrm{L}} = PH_{\mathrm{L}}P = LP\left(r_1 + r_1^{\dagger} \right)P,$$

i.e., deriving only one of the creation or annihilation matrices in this basis. To perform this task we use the fact that only subspaces with a number of excitations (or 1's in the bracelets' notation) that differ by one are connected by the matrices. Let us consider the creation matrix $Pr_1^{\dagger}P$. The matrix elements connecting the initial $|b_i\rangle$ (with $N - 1$ excitations) with the final $|b_f\rangle$ (with N excitations) states yield

$$
\begin{aligned}
\langle b_i | Pr_1^{\dagger}P | b_f \rangle &= \langle b_i | r_1^{\dagger} | b_f \rangle = \frac{1}{\sqrt{M_i M_f}} \left(\left(\langle b_{i1}| + \cdots + \langle b_{iM_i}| \right) r_1^{\dagger} \left(|b_{f1}\rangle + \cdots + |b_{fM_f}\rangle \right) \right) \\
&= \frac{1}{\sqrt{M_i M_f}} \left(\langle b_{i1}| r_1^{\dagger} |b_{f1}\rangle + \cdots + \langle b_{iM_i}| r_1^{\dagger} |b_{fM_f}\rangle \right),
\end{aligned}
$$

where the bracelets $|b_i\rangle$ and $|b_f\rangle$ have been expanded in terms of their M_i and M_f different equivalent states under rotation and reversal. Numerically, these elements are obtained as follows:

- Two bracelets with number of excitations differing by one are taken. For example, for $L = 6$, let us consider $|b_i\rangle = (000111)$ and $|b_f\rangle = (001111)$.

- These two states are rotated and reversed so that all the possible equivalent configurations are achieved. In our example,

$$
(000111) \rightarrow
\begin{array}{c}
(001110) \\
(011100) \\
(111000) \\
(110001) \\
(100011) \\
(000111)
\end{array}
\qquad
(001111) \rightarrow
\begin{array}{c}
(011110) \\
(111100) \\
(111001) \\
(110011) \\
(100111) \\
(001111)
\end{array}\;.
$$

- In the set formed by the state with fewer number of excited atoms, we transform a 0 to 1 in the first position when possible, i.e., we apply the $r_1^\dagger$ matrix,

$$
\begin{matrix}
(001110) \\
(011100) \\
(111000) \\
(110001) \\
(100011) \\
(000111)
\end{matrix}
\quad \rightarrow \quad
\begin{matrix}
(101110) \\
(111100) \\
(100111)
\end{matrix}
\quad .
$$

- The latter set of strings is compared with the one formed by the state with higher number of excited atoms and count the number of coincidences, which for this example is two,

$$
\begin{matrix}
(101110) \\
(\mathbf{111100}) \\
(\mathbf{100111})
\end{matrix}
\qquad
\begin{matrix}
(011110) \\
(\mathbf{111100}) \\
(111001) \\
(110011) \\
(\mathbf{100111}) \\
(001111)
\end{matrix}
\quad .
$$

- Finally, this number is divided by the square root of the multiplicity of the considered states. We obtain in our case $\langle 000111 | \, Pr_1^\dagger P \, | 001111 \rangle = 2/\sqrt{6 \cdot 6} = 1/3$.

Bibliography

[1] S. B. Sears, R. G. Parr, and U. Dinur, "On the quantum-mechanical kinetic energy as a measure of the information in a distribution," *Israel J. Chem.*, vol. 19, p. 165, 1980.

[2] E. Romera and J. S. Dehesa, "Weiszäcker energy of many-electron systems," *Phys. Rev. A*, vol. 50, p. 256, 1994.

[3] E. Romera, J. S. Dehesa, and R. J. Yáñez, "The Weizsäcker functional: Some rigorous results," *Int. J. Quantum Chem.*, vol. 56, p. 627, 1995.

[4] B. R. Frieden and B. H. Soffer, "Lagrangians of physics and the game of Fisher-information transfer," *Phys. Rev. E*, vol. 52, p. 2274, 1995.

[5] M. Reginatto, "Derivation of the equations of nonrelativistic quantum mechanics using the principle of minimum Fisher information," *Phys. Rev. A*, vol. 58, p. 1775, 1998.

[6] B. R. Frieden, *Physics from Fisher Information*. Cambridge University Press, 1999.

[7] M. J. W. Hall, "Quantum properties of classical Fisher information," *Phys. Rev. A*, vol. 62, p. 012107, 2000.

[8] M. J. W. Hall, "Exact uncertainty relations," *Phys. Rev. A*, vol. 64, p. 052103, 2001.

[9] B. R. Frieden, A. Plastino, A. R. Plastino, and B. H. Soffer, "Schrödinger link between nonequilibrium thermodynamics and Fisher information," *Phys. Rev. E*, vol. 66, p. 046128, 2002.

[10] A. Nagy, "Fisher information in density functional theory," *J. Chem. Phys.*, vol. 119, p. 9401, 2003.

[11] B. R. Frieden, *Science from Fisher Information*. Cambridge University Press, 2004.

[12] E. Romera and J. S. Dehesa, "The Fisher-Shannon information plane, an electron correlation tool," *J. Chem. Phys.*, vol. 120, p. 8096, 2004.

[13] R. González-Férez and J. S. Dehesa, "Characterization of atomic avoided crossings by means of Fisher information," *Eur. Phys. J. D*, vol. 32, p. 39, 2005.

[14] R. F. Nalewajski, *Information Theory of Molecular Systems*. Elsevier Science, 2006.

[15] A. Plastino, A. R. Plastino, and B. H. Soffer, "Fisher info and thermodynamics first law," *Physica A*, vol. 369, p. 432, 2006.

[16] J. S. Dehesa, A. Martínez-Finkelshtein, and V. N. Sorokin, "Information-theoretic measures for Morse and Pöschl-Teller potentials," *Mol. Phys.*, vol. 104, p. 613, 2006.

[17] S. H. Patil and K. D. Sen, "Net information measures for modified Yukawa and Hulthen potentials," *Int. J. Quantum Chem.*, vol. 107, p. 1864, 2007.

[18] S. H. Patil, K. D. Sen, N. A. Watson, and H. E. Montgomery Jr., "Characteristics features of net information measures for constrained Coulomb potentials," *J. Phys. B*, vol. 40, p. 2147, 2007.

[19] R. J. Yáñez, W. van Assche, and J. S. Dehesa, "Position and momentum information entropies of the D-dimensional harmonic oscillator and hydrogen atom," *Phys. Rev. A*, vol. 50, p. 3065, 1994.

[20] J. S. Dehesa, S. López-Rosa, A. Martínez-Finkelshtein, and R. J. Yáñez, "Information theory of D-dimensional hydrogenic systems: Application to circular and Rydberg states," *Int. J. Quantum Chem., Accepted*, vol. 109, 2010.

[21] J. S. Dehesa, A. Martínez-Finkelshtein, and V. N. Sorokin, "Short-wave asymptotics of the information entropy of a circular membrane," *Int. J. Bifurcation and Chaos*, vol. 12, p. 2387, 2002.

[22] K. D. Sen, "Shell-confined hydrogen atom," *J. Chem Phys.*, vol. 122, p. 194324, 2005.

[23] K. D. Sen, V. I. Pupyshev, and H. E. Montgomery Jr., "Exact relations for confined one-electron systems," *Adv. Quantum Chem.*, vol. 57, p. 25, 2009.

[24] J. C. Angulo and J. S. Dehesa, "Tight rigorous bounds to atomic information entropies," *J. Chem. Phys.*, vol. 97, p. 6485, 1992.

[25] R. O. Esquivel, N. Flores-Gallegos, E. Carrera, J. S. Dehesa, J. Antolín, and C. Soriano-Correa, "Theoretic-information entropies analysis of nanostructures: ab initio study of PA-MAM precursors and dendrimers G0 to G3," *Mol. Simul.*, vol. 35, p. 498, 2009.

[26] S. López-Rosa, J. C. Angulo, and J. S. Dehesa, "Spreading measures of information-extremizer distributions: applications to atomic electron densities in position and momentum spaces," *Eur. Phys. J. D*, vol. 51, p. 321, 2009.

[27] S. López-Rosa, R. O. Esquivel, J. C. Angulo, J. Antolín, J. S. Dehesa, and N. Flores-Gallegos, "Fisher information study in position and momentum spaces from elementary chemical reactions," *J. Chem. Theory Comput.*, vol. 6, p. 145, 2010.

[28] J. Sánchez-Ruiz and J. S. Dehesa, "Entropic integrals of orthogonal hypergeometric polynomials with general supports," *J. Comput. Appl. Math.*, vol. 118, p. 311, 2000.

[29] J. S. Dehesa, A. Martínez-Finkelshtein, and J. Sánchez-Ruiz, "Quantum information entropies and orthogonal polynomials," *J. Comput. Appl. Math.*, vol. 133, p. 23, 2001.

[30] J. Sánchez-Ruiz, "Information entropy of Gegenbauer polynomials and Gaussian quadrature," *J. Phys. A: Math. Gen.*, vol. 36, p. 4857, 2003.

[31] J. Sánchez-Ruiz and J. S. Dehesa, "Fisher information of orthogonal hypergeometric polynomials," *J. Comput. Appl. Math.*, vol. 182, p. 150, 2005.

[32] V. S. Buyarov, J. S. Dehesa, A. Martínez-Finkelshtein, and J. Sánchez-Lara, "Computation of the entropy of polynomials orthogonal on an interval," *SIAM J. Sci. Comput.*, vol. 26, p. 488, 2005.

[33] R. A. Fisher, "Theory of statistical estimation," *Proc. Cambridge Phil. Sec.*, vol. 22, p. 700, 1925.

[34] T. M. Cover and J. A. Thomas, *Elements of Information Theory*. Wiley, 2006.

[35] S. Amari, *Differential Geometrical Methods in Statistics*. Springer, 1985.

[36] M. J. Schervish, *Theory of Statistics*. Springer-Verlag, 1995.

[37] C. Vignat and J.-F. Bercher, "Analysis of signals in the Fisher-Shannon information plane," *Phys. Lett. A*, vol. 312, p. 27, 2003.

[38] J. W. Harris and H. Stocker, *Handbook of Mathematics and Computational Science*. Springer-Verlag, 1998.

[39] C. E. Shannon, "A mathematical theory of communication," *Bell Syst. Tech.*, vol. 27, p. 379, 1948.

[40] A. Stam, "Some inequalities satified by the quantities of information of Fisher and Shannon," *Inf. Control*, vol. 2, p. 101, 1959.

[41] S. Luo, "Fisher information, kinetic energy and uncertainty relation inequalities," *J. Phys. A: Math. Gen.*, vol. 35, p. 5181, 2002.

[42] M. Hayasi, "Two quantum analogues of Fisher information from a large deviation viewpoint of quantum estimation," *J. Phys. A: Math. Gen.*, vol. 35, p. 7689, 2002.

[43] S. Luo, "Quantum Fisher information and uncertainty relations," *Lett. Math. Phys.*, vol. 53, p. 243, 2000.

[44] S. Luo, "Wigner-Yanase skew information and uncertainty relations," *Phys. Rev. Lett.*, vol. 91, p. 180403, 2003.

[45] E. Romera, J. C. Angulo, and J. S. Dehesa, "Fisher entropy and uncertainty-like relationships in many-particle systems," *Phys. Rev. A*, vol. 59, p. 4064, 1999.

[46] E. Romera, "Stam's principle, D-dimensional uncertainty-like relationships and some atomic properties," *Mol. Phys.*, vol. 100, p. 3325, 2002.

[47] C. E. Shannon and W. Weaver, *The Mathematical Theory of Communication*. University of Illinois Press, 1949.

[48] B. Lohman and E. Weigold, "Direct measurement of the electron momentum probability distribution in atomic hydrogen," *Phys. Lett. A*, vol. 86, p. 139, 1981.

[49] A. Goldberg, M. Schey, and J. L. Schwarz, "One-dimensional scattering in configuration space and momentum space," *Am. J. Phys.*, vol. 36, p. 454, 1968.

[50] J. S. Briggs and L. Dubé, "The second Born approximation to the electron transfer cross section," *J. Phys. B*, vol. 13, p. 771, 1980.

[51] J. Avery, *Hyperspherical Harmonics. Applications in Quantum Theory*. Kluwer Acad. Publ., 1989.

[52] J. D. Louck, "Generalized orbital angular momentum and the n-fold degenerate quantum-mechanical oscillator," *J. Mol. Spectrosc.*, vol. 4, p. 334, 1960.

[53] J. Avery, *Hyperspherical Harmonics and Generalized Sturmians*. Kluwer Acad. Publ., 2000.

[54] B. Podolsky and L. Pauling, "The momentum distribution in hydrogen-like atoms," *Phys. Rev.*, vol. 34, p. 109, 1929.

[55] W. research, "The Wolfram function site," http://functions.wolfram.com.

[56] E. Romera, P. Sánchez-Moreno, and J. S. Dehesa, "Uncertainty relation for Fisher information of D-dimensional single-particle systems with central potentials," *J. Math. Phys.*, vol. 47, p. 103504, 2006.

[57] J. S. Dehesa, S. López-Rosa, B. Olmos, and R. J. Yáñez, "Information measures of hydrogenic systems, Laguerre polynomials and spherical harmonics," *J. Comput. Appl. Math.*, vol. 179, p. 185, 2005.

[58] E. Romera, P. Sánchez-Moreno, and J. S. Dehesa, "The Fisher information of single-particle systems with a central potential," *Chem. Phys. Lett.*, vol. 414, p. 468, 2005.

[59] J. S. Dehesa, S. López-Rosa, B. Olmos, and R. J. Yáñez, "The Fisher information of D-dimensional hydrogenic systems in position and momentum spaces," *J. Math. Phys.*, vol. 47, p. 052104, 2006.

[60] E. A. Rakhmanov, "On the asymptotics of the ratio of orthogonal polynomials," *Math. USSR Sb.*, vol. 32, p. 199, 1977.

[61] B. Simon, "Ratio asymptotics and weak asymptotic measures for orthogonal polynomials on the real line," *J. Approx. Theory*, vol. 126, p. 198, 2004.

[62] J. S. Dehesa, W. van Assche, and R. J. Yáñez, "Information entropy of classical orthogonal polynomials and their application to the harmonic oscillator and Coulomb potentials," *Meth. Appl. Anal.*, vol. 4, p. 91, 1997.

[63] J. S. Dehesa, P. Sánchez-Moreno, and R. J. Yáñez, "Cramer-Rao information plane of orthogonal hypergeometric polynomials," *J. Comput. Appl. Math.*, vol. 186, p. 523, 2006.

[64] A. Nikiforov and V. Uvarov, *Special Functions in Mathematical Physics*. Birkhauser Verlag, 1988.

[65] J. Froehlich, "Parameter derivatives of the Jacobi polynomials and the Gaussian hypergeometric function," *Int. Transf. and Special Functions*, vol. 2, p. 253, 1994.

[66] W. Koepf and D. Schmersau, "Representations of orthogonal polynomials," *J. Comput. Appl. Math.*, vol. 90, p. 57, 1998.

[67] A. Ronveaux, A. Zarzo, I. Area, and E. Gogoy, "Classical orthogonal polynomials: Dependence of parameters," *J. Comput. Appl. Math.*, vol. 121, p. 95, 2000.

[68] W. van Assche, R. J. Yáñez, R. González-Ferez, and J. S. Dehesa, "Functionals of Gegenbauer polynomials and D-dimensional hydrogenic momentum expectation values," *J. Math. Phys.*, vol. 41, p. 6600, 2000.

[69] C. C. Grosjean, "The weight functions, generating functions and miscellaneous properties of the sequences of orthogonal polynomials of second kind associated with the Jacobi and Gegenbauer polynomials," *J. Comput. Appl. Math.*, vol. 16, p. 259, 1986.

[70] A. Ronveaux and W. van Assche, "Upward extension of the Jacobi matrix for orthogonal polynomials," *J. Approx. Th.*, vol. 86, p. 335, 1996.

[71] A. Ronveaux, J. S. Dehesa, A. Zarzo, and R. J. Yáñez, "A note on the zeroes of Grosjean polynomials," *Newsletter of the SIAM activity group on Orthogonal Polynomials and Special Functions*, vol. 6, p. 15, 1996.

[72] J. S. Dehesa, B. Olmos, and R. J. Yáñez, "Parameter-based Fisher information of orthogonal polynomials," *J. Comput. Appl. Math.*, vol. 214, p. 136, 2008.

[73] M. H. Anderson, J. R. Ensher, M. R. Matthews, C. E. Wieman, and E. A. Cornell, "Observation of Bose-Einstein condensation in a dilute atomic vapor," *Science*, vol. 269, p. 198, 1995.

[74] C. C. Bradley, C. A. Sackett, J. J. Tollett, and R. G. Hulet, "Evidence of Bose-Einstein condensation in an atomic gas with attractive interactions," *Phys. Rev. Lett.*, vol. 75, p. 1687, 1995.

[75] K. B. Davis, M.-O. Mewes, M. R. Andrews, N. J. van Druten, D. S. Durfee, D. M. Kurn, and W. Ketterle, "Bose-Einstein condensation in a gas of sodium atoms," *Phys. Rev. Lett.*, vol. 75, p. 3969, 1995.

[76] F. Schreck, L. Khaykovich, K. L. Corwin, G. Ferrari, T. Bourdel, J. Cubizolles, and C. Salomon, "Quasipure Bose-Einstein condensate immersed in a Fermi Sea," *Phys. Rev. Lett.*, vol. 87, p. 080403, 2001.

[77] I. Bloch, J. Dalibard, and W. Zwerger, "Many-body physics with ultracold gases," *Rev. Mod. Phys.*, vol. 80, p. 885, 2008.

[78] T. Gallagher, *Rydberg Atoms.* Cambridge University Press, 1994.

[79] I. Mourachko, D. Comparat, F. de Tomasi, A. Fioretti, P. Nosbaum, V. M. Akulin, and P. Pillet, "Many-body effects in a frozen Rydberg gas," *Phys. Rev. Lett.*, vol. 80, p. 253, 1998.

[80] W. R. Anderson, J. R. Veale, and T. F. Gallagher, "Resonant dipole-dipole energy transfer in a nearly frozen Rydberg gas," *Phys. Rev. Lett.*, vol. 80, p. 249, 1998.

[81] B. Sun and F. Robicheaux, "Numerical study of two-body correlation in a 1D lattice with perfect blockade," *New J. Phys.*, vol. 10, p. 045032, 2008.

[82] H. Weimer, R. Löw, T. Pfau, and H. P. Büchler, "Quantum critical behavior in strongly interacting Rydberg gases," *Phys. Rev. Lett.*, vol. 101, p. 250601, 2008.

[83] U. Raitzsch, V. Bendkowsky, R. Heidemann, B. Butscher, R. Löw, and T. Pfau, "Echo experiments in a strongly interacting Rydberg gas," *Phys. Rev. Lett.*, vol. 100, p. 013002, 2008.

[84] M. Reetz-Lamour, T. Amthor, J. Deiglmayr, and M. Weidemüller, "Rabi oscillations and excitation trapping in the coherent excitation of a mesoscopic frozen Rydberg gas," *Phys. Rev. Lett.*, vol. 100, p. 253001, 2008.

[85] D. Jaksch, J. I. Cirac, P. Zoller, S. L. Rolston, R. Côté, and M. D. Lukin, "Fast quantum gates for neutral atoms," *Phys. Rev. Lett.*, vol. 85, p. 2208, 2000.

[86] M. Lukin, M. Fleischhauer, and R. Côté, "Dipole blockade and quantum information processing in mesoscopic atomic ensembles," *Phys. Rev. Lett.*, vol. 87, p. 037901, 2001.

[87] K. Singer, M. Reetz-Lamour, T. Amthor, L. G. Marcassa, and M. Weidemüller, "Suppression of excitation and spectral broadening induced by interactions in a cold gas of Rydberg atoms," *Phys. Rev. Lett.*, vol. 93, p. 163001, 2004.

[88] D. Tong, S. Farooqi, J. Stanojevic, S. Krishnan, Y. Zhang, R. Côté, E. Eyler, and P. Gould, "Local blockade of Rydberg excitation in an ultracold gas," *Phys. Rev. Lett.*, vol. 93, p. 063001, 2001.

[89] R. Heidemann, U. Raitzsch, V. Bendkowsky, B. Butscher, R. Löw, L. Santos, and T. Pfau, "Evidence for coherent collective Rydberg excitation in the strong blockade regime," *Phys. Rev. Lett.*, vol. 99, p. 163601, 2007.

[90] R. Heidemann, U. Raitzsch, V. Bendkowsky, B. Butscher, R. Löw, and T. Pfau, "Rydberg excitation of Bose-Einstein condensates," *Phys. Rev. Lett.*, vol. 100, p. 033601, 2008.

[91] E. Urban, T. A. Johnson, T. Henage, L. Isenhower, D. D. Yavuz, T. G. Walker, and M. Saffman, "Observation of Rydberg blockade between two atoms," *Nature Phys.*, vol. 5, p. 110, 2009.

[92] A. Gaëtan, Y. Miroshnychenko, T. Wilk, A. Chotia, M. Viteau, D. Comparat, P. Pillet, A. Browaeys, and P. Grangier, "Observation of collective excitation of two individual atoms in the Rydberg blockade regime," *Nature Phys.*, vol. 5, p. 115, 2009.

[93] L. Isenhower, E. Urban, X. L. Zhang, A. T. Gill, T. Henage, T. A. Johnson, T. G. Walker, and M. Saffman, "Demonstration of a neutral atom Controlled-NOT quantum gate," *Phys. Rev. Lett.*, vol. 104, p. 010503, 2010.

[94] T. Wilk, A. Gaëtan, C. Evellin, J. Wolters, Y. Miroshnychenko, P. Grangier, and A. Browaeys, "Entanglement of two individual neutral atoms using Rydberg blockade," *Phys. Rev. Lett.*, vol. 104, p. 010502, 2010.

[95] M. Müller, I. Lesanovsky, H. Weimer, H. P. Büchler, and P. Zoller, "Mesoscopic Rydberg gate based on electromagnetically induced transparency," *Phys. Rev. Lett.*, vol. 102, p. 170502, 2009.

[96] H. Weimer, M. Müller, I. Lesanovsky, P. Zoller, and H. P. Büchler, "Digital coherent and dissipative quantum simulations with Rydberg atoms," *arXiv:0907.1657*, 2009.

[97] B. Olmos, M. Müller, and I. Lesanovsky, "Thermalization of a strongly interacting 1D Rydberg lattice gas," *New J. Phys.*, vol. 12, p. 013024, 2010.

[98] M. Saffman, T. G. Walker, and K. Mølmer, "Quantum information with Rydberg atoms," *arXiv:0909.4777v1*, 2009.

[99] J. M. Deutsch, "Quantum statistical mechanics in a closed system," *Phys. Rev. A*, vol. 43, p. 2046, 1991.

[100] M. Srednicki, "Chaos and quantum thermalization," *Phys. Rev. E*, vol. 50, p. 888, 1994.

[101] T. Kinoshita, T. R. Wenger, and D. S. Weiss, "A quantum Newton's cradle," *Nature*, vol. 440, p. 900, 2006.

[102] M. Rigol, V. Dunjko, V. Yurovsky, and M. Olshanii, "Relaxation in a completely integrable many-body quantum system: An ab initio study of the dynamics of the highly excited states of 1D lattice hard-core bosons," *Phys. Rev. Lett.*, vol. 98, p. 050405, 2007.

[103] C. Kollath, A. M. Läuchli, and E. Altman, "Quench dynamics and nonequilibrium phase diagram of the Bose-Hubbard model," *Phys. Rev. Lett.*, vol. 98, p. 180601, 2007.

[104] S. Hofferberth, I. Lesanovsky, B. Fischer, T. Schumm, and J. Schmiedmayer, "Non-equilibrium coherence dynamics in one-dimensional Bose gases," *Nature*, vol. 449, p. 324, 2007.

[105] M. Rigol, V. Dunjko, and M. Olshanii, "Thermalization and its mechanism for generic isolated quantum systems," *Nature*, vol. 452, p. 854, 2008.

[106] D. Porras and J. I. Cirac, "Collective generation of quantum states of light by entangled atoms," *Phys. Rev. A*, vol. 78, p. 053816, 2008.

[107] G. M. D'Ariano, P. Lo Presti, and M. G. A. Paris, "Using entanglement improves the precision of quantum measurements," *Phys. Rev. Lett.*, vol. 87, p. 270404, 2001.

[108] K. Singer, J. Stanojevic, M. Weidemüller, and R. Côté, "Long-range interactions between alkali Rydberg atom pairs correlated to the ns-ns, np-np and nd-nd asymptotes," *J. Phys. B*, vol. 38, p. S295, 2005.

[109] M. Marinescu, J. F. Babb, and A. Dalgarno, "Long-range potentials including retardation for the interaction of two alkali-metal atoms," *Phys. Rev. A*, vol. 50, p. 003096, 1994.

[110] K. D. Nelson, X. Li, and D. S. Weiss, "Imaging single atoms in a three-dimensional array," *Nature Phys.*, vol. 3, p. 556, 2007.

[111] S. Whitlock, R. Gerritsma, T. Fernholz, and R. J. C. Spreeuw, "Two-dimensional array of microtraps with atomic shift register on a chip," *New J. Phys.*, vol. 11, p. 023021, 2009.

[112] P. Würtz, T. Langen, T. Gericke, A. Koglbauer, and H. Ott, "Experimental demonstration of single-site addressability in a two-dimensional optical lattice," *Phys. Rev. Lett.*, vol. 103, p. 080404, 2009.

[113] J. Sawada, "Generating bracelets in constant amortized time," *SIAM J. Comput.*, vol. 31, p. 259, 2001.

[114] B. Olmos, R. González-Férez, and I. Lesanovsky, "Collective Rydberg excitations of an atomic gas confined in a ring lattice," *Phys. Rev. A*, vol. 79, p. 043419, 2009.

[115] J. Schachenmayer, I. Lesanovsky, and A. Daley, "Dynamical state preparation of Rydberg and polar molecular crystals in an optical lattice," *in preparation*, 2010.

[116] D. L. Zhou, B. Zeng, Z. Xu, and L. You, "Multiparty correlation measure based on the cumulant," *Phys. Rev. A*, vol. 74, p. 052110, 2006.

[117] W. K. Wootters, "Entanglement of formation of an arbitrary state of two qubits," *Phys. Rev. Lett.*, vol. 80, p. 2245, 1998.

[118] M. A. Nielsen and I. L. Chuang, *Quantum Computation and Quantum Information*. Cambridge University Press, 2000.

[119] T. C. Liebisch, A. Reinhard, P. R. Berman, and G. Raithel, "Atom counting statistics in ensembles of interacting Rydberg atoms," *Phys. Rev. Lett.*, vol. 95, p. 253002, 2005.

[120] C. Ates, T. Pohl, T. Pattard, and J. M. Rost, "Strong interaction effects on the atom counting statistics of ultracold Rydberg gases," *J. Phys. B*, vol. 39, p. L233, 2006.

[121] B. L. Altshuler, Y. Gefen, A. Kamenev, and L. S. Levitov, "Quasiparticle lifetime in a finite system: A nonperturbative approach," *Phys. Rev. Lett.*, vol. 78, p. 2803, 1997.

[122] R. Berkovits and Y. Avishai, "Localization in Fock space: A finite-energy scaling hypothesis for many-particle excitation statistics," *Phys. Rev. Lett.*, vol. 80, p. 568, 1998.

[123] A. De Pasquale and P. Facchi, "XY model on the circle: diagonalization, spectrum, and forerunners of the quantum phase transition," *Phys. Rev. A*, vol. 80, p. 032102, 2009.

[124] T. Pohl, E. Demler, and M. D. Lukin, "Dynamical crystallization in the dipole blockade of ultracold atoms," *Phys. Rev. Lett. (Accepted) arXiv:0911.1427*, 2010.

[125] A. P. Peirce, M. A. Dahleh, and H. Rabitz, "Optimal control of quantum-mechanical systems: Existence, numerical approximation, and applications," *Phys. Rev. A*, vol. 37, p. 4950, 1988.

[126] T. Calarco, U. Dorner, P. S. Julienne, C. J. Williams, and P. Zoller, "Quantum computations with atoms in optical lattices: Marker qubits and molecular interactions," *Phys. Rev. A*, vol. 70, p. 012306, 2004.

[127] J. Somlói, V. A. Kazakov, and D. J. Tannor, "Controlled dissociation of I_2 via optical transitions between the X and B electronic states," *Chem. Phys.*, vol. 172, p. 85, 1993.

[128] J. Grond, J. Schmiedmayer, and U. Hohenester, "Optimizing number squeezing when splitting a mesoscopic condensate," *Phys. Rev. A*, vol. 79, p. 021603(R), 2009.

[129] P. W. Anderson, "Absence of diffusion in certain random lattices," *Phys. Rev.*, vol. 109, p. 1492, 1958.

[130] J. Billy, V. Josse, Z. Zuo, A. Bernard, B. Hambrecht, P. Lugan, D. Clément, L. Sánchez-Palencia, P. Bouyer, and A. Aspect, "Direct observation of Anderson localization of matter waves in a controlled disorder," *Nature*, vol. 453, p. 891, 2008.

[131] G. Roati, C. D'Errico, L. Fallani, M. Fattori, C. Fort, M. Zaccanti, G. Modugno, M. Modugno, and M. Inguscio, "Anderson localization of a non-interacting Bose-Einstein condensate," *Nature*, vol. 453, p. 895, 2008.

[132] B. Olmos, R. González-Férez, and I. Lesanovsky, "Fermionic collective excitations in a lattice gas of Rydberg atoms," *Phys. Rev. Lett.*, vol. 103, p. 185302, 2009.

[133] B. Olmos, R. González-Férez, and I. Lesanovsky, "Creating collective many-body states with highly excited atoms," *Phys. Rev. A (Accepted) arXiv:0911.2335*, 2010.

[134] V. Aquilanti, S. Cavalli, and C. Coletti, "Hyperspherical symmetry of hydrogenic orbitals and recoupling coefficients among alternative bases," *Phys. Rev. Lett.*, vol. 80, p. 3209, 1998.

[135] V. Aquilanti, A. Caligiana, and S. Cavalli, "Hydrogenic elliptic orbitals, Coulomb Sturmian sets, and recoupling coefficients among alternative bases," *Int. J. Quantum Chem.*, vol. 92, p. 99, 2003.

[136] V. Aquilanti, A. Caligiana, S. Cavalli, and C. Coletti, "Hydrogenic orbitals in momentum space and hyperspherical harmonics: Elliptic Sturmian basis sets," *Int. J. Quantum Chem.*, vol. 92, p. 212, 2003.

[137] P. Sánchez-Moreno, R. J. Yáñez, and J. S. Dehesa, "Discrete densities and Fisher information," *Proceedings of the 14th Int. Conf. on Difference Equations and Applications*, p. 291, 2009.

[138] J. S. Dehesa, P. Sánchez-Moreno, and R. J. Yáñez, "Relative Fisher information of discrete classical orthogonal polynomials," *J. Difference Eq. Appl., Accepted*, 2010.

[139] A. Micheli, G. K. Brennen, and P. Zoller, "A toolbox for lattice-spin models with polar molecules," *Nature Phys.*, vol. 2, p. 341, 2006.

[140] A. Micheli, G. Pupillo, H. P. Büchler, and P. Zoller, "Cold polar molecules in two-dimensional traps: Tailoring interactions with external fields for novel quantum phases," *Phys. Rev. A*, vol. 76, p. 043604, 2007.

[141] L. Pezzé and A. Smerzi, "Entanglement, nonlinear dynamics, and the Heisenberg limit," *Phys. Rev. Lett.*, vol. 102, p. 100401, 2009.

[142] P. Hyllus, O. Gühne, and A. Smerzi, "Not all pure entangled states are useful for sub shot-noise interferometry," *arXiv:0912.4349*, 2009.

[143] K. Cattell, F. Ruskey, J. Sawada, M. Serra, and C. R. Miers, "Fast algorithms to generate necklaces, unlabeled necklaces, and irreducible polynomials over GF(2)," *J. Algorithms*, vol. 37, p. 267, 2000.